



NTNU – Trondheim
Norwegian University of
Science and Technology

High Precision, Full Potential Electronic Transport Simulator

Implementation and First Results

Juri Selvåg

June 2014

Supervisors: Trond Brudevoll, Forsvarets forskningsinstitutt
Asta Katrine Storebø, Forsvarets forskningsinstitutt
Jon Andreas Støvneng, NTNU

Preface

This master's thesis is the fulfilment of my Master's Degree in 'Applied Physics and Mathematics' at Norwegian University of Science and Technology (NTNU). The work has been carried out in cooperation with Norwegian Defence Research Establishment (FFI) under the supervision of Asta Katrine Storebø (FFI), Trond Brudevoll (FFI) and Jon Andreas Støvneng (NTNU). They have provided reliable help and assistance whenever requested and I send my sincerest thanks to all of them.

I would also thank my girlfriend, family and friends, for their support and encouragement throughout this work.

Abstract

During the work with this master's thesis a number of important upgrades has been made to the Full Band Monte Carlo program that is under development at FFI.

The program is now able to simulate charge transport in $\text{Hg}_{0.72}\text{Cd}_{0.28}\text{Te}$, thanks to introductions of a new *ab initio* numerical band structure. All necessary changes has been made to include electrons in the simulations, in addition to holes. The implemented algorithm used to calculate scattering rates has been modified to utilize interpolated values, and generalized to calculate both electron- and hole scattering rates. The selection of final states is now performed with very high precision, where the energy represented by the selected final state deviate by less than 10^{-6} eV from the predetermined final energy.

The most important change is the fact that the Monte Carlo program is now able to simulate both electrons and holes in bulk $\text{Hg}_{0.72}\text{Cd}_{0.28}\text{Te}$, using a full band model for the valence and the conduction bands.

The program was finally used to calculate electron mobility in bulk $\text{Hg}_{0.72}\text{Cd}_{0.28}\text{Te}$, and the calculated electron mobility is in good agreement with other published simulation results.

Sammendrag

Under arbeidet med denne masteroppgaven har det blitt gjort en rekke viktige forbedringer til Monte Carlo programmet som er under utvikling ved FFI.

Programmet har blitt i stand til å simulere transport av ladningsbærere i $\text{Hg}_{0.72}\text{Cd}_{0.28}\text{Te}$, takket være innføringen av en ny *ab initio* numerisk båndstruktur. Alle nødvendige endringer har blitt gjort for å få med elektroner i simuleringene, i tillegg til hull. Algoritmen som brukes til å beregne spredninger har blitt modifisert for å utnytte interpolerte verdier, og generalisert for å beregne spredninger for både elektroner og hull. Valg av slutttilstander blir nå gjort med svært høy presisjon, hvor energien til den valgte slutttilstanden avviker med mindre enn 10^{-6} eV fra den forhåndsvalgte sluttenergien.

Den aller viktigste forandringen er at Monte Carlo programmet er nå i stand til å simulere både elektroner og hull i bulk $\text{Hg}_{0.72}\text{Cd}_{0.28}\text{Te}$, ved bruk av en fullbåndmodell for valens- og ledningsbåndene.

Programmet ble til slutt brukt til å beregne elektronmobilitet i bulk $\text{Hg}_{0.72}\text{Cd}_{0.28}\text{Te}$, og den beregnede elektronmobiliteten stemmer godt overens med andre publiserte simuleringresultater.

Table of Contents

Preface	i
Abstract/Sammendrag	iii
1 Introduction	1
2 The Monte Carlo method	3
2.1 Scattering rates	4
2.2 Duration of the Free Flights	5
2.3 Monte Carlo selection of scattering mechanism	7
2.4 Selection of final states	8
3 Numerical approach	9
3.1 Numerical band representation	9
3.1.1 Energy band structure	11
3.2 Energy interpolation	12
3.2.1 Gradient interpolation	13
3.3 Numerical calculation of the scattering rates	14
3.3.1 Area of the constant energy plane	17
3.3.2 Average of the squared matrix elements	18
3.4 Scattering rate interpolation	21
3.5 Selection of final states	22
3.5.1 Selecting final cube	22
3.5.2 High precision selection of final states	25
4 Results	35
4.1 Scattering rates	35
4.2 Monte Carlo simulations	40
4.3 Electron Mobility in bulk $\text{Hg}_{0.72}\text{Cd}_{0.28}\text{Te}$	43

5	Conclusions	47
5.1	Future work	48
	Bibliography	48
	Appendix A: List of parameters	51
	Appendix B: Expressions for the coefficients	52

Chapter 1

Introduction

The electronic transport properties of semiconductors are determined by the solution of the Boltzmann transport equation (BTE) for the system. The Boltzmann transport equation is commonly solved using two very different approaches, either by explicitly solving the equation, or by performing Monte Carlo simulations. The first method relies on equation solving techniques, while the Monte Carlo method uses (computer generated) pseudo-random numbers to simulate the behaviour of individual charge carriers and thereby indirectly solving the transport equation. Monte Carlo simulations offers great level of details, but tends to be very CPU intensive and time consuming.

Such a Monte Carlo simulator is under development at FFI, and several students have and continue to contribute to its development. The ultimate goal is to make a state of the art Monte Carlo program to simulate transport of charge carriers in both bulk materials, as well as electronic and optoelectronic devices. The opportunity to accurately simulate charge carrier transport in various materials and devices without building the actual devices, will be an invaluable resource.

The semiconductor mercury cadmium telluride(MCT), with the chemical formula $\text{Hg}_{1-x}\text{Cd}_x\text{Te}$, will serve as a test material for the Monte Carlo program under development. MCT is an alloy of the semimetal HgTe and the semiconductor CdTe. The bandgap in MCT can be tuned by changing the alloy fraction x of CdTe, thereby having any value between 0 and 1.5eV. The tunable bandgap in the infrared region and high absorption coefficient, makes MCT well suited as detector material in infrared detectors. With the unique impact ionization properties can MCT also be used in Avalanche Photo Diodes (APDs). MCT is also the only common material able to detect infrared radiation in both accessible atmospheric windows.

The Monte Carlo program was recently upgraded from a less accurate analytical model to a Full Band model, where the bands are represented numerically over the whole Brillouin zone. Prior to this work, the Full Band Monte Carlo program was able to only simulate holes in the light- and heavy hole bands, and the method used to select final

states offered too low precision. The low precision in selection of final states was a serious problem which could potentially lead to artificial heating of the carriers. So a high precision method, to select final states with correct energy, was proposed in the specialization project [1]. The proposed method was found to be reliable and effective, and proper implementation of this method into the Full Band Monte Carlo program became an important task. The resulting implementation is a further developed approach (used in the specialization project [1]) with improved efficiency and a more convenient managing of final states within the final cubes.

Another important part of this work was to include electrons in the simulations. A task that includes calculation of electron scattering rates, modifying the routine that is used to select final states, and writing new routines that take care of electron scattering. The routine that is responsible for calculation of scattering rates has been generalized to include calculation of electron scattering rates in addition to holes. And the routine that selects final states has been modified to find final states for electrons in the conduction band.

Also great effort was devoted to include an *ab initio* energy band structure for $\text{Hg}_{0.72}\text{Cd}_{0.28}\text{Te}$, that was calculated using the electronic structure code ABINIT [2] by Bjørnar Karlsen [3].

Of the many existing charge transport Monte Carlo programs, only a handful share the capabilities of the Full Band Monte Carlo program presented in this work.

Chapter 2 of this work will give a theoretical introduction to how the Monte Carlo method is applied to simulate charge carrier transport in semiconductors. Chapter 3 will describe the most important numerical methods and algorithms that are used in the Full Band Monte Carlo program. Chapter 4 will show and discuss the results of the present work.

The Monte Carlo method

The Monte Carlo method is a very powerful numerical method used to describe stochastic processes. The method has found a large number of applications in science, including electronic transport. This chapter intends to give a theoretical introduction to how the Monte Carlo method is applied to semiclassical electronic transport in semiconductors.

The essence of the method is to simulate the charge carriers, in this case electrons and holes, through a series of free flights and scattering events. The charge carriers are treated semiclassically. During the free flights the carriers are treated as classical particles, while the scattering events are treated according to quantum mechanical laws.

Charge carriers in semiconductors can be described by Bloch states $|n, \vec{k}\rangle$, being in an energy band n with wavevector (crystal momentum) \vec{k} , thus having energy $E_n(\vec{k})$. The evolution of charge carriers position and wavevector during free flights is given by the semiclassical equations of motion

$$\vec{v} = \frac{d\vec{r}}{dt} = \frac{1}{\hbar} \nabla_{\vec{k}} E_n(\vec{k}), \tag{2.1}$$

$$\frac{d\vec{k}}{dt} = \frac{q}{\hbar} (\vec{F} + \vec{v} \times \vec{B}) \tag{2.2}$$

where \vec{v} is carriers velocity, q is the charge, \vec{F} is the electric field and \vec{B} is the magnetic field.

The scattering events are a consequence of semiconductors not being perfect crystals. Semiconductors contain various imperfections, such as lattice vibrations and ionized impurities. These imperfections are treated as perturbations to the perfect crystal potential, which may instantly change carriers Bloch state from $|n, \vec{k}\rangle$ to $|n', \vec{k}'\rangle$, in a so called scattering event. The scattering events are taken into account by the scattering rates, that are the probability (per unit time) for a scattering event to occur. The scattering rates tell how often scattering events should occur, and hence affect the length of the free flights.

Performing the free flights and scattering events are the two main tasks of a Monte Carlo program. Performing a free flight is just a matter of finding the change in carrier position and wavevector over a time step, using the semiclassical equations of motion. The scattering events are more complicated tasks. A scattering event can be divided into three parts: calculating the free flight duration, selecting the scattering mechanism, and selecting a final Bloch state for the carrier. Both the duration of the free flights and selection of the scattering mechanism will depend on the scattering rates, as will be shown later in this chapter. But first a section describing how the scattering rates are calculated.

2.1 Scattering rates

There are number of mechanisms that can cause a charge carrier to scatter between two Bloch states, and the importance of each mechanisms varies based on material and temperature. Following mechanisms are considered in the present work:

- Acoustic deformation potential phonon scattering (absorption and emission)
- Polar optical phonon scattering (absorption and emission)
- Nonpolar optical phonon scattering (absorption and emission)
- Ionized impurity scattering
- Alloy scattering

As already mentioned, scattering mechanisms may change carriers Bloch state from $|n, \vec{k}\rangle$ to a new state $|n', \vec{k}'\rangle$. The probability of this transition is given by Fermi's golden rule

$$P_{nn'}^m(\vec{k}, \vec{k}') = \frac{2\pi}{\hbar} \left| \langle \vec{k}', n' | \Delta H^m | n, \vec{k} \rangle \right|^2 \delta(E_n(\vec{k}) - E_{n'}(\vec{k}') + \Delta E^m(\vec{q})), \quad (2.3)$$

where the spin flip has been neglected. m is the mechanism causing the transition, ΔH^m is the perturbing potential, $\langle \vec{k}', n' | \Delta H^m | n, \vec{k} \rangle$ is the interaction matrix element. $E_n(\vec{k})$ and $E_{n'}(\vec{k}')$ are carrier's initial and final energies, and $\Delta E^m(\vec{q})$ is the energy transferred to the carrier during the scattering. \vec{q} is the shift in carriers wavevector caused by the scattering.

The squared matrix element is often factorized into two parts, an overlap factor denoted by $G_{nn'}(\vec{k}, \vec{k}')$ and a matrix element $|M^m(\vec{k}, \vec{k}')|^2$:

$$\left| \langle \vec{k}', n' | \Delta H^m | n, \vec{k} \rangle \right|^2 = |M^m(\vec{k}, \vec{k}')|^2 G_{nn'}(\vec{k}, \vec{k}') \quad (2.4)$$

The overlap factor is given by

$$G_{nn'}(\vec{k}, \vec{k}') = \left| \int_{unit\ cell} d^3r u_{n', \vec{k}'}^*(\vec{r}) u_{n, \vec{k}}(\vec{r}) \exp(i\vec{G} \cdot \vec{r}) \right|^2 \quad (2.5)$$

where $u_{n,\vec{k}}(\vec{r})$ is the cell periodic part of the Bloch wavefunction, \vec{G} is a reciprocal lattice vector.

The Fermi's golden rule includes conservation of both energy and crystal momentum. The Dirac's δ -function ensures the energy conservation, while the matrix element makes sure that the crystal momentum is conserved. The conservation of crystal momentum is given by

$$\vec{k} - \vec{k}' + \vec{q} = \vec{G}. \quad (2.6)$$

\vec{q} is the shift in carriers wavevector, and \vec{G} is a reciprocal lattice vector. Processes where $\vec{G} = 0$ are called normal processes, while $\vec{G} \neq 0$ are known as Umklapp processes, implying scattering into an another Brillouin zone. Umklapp processes are usually very weak compared to normal processes, and are therefore neglected in the present work.

The total scattering rate for a carrier in energy band n with wavevector \vec{k} , to the energy band n' caused by mechanism m is found by summing the transition probability 2.3 over all possible final wavevectors \vec{k}'

$$S_{nn'}^m(\vec{k}) = \sum_{\vec{k}'} P_{nn'}^m(\vec{k}, \vec{k}') = \frac{2\pi}{\hbar} \sum_{\vec{k}'} |M^m(\vec{k}, \vec{k}')|^2 G_{nn'}(\vec{k}, \vec{k}') \delta(E_n(\vec{k}) - E_{n'}(\vec{k}') + \Delta E^m(\vec{q})). \quad (2.7)$$

Since the final wavevector-space (\vec{k}' -space) is very dense, can the summation over final wavevectors be well approximated by an integral

$$S_{nn'}^m(\vec{k}) = \frac{2\pi}{\hbar} \cdot \frac{V}{(2\pi)^3} \int_{\vec{k}'} |M^m(\vec{k}, \vec{k}')|^2 G_{nn'}(\vec{k}, \vec{k}') \delta(E_n(\vec{k}) - E_{n'}(\vec{k}') + \Delta E^m(\vec{q})) d^3 k'. \quad (2.8)$$

where V is the crystal volume. The integrand in equation 2.8 can be interpreted as a density function of final states, and becomes very important in selection of final states.

The total scattering rate for a carrier in Bloch state $|n, \vec{k}\rangle$ is found by simply summing the equation 2.8 over all possible final bands n' and mechanisms m :

$$S_n(\vec{k}) = \sum_m \left[\sum_{n'} S_{nn'}^m(\vec{k}) \right] \quad (2.9)$$

2.2 Duration of the Free Flights

The scattering rates represents the probability (per unit time) for a carrier to get scattered, which implies that the durations of the free flights are random by nature. The purpose of this section is to describe how the duration of a free flight can be generated using a random number r , that is uniformly distributed between 0 and 1.

The probability density, $p(t)$, for the duration of the free flight is given by

$$p(t) = Q(t) \cdot S_n(\vec{k}(t)), \quad (2.10)$$

where $S_n(\vec{k}(t))$ is the total scattering rate for carrier in state $|n, \vec{k}\rangle$, and $Q(t)$ denotes the probability that the carrier has **not** been scattered in the interval $[0, t]$.

The probability $Q(t + dt)$ that a carrier does not get scattered in the interval $[0, t + dt]$ can be written

$$Q(t + dt) = Q(t) \cdot [1 - S(\vec{k}(t))dt], \quad (2.11)$$

and by letting $dt \rightarrow 0$, the following relation emerges

$$\frac{dQ(t)}{dt} = -S(\vec{k}(t)) \cdot Q(t). \quad (2.12)$$

The solution, $Q(t)$, to equation 2.12 becomes

$$Q(t) = \exp \left[- \int_0^t S_n(\vec{k}(t')) dt' \right]. \quad (2.13)$$

The probability density, $p(t)$, for the duration of the free flight is now given by

$$p(t) = S_n(\vec{k}(t)) \cdot \exp \left[- \int_0^t S_n(\vec{k}(t')) dt' \right]. \quad (2.14)$$

The probability density, $p_r(r)$, of the uniformly distributed random number r , may be related to the probability density for the duration of the free flights by

$$p_r(r) dr = p(t) dt. \quad (2.15)$$

Which, with $p_r(r) = 1$ and after integration, gives

$$r = \int_0^t p(t') dt'. \quad (2.16)$$

Substituting the equation 2.14 for $p(t)$, and the integration could of course be performed, but may be solved using a simpler approach. The integration of $p(t')$ from 0 to t is nothing more than the cumulative probability $P(t)$ for the duration of the free flight, which is the probability that a carrier **will** get scattered somewhere in the interval $[0, t]$. Using the definition of $Q(t)$, $P(t)$ is simply

$$\int_0^t p(t') dt' = P(t) = 1 - Q(t). \quad (2.17)$$

And the random number r is related to the free flight duration t by

$$r = 1 - Q(t) = 1 - \exp \left[- \int_0^t S_n(\vec{k}(t')) dt' \right]. \quad (2.18)$$

Since r is a random number between 0 and 1, it is equivalent to $1 - r$. Thus, replacing r by $1 - r$ in equation 2.18 and taking the natural logarithm of both sides, results in

$$-\ln r = \int_0^t S_n(\vec{k}(t')) dt'. \quad (2.19)$$

An elegant way to solve the equation 2.19 for t , is by introducing self-scattering, a fictitious scattering mechanism that does not alter the carriers state $|n, \vec{k}\rangle$. The self-scattering is described by an arbitrary positive scattering rate $S_0(\vec{k}(t))$, and the new total scattering rate $\Gamma(\vec{k}(t)) = S_n(\vec{k}(t)) + S_0(\vec{k}(t))$ replaces the $S_n(\vec{k}(t))$ in equation 2.19. The integral in 2.19 is converted to a sum over fixed time increments, t_{inc} , over which the Γ has a constant value. The value for Γ during each time interval, has to be equal or greater than the highest real scattering rate the carrier in question can encounter during the time interval. The integral over each time interval becomes a simple product of Γ and the length of the time interval.

The integrals over the time intervals accumulate after each time step, and the free flight ends at the particular time interval when the accumulated sum exceeds the value of $-\ln r$. The carrier's state $|n, \vec{k}\rangle$ changes according to the scattering mechanism, before a new value for $-\ln r$ is generated and a new free flight starts. This particular method of determining the duration of the free flights is the so called constant-time method given by Yorston [4].

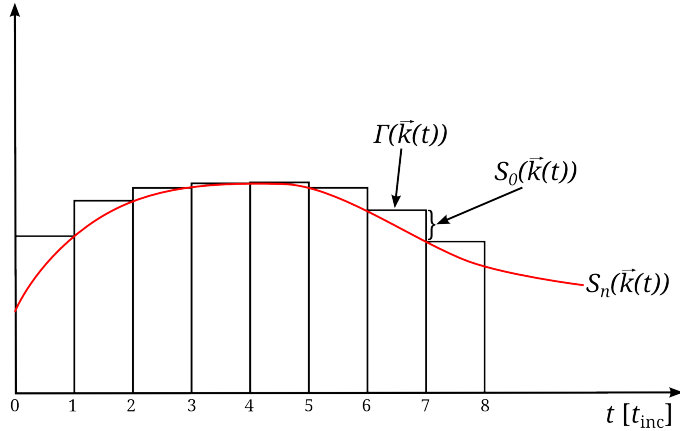


Figure 2.1: Illustrating the constant-time method by Yorston.

2.3 Monte Carlo selection of scattering mechanism

At the end of each free flight, the carriers get scattered by one of the scattering mechanisms. The probability for choosing a scattering mechanism has to be proportional to mechanism's scattering rate at the end of the free flight. The mechanism is chosen by generating a random number r , that is uniformly distributed between 0 and 1, multiplying

it with the total scattering rate $\Gamma(\vec{k}_e)$, and picking out the mechanism m that satisfies the relation

$$\sum_{i=0}^{m-1} S^i(\vec{k}_e) < r\Gamma(\vec{k}_e) < \sum_{i=0}^m S^i(\vec{k}_e) \quad (2.20)$$

where \vec{k}_e is the wavevector at the end of the free flight, and $S^i(\vec{k}_e)$ is the scattering rate for mechanism i at \vec{k}_e . The self-scattering mentioned in the previous section is given by the rate $S^0(\vec{k}_e)$, and is included in the total scattering rate $\Gamma(\vec{k}_e)$.

2.4 Selection of final states

After a scattering mechanism is chosen comes the last part of the scattering event, the assignment of a final state \vec{k}' to the scattered carrier. The final state \vec{k}' , has to be chosen so that both the energy and crystal momentum are conserved in the transition. Recall the calculation of scattering rates where the crystal momentum and the energy has to be conserved, so the only transitions that contribute to the scattering rates are the ones that conserve the energy and crystal momentum. Hence one of the final states that contribute to the scattering rate should be assigned to the carrier after scattering. The state to be assigned should be chosen at random, with a probability that is proportional to the state's contribution to the scattering rate.

However, how the selection of final states is performed in practice depends on the band model. For instance, when analytical band model is used, the selection of final states is a matter of selecting polar and azimuthal angles with given probabilities.

When a full band model is used, the selection of final states becomes more challenging. An algorithm that can be used to select final states is described in section 3.5 in the next chapter.

Numerical approach

The implementation of a properly working full band model has been the main focus of the present work. This chapter will describe and discuss the most important numerical models and algorithms that have been implemented in the Full Band Monte Carlo program.

The basis of the full band model, is that all of the information concerning the band structure is only given at discrete points in \vec{k} -space. This information includes the energy $E_n(\vec{k})$, \vec{k} -space energy gradient and 2nd derivatives, and for some purposes also the wavefunction. The energy and energy gradient are very important quantities in Monte Carlo simulations, since they are used in the semiclassical equations of motion to determine the carriers' free flight trajectories. These quantities have to be known at any \vec{k} , so the values has to be approximated when \vec{k} is somewhere between the discrete points.

The first sections of this chapter intend to describe the layout of the discrete points in \vec{k} -space where the band structure is given, and describe the interpolation schemes that are used to approximate the quantities of interest between the discrete points. And finally the algorithms that are used to calculate the scattering rates and select final states, are described and discussed.

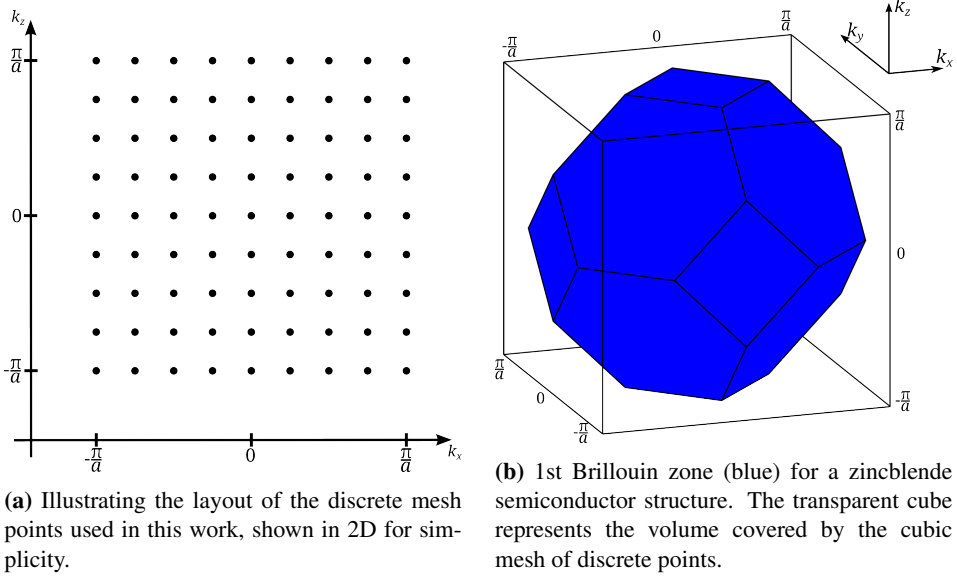
3.1 Numerical band representation

As mentioned, is all of the information about the band structure given at discrete points in \vec{k} -space. These discrete points are evenly spaced in the 3 dimensions of the \vec{k} -space, forming a cubic mesh. The cubic mesh has a total length of $\frac{2\pi}{a}$ (in each dimension), where a is semiconductor's lattice constant, thereby completely covering the whole 1st Brillouin zone as shown in figure 3.1b.

In addition to the coarse mesh that covers the whole 1st Brillouin zone, a fine mesh is present in the center of the Brillouin zone. The fine mesh only covers a small fraction of the zone center, to offer a much more detailed description of the region. This is done because the band structure and specially the scattering rates can change very abruptly near

$\vec{k} = 0$, and a higher resolution of this region is therefore required.

The size of both coarse and fine mesh was set to 33x33x33 in the present work.



It is important to notice that the mesh used in this work is somewhat different from the mesh used by Einar Halvorsen [5]. The difference is not only in the mesh size, but also in the layout. The main difference is that the mesh used in this work contains the origin as one of the mesh points, while Halvorsen's mesh does *not*, as shown in figure 3.1.

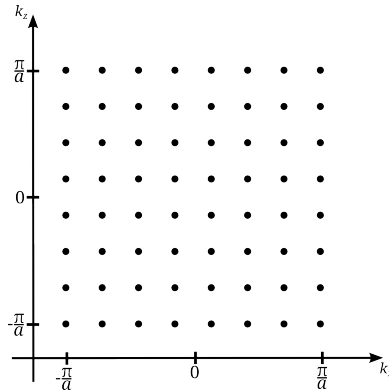


Figure 3.1: Layout of the mesh used by Einar Halvorsen [5]. Notice: the origin is *not* one of the meshpoints.

Halvorsen's mesh was only used to calculate the scattering rates, that did not require any

interpolation between the mesh points, and to avoid various calculation difficulties the origin could not be part of the mesh. Thanks to the interpolation routines, these calculation difficulties are avoided in this work, which allows a more convenient layout of the mesh to be used.

3.1.1 Energy band structure

One of the main changes that has been made to the Monte Carlo program, is introduction of a new energy band structure for $\text{Hg}_{0.72}\text{Cd}_{0.28}\text{Te}$. The energy band structure was calculated using an *ab initio* pseudopotential method, by the electronic structure program ABINIT [2]. Bjørnar Karlsen performed the band structure calculations on a $40 \times 40 \times 40$ cubic mesh during the work with his master's thesis, and all of the details about the calculations are well described in his master's thesis [3]. The band structure for the $33 \times 33 \times 33$ cubic mesh used in the present work, was *interpolated* from Karlsen's original $40 \times 40 \times 40$ cubic mesh, using the interpolation scheme described in the next section.

The energy band structure for the 3 highest valence and 4 lowest conduction bands in $\text{Hg}_{0.72}\text{Cd}_{0.28}\text{Te}$, is shown in figure 3.2.

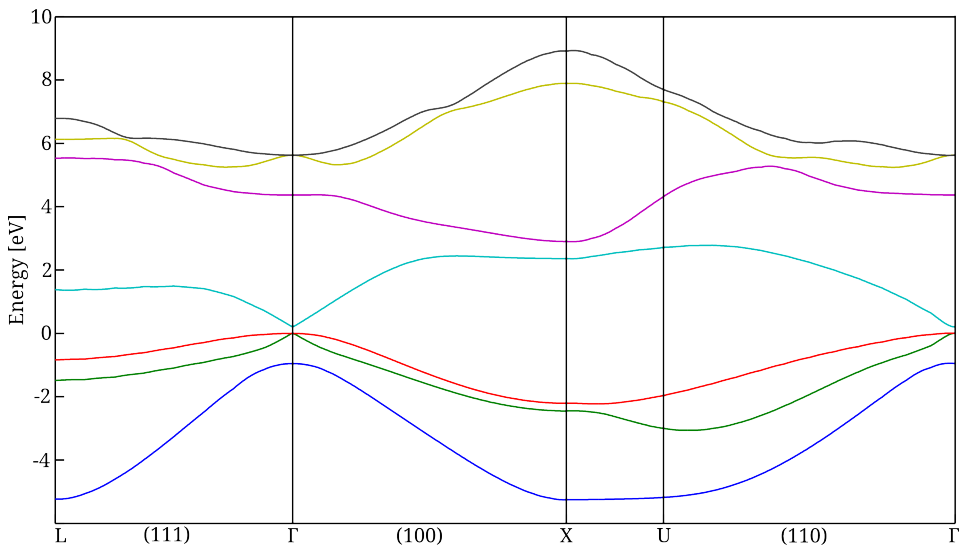


Figure 3.2: Band structure plots for the 3 highest valence and the lowest 4 conduction bands in $\text{Hg}_{0.72}\text{Cd}_{0.28}\text{Te}$.

All of the energy values in figure 3.2 were interpolated using the interpolation scheme described in the next section.

Other programs, such as WIEN2k [6], could also be used to calculate *ab initio* band structures to be used as input data for the Monte Carlo program. Even for alloy compounds such as $\text{Hg}_{1-x}\text{Cd}_x\text{Te}$.

3.2 Energy interpolation

Since the energy is only given at discrete mesh points, interpolation is used to approximate the energy at arbitrary \vec{k} . The interpolation scheme used is identical to the one used by Fischetti and Laux [7].

The interpolation scheme requires a three-dimensional cubic mesh where the energy, first and second derivatives of the energy are known at all mesh points. The first step of the interpolation routine is to find the eight mesh points that form a cube that surrounds the \vec{k} , as shown in figure 3.3.

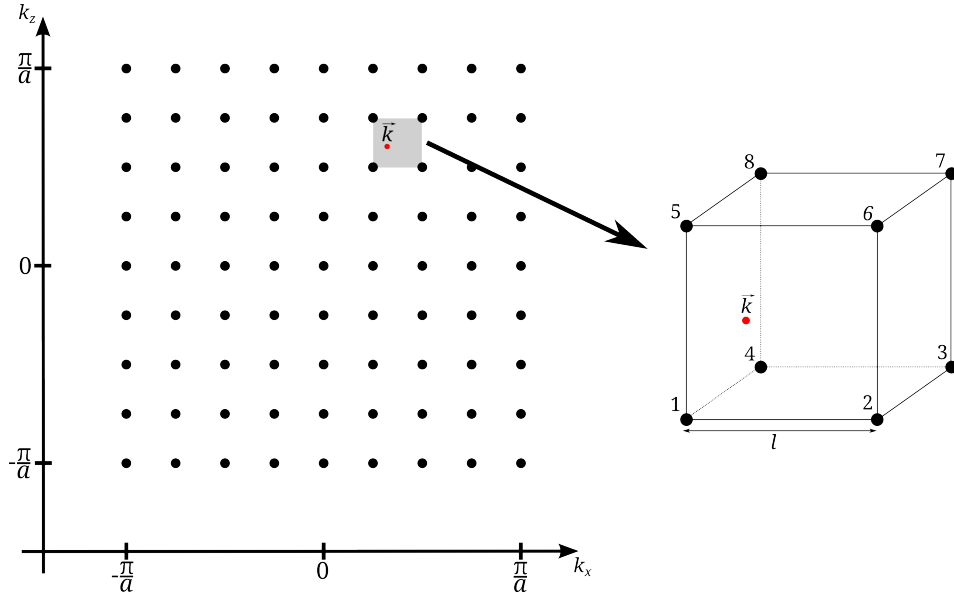


Figure 3.3: Showing the cube formed by the eight mesh points that surrounds the arbitrary \vec{k} (red dot), with the \vec{k} inside the cube.

After finding the eight corners (mesh points), the energy is expanded to second order around each of the corners:

$$E_{n,\lambda}(\vec{k}) = E_n(\vec{k}_\lambda) + \frac{\partial E_n}{\partial k_i} \Big|_{\vec{k}_\lambda} \cdot (k_i - k_{i,\lambda}) + \frac{1}{2} \frac{\partial^2 E_n}{\partial k_i \partial k_j} \Big|_{\vec{k}_\lambda} \cdot (k_i - k_{i,\lambda})(k_j - k_{j,\lambda}) \quad (3.1)$$

where summation must be made over identical indices (i, j). n is the energy band, λ is the corners (1-8), and $\vec{k} = [k_x, k_y, k_z]$.

Energy contribution from each corner have to be multiplied with appropriate weight,

$$W_\lambda(\vec{k}) = \left(1 - \frac{|k_x - k_{x,\lambda}|}{l}\right) \left(1 - \frac{|k_y - k_{y,\lambda}|}{l}\right) \left(1 - \frac{|k_z - k_{z,\lambda}|}{l}\right), \quad (3.2)$$

where l is side length of the cube spanned by the eight corners, as shown in Figure 3.3. Finally the contributions from all corners are added up, giving the interpolated energy

$$\begin{aligned}
E_n(\vec{k}) &= \sum_{\lambda=1}^8 E_{n,\lambda}(\vec{k}) \cdot W_\lambda(\vec{k}) \\
&= \sum_{\lambda=1}^8 \left(E_n(\vec{k}_\lambda) + \frac{\partial E_n}{\partial k_x} \Big|_{\vec{k}_\lambda} \cdot (k_x - k_{x,\lambda}) + \frac{\partial E_n}{\partial k_y} \Big|_{\vec{k}_\lambda} \cdot (k_y - k_{y,\lambda}) + \frac{\partial E_n}{\partial k_z} \Big|_{\vec{k}_\lambda} \right. \\
(3.3) \quad &\quad \cdot (k_z - k_{z,\lambda}) + \frac{\partial^2 E_n}{\partial k_x \partial k_y} \Big|_{\vec{k}_\lambda} \cdot (k_x - k_{x,\lambda})(k_y - k_{y,\lambda}) + \frac{\partial^2 E_n}{\partial k_y \partial k_z} \Big|_{\vec{k}_\lambda} \\
&\quad \cdot (k_y - k_{y,\lambda})(k_z - k_{z,\lambda}) + \frac{\partial^2 E_n}{\partial k_z \partial k_x} \Big|_{\vec{k}_\lambda} \cdot (k_z - k_{z,\lambda})(k_x - k_{x,\lambda}) + \frac{1}{2} \frac{\partial^2 E_n}{\partial k_x^2} \Big|_{\vec{k}_\lambda} \\
&\quad \cdot (k_x - k_{x,\lambda})^2 + \frac{1}{2} \frac{\partial^2 E_n}{\partial k_y^2} \Big|_{\vec{k}_\lambda} \cdot (k_y - k_{y,\lambda})^2 + \frac{1}{2} \frac{\partial^2 E_n}{\partial k_z^2} \Big|_{\vec{k}_\lambda} \cdot (k_z - k_{z,\lambda})^2 \Big) \\
&\quad \cdot \left(1 - \frac{|k_x - k_{x,\lambda}|}{l} \right) \left(1 - \frac{|k_y - k_{y,\lambda}|}{l} \right) \left(1 - \frac{|k_z - k_{z,\lambda}|}{l} \right).
\end{aligned}$$

This interpolation scheme is found to be very accurate, and ensures continuous and smooth energy.

3.2.1 Gradient interpolation

\vec{k} -space energy gradient is another very important quantity that is needed to perform simulations, and must therefore be interpolated. The interpolation scheme for the gradient is very similar to the one used for energy.

After finding the eight mesh points that surround the (arbitrary) \vec{k} , the gradient is expanded to first order around each corner:

$$\frac{\partial E_{n,\lambda}}{\partial k_i}(\vec{k}) = \frac{\partial E_n}{\partial k_i} \Big|_{\vec{k}_\lambda} + \frac{\partial^2 E_n}{\partial k_i \partial k_j} \Big|_{\vec{k}_\lambda} \cdot (k_j - k_{j,\lambda}) \quad (3.4)$$

where the summation is performed over j , giving i 'th component of the gradient. n is the energy band, λ is the corner (1-8), and $\vec{k} = [k_x, k_y, k_z]$.

The contribution from each corner is multiplied with appropriate weight given by equation 3.2, and finally added up giving the i 'th component of the gradient

$$\frac{\partial E_n}{\partial k_i}(\vec{k}) = \sum_{\lambda=1}^8 \frac{\partial E_{n,\lambda}}{\partial k_i}(\vec{k}) \cdot W_\lambda(\vec{k}). \quad (3.5)$$

Figure 3.4 shows a plot of the k_x -component of the energy gradient along two different lines in \vec{k} -space. All of the values in the plot are interpolated, and the gradient is clearly continuous and smooth.

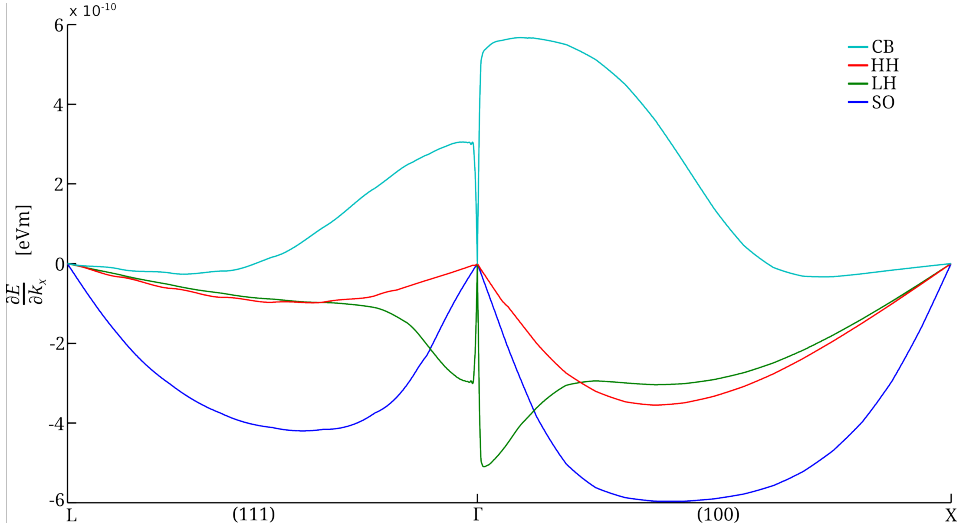


Figure 3.4: Plot of the k_x -component of the energy gradient for the 3 highest valence bands and the lowest conduction band in $\text{Hg}_{0.72}\text{Cd}_{0.28}\text{Te}$.

One thing should be noted about figure 3.4. There is a small sign of tiny ripples along the (111)-direction in HH and CB bands. The ripples are believed to be an artefact of the numerical derivatives, that are known to be notorious sources of noise. However, these defects are minimal, and should not affect the simulations in ANY way.

3.3 Numerical calculation of the scattering rates

The scattering rate for a particle in state $|n, \vec{k}\rangle$ to final band n' is given by equation 2.8, where the transitional probability (2.3) is integrated over the whole \vec{k}' -space. If \vec{k}' -space is divided up into cubes, can the integration over the whole \vec{k}' -space in 2.8 be replaced by a sum of integrals over each cube.

$$S_{nn'}^m(\vec{k}) = \sum_i^{\text{all cubes}} \frac{2\pi}{\hbar} \frac{V}{(2\pi)^3} \int_{\vec{k}' \in \text{cube } i} |M^m(\vec{k}, \vec{k}')|^2 G_{nn'}(\vec{k}, \vec{k}') \delta(E_n(\vec{k}) - E_{n'}(\vec{k}') + \Delta E^m(\vec{q})) d^3 k', \quad (3.6)$$

where i denotes a cube.

The integral over the whole \vec{k}' -space, has simply been replaced by a sum of many integrals, each over a small portion of \vec{k}' -space (cube). Now, if the integral over a cube i is denoted by a weight \mathbb{W}_i , the scattering rate becomes a sum of the weights:

$$S_{nn'}^m(\vec{k}) = \sum_i^{\text{all cubes}} \mathbb{W}_i, \quad (3.7)$$

where each weight is given by

$$\mathbb{W}_i = \frac{2\pi}{\hbar} \frac{V}{(2\pi)^3} \int_{\vec{k}' \in \text{cube } i} |M^m(\vec{k}, \vec{k}')|^2 G_{nn'}(\vec{k}, \vec{k}') \delta(E_n(\vec{k}) - E_{n'}(\vec{k}') + \Delta E^m(\vec{q})) d^3 k'. \quad (3.8)$$

And the scattering rate calculation has been reduced to calculation of the cube weights.

A consequence of the energy conservation, is that all of the final states that contribute to the scattering rate lie on the so called energy conserving surface. That is a surface in \vec{k}' -space where the energy conserving δ -function is $\neq 0$. Which implies that the only cubes that will have a non-zero weight \mathbb{W} , are those that are intersected by the energy conserving surface. The energy along the energy conserving surface varies in general with $\Delta E^m(\vec{q})$. However, $\Delta E^m(\vec{q})$ is either a constant or changes very slowly, for all of the mechanisms considered in this work. So the energy *along* the energy conserving surface can be considered to be constant inside each of the intersected cubes. Of course, this also requires the cubes to be sufficiently small.

The final state energy inside each cube can be well approximated by a first order Taylor expansion away from the cube center. The energy inside a cube i is then given by

$$E_{n'}(\vec{k}') = E_{n'}(\vec{k}_i) + (\vec{k}' - \vec{k}_i) \cdot \nabla_{\vec{k}} E_{n'}(\vec{k}_i), \quad (3.9)$$

where \vec{k}_i denotes the center of cube i , and \vec{k}' is somewhere inside the cube i . This implies that the energy conserving surface inside an intersected cube, is approximated by a constant energy plane, normal to the energy gradient at the center of the cube. This idea was taken from Gilat and Raubenheimer [8], who used it to calculate the density of states for phonons.

Any final state \vec{k}' that lies on the constant energy plane inside a cube i , can be described by a sum of three wavevectors

$$\vec{k}' = \vec{k}_i + \vec{k}_{\parallel} + \vec{k}_{\perp}. \quad (3.10)$$

\vec{k}_i denotes the center of cube i . \vec{k}_{\parallel} is a vector from the cube center to the constant energy plane, along the energy gradient. And \vec{k}_{\perp} is a vector along the constant energy plane, thereby normal to the energy gradient. As shown in figure 3.5.

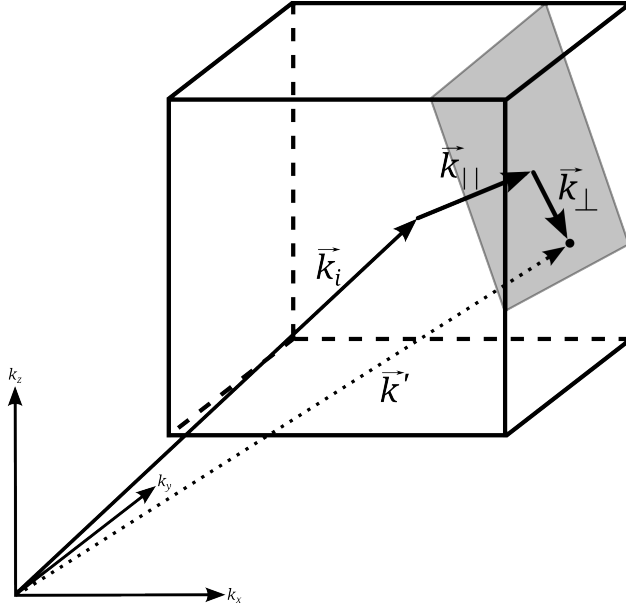


Figure 3.5: Showing the decomposition \vec{k}' . \vec{k}' lies on the constant energy plane (marked gray).

The approximations mentioned above, makes it possible to rewrite the expression for the cube weight \mathbb{W}_i . Equation 3.8 becomes

$$\begin{aligned}
 \mathbb{W}_i &= \frac{2\pi}{\hbar} \frac{V}{(2\pi)^3} \int_{\vec{k}' \in \text{cube } i} |M^m(\vec{k}, \vec{k}')|^2 G_{nn'}(\vec{k}, \vec{k}') \delta(E_n(\vec{k}) - E_{n'}(\vec{k}') + \Delta E^m(\vec{q})) d^3 k' \\
 &\approx \frac{2\pi}{\hbar} \frac{V}{(2\pi)^3} \int \delta \left(E_{n'}(\vec{k}_i) + k_{\parallel} |\nabla_{\vec{k}} E_{n'}(\vec{k}_i)| - E_n(\vec{k}) - \Delta E^m(\vec{k}_i - \vec{k}) \right) dk_{\parallel} \\
 &\times \int_{S(k_{\parallel})} |M^m(\vec{k}, \vec{k}')|^2 G_{nn'}(\vec{k}, \vec{k}') d^2 k_{\perp}. \tag{3.11}
 \end{aligned}$$

$S(k_{\parallel})$ represents the cross-section of the constant energy plane confined by the cube. The integral of the δ -function is found by using the generalized scaling property of the Dirac's δ -function

$$\int \delta \left(E_{n'}(\vec{k}_i) + k_{\parallel} |\nabla_{\vec{k}} E_{n'}(\vec{k}_i)| - E_n(\vec{k}) - \Delta E^m(\vec{k}_i - \vec{k}) \right) dk_{\parallel} = \frac{1}{|\nabla_{\vec{k}} E_{n'}(\vec{k}_i)|}. \tag{3.12}$$

The last term in equation 3.11, containing the integral of the squared matrix element over the surface $S(k_{\parallel})$, can be replaced using

$$\left\langle |M^m(\vec{k}, \vec{k}')|^2 G_{nn'}(\vec{k}, \vec{k}') \right\rangle_{S(k_{\parallel})} = \frac{1}{S(k_{\parallel})} \int_{S(k_{\parallel})} |M^m(\vec{k}, \vec{k}')|^2 G_{nn'}(\vec{k}, \vec{k}') d^2 k_{\perp}, \tag{3.13}$$

which is the definition of the average value of the squared matrix element over the surface $S(k_{\parallel})$.

Inserting equation 3.12 and 3.13 into 3.11, gives the final expression for the cube weights

$$\mathbb{W}_i \approx \frac{2\pi}{\hbar} \frac{V}{(2\pi)^3} \frac{S(k_{\parallel})}{|\nabla_{\vec{k}} E_{n'}(\vec{k}_i)|} \left\langle |M^m(\vec{k}, \vec{k}')|^2 G_{nn'}(\vec{k}, \vec{k}') \right\rangle_{S(k_{\parallel})}. \quad (3.14)$$

In order to evaluate 3.14 for a chosen cube, one has to find the area of the constant energy plane $S(k_{\parallel})$ confined by the cube, the averaged value of the squared matrix element, and the energy gradient at the center of the cube.

3.3.1 Area of the constant energy plane

The area of the constant energy plane, confined by a cube i , is calculated using a method given by Gilat and Raubenheimer [8]. First of all, each cube has a side length $2b$, and the absolute distance to the constant energy plane from the cube center along the gradient, w , is given by

$$w = |k_{\parallel}| = \left| \frac{E_n(\vec{k}) + \Delta E^m(\vec{k}_i - \vec{k}) - E_{n'}(\vec{k}_i)}{|\nabla_{\vec{k}} E_{n'}(\vec{k}_i)|} \right| \quad (3.15)$$

where \vec{k}_i denotes the cube center, \vec{k} is the initial wavevector, n and n' are initial and final bands respectively.

The unit normal vector to the constant energy plane, $\vec{n} = [l_1, l_2, l_3]$, is derived from the energy gradient at the center of the cube. \vec{n} is transformed so that all of the components are positive, and satisfy

$$l_1 \geq l_2 \geq l_3 \geq 0. \quad (3.16)$$

Because of the cube symmetry, this transformation does not affect the cross-section area. The shape of the cross-section, and thereby the formula used to calculate the area, depends on how many corners are "cut" away by the plane. The distances between a plane, given by \vec{n} and intersecting the center of the cube, and the 4 corners that may possibly be "cut" away, are used to determine the shape and area of the cross-section. The distances are given by:

$$w_1 = b|l_1 - l_2 - l_3| \quad (3.17)$$

$$w_2 = b(l_1 - l_2 + l_3) \quad (3.18)$$

$$w_3 = b(l_1 + l_2 - l_3) \quad (3.19)$$

$$w_4 = b(l_1 + l_2 + l_3) \quad (3.20)$$

And the formulas for the cross-section areas $S(k_{\parallel})$, for all possible combinations of w and $w_{1,2,3,4}$, are:

$$S(k_{\parallel}) = \frac{4b^2}{l_1}, \text{ when } 0 < w < w_1 \text{ and } l_1 \geq l_2 + l_3 \quad (3.21)$$

$$S(k_{\parallel}) = \frac{2b^2(l_1l_2 + l_1l_3 + l_2l_3) - (w^2 + b^2)}{l_1l_2l_3}, \text{ when } 0 < w < w_1 \text{ and } l_1 < l_2 + l_3 \quad (3.22)$$

$$S(k_{\parallel}) = \frac{b^2(3l_2l_3 + l_1l_2 + l_1l_3) + wb(l_1 - l_2 - l_3) - (w^2 + b^2)/2}{l_1l_2l_3}, \text{ when } w_1 < w < w_2 \quad (3.23)$$

$$S(k_{\parallel}) = \frac{2b^2(l_1 + l_1) - 2wb}{l_1l_2}, \text{ when } w_2 < w < w_3 \quad (3.24)$$

$$S(k_{\parallel}) = \frac{[b(l_1 + l_2 + l_3) - w]^2}{2l_1l_2l_3}, \text{ when } w_3 < w < w_4 \quad (3.25)$$

The equations 3.21-3.25 are based on formulas for the area of the following shapes: parallelogram, hexagon, pentagon, trapezoid and triangle respectively. All of the formulas are taken from Gilat and Raubenheimer [8], except for equation 3.23, which contained a typographical error in [8]. The error that was corrected by Einar Halvorsen [5].

3.3.2 Average of the squared matrix elements

The average squared matrix element, is another quantity needed to calculate the scattering rates. Formulas for the squared matrix elements, for all scattering mechanisms except the alloy scattering, are taken from Brudevoll et al. [9]. While the matrix element for alloy scattering is given by Ridley [10]. The squared matrix elements are all given as functions of $q = |\vec{k}' - \vec{k}|$, and does not include overlap factors. The scattering mechanisms considered in this work are, as mentioned in section 2.1:

- Acoustic deformation potential phonon scattering (absorption and emission)
- Polar optical phonon scattering (absorption and emission)
- Nonpolar optical phonon scattering (absorption and emission)
- Ionized impurity scattering
- Alloy scattering

The squared matrix element for all phonon scattering mechanisms is also proportional to the number of existing phonons, $N(q)$, given by Bose-Einstein statistics

$$N(q) = \frac{1}{\exp\left(\frac{E(q)}{k_B T}\right) - 1} \quad (3.26)$$

where q is the phonon's wavevector and $E(q)$ is the energy of the absorbed or emitted phonon, k_B is Boltzmann's constant and T is the temperature. All the optical phonons are

assumed to have same frequency ω_0 , and therefore energy $E(q) = \hbar\omega_0$, that is independent of q . The acoustic phonon energy is approximated by

$$E(q) = \hbar v_s q, \quad (3.27)$$

where v_s is the average sound velocity. Alloy and ionized impurity scatterings are elastic, which means that the carriers have the same energy after scattering as before.

To calculate the average squared matrix element inside a cube, Fischetti and Laux assumed that the squared matrix element varies slowly over a cube, and used the squared matrix element at the center of the cube as the averaged value. This approximation is good for most mechanisms, but could lead to some trouble when dealing with polar optical phonon and ionized impurity scattering. The formula for the squared matrix element, for both polar optical phonon and ionized impurity scatterings, has q in the denominator, which leads to very rapid changes of the squared matrix element for small q . This is typically the case when the initial \vec{k} is in the same cube as the final state \vec{k}' . The polar optical phonon scattering is saved by the high energy transfer, which makes it unlikely to find any final states very close to the initial state. Ionized impurity scattering is elastic, so final states could be found very close to the initial state. But the screening factor β in the denominator of the squared matrix element, saves the scattering rate from being calculated to infinity.

Using a point on the constant energy plane, $\vec{k}_i + \vec{k}_{\parallel}$, instead of just the cube center \vec{k}_i , to calculate q and then the squared matrix element, will first of all give more accurate scattering rate calculations. Because the squared matrix element must be averaged on the constant energy plane, and a point value on this plane must be a better approximation than point value in the center of the cube. This method will in addition further reduce the chance of getting $q = 0$ for polar optical scattering. Which is why this method is used in scattering rate calculations for the Monte Carlo simulations.

The overlap factor is a part of the squared matrix element, and is calculated using the $\vec{k} \cdot \hat{p}$ eigenfunctions. The eigenfunctions are only given at the discrete mesh points, so the eigenfunctions from the nearest mesh points are used to calculate the overlap factor between the initial and final state. The overlap factor using the $\vec{k} \cdot \hat{p}$ -eigenfunctions is then given by

$$G_{nn'}(\vec{k}, \vec{k}') = \frac{1}{2} \sum_{\mu=1}^2 \sum_{\mu'=1}^2 |\mathcal{F}_{n'\mu'\vec{k}'}^\dagger \mathcal{F}_{n\mu\vec{k}}|^2 \quad (3.28)$$

Where $\mathcal{F}_{n\mu\vec{k}}$ is the $\vec{k} \cdot \hat{p}$ -eigenfunction describing the state $|n, \vec{k}\rangle$ with spin μ . But at the present stage, the carriers are only described by the energy band n and crystal momentum \vec{k} (and not the spin), so the overlap factor is therefore averaged over the two spin eigenfunctions.

So far, the only thing that has been said about the division of the Brillouin zone, is that it has to be divided up into small cubes, in order to use the mentioned method to calculate scattering rates. Einar Halvorsen [5] implemented this method in the original program that has served as a basis for the scattering rate calculations. The program was recently revised by Bjørnar Karlsen [3] who included the alloy scattering, before Tore Bergslid[11]

included it in the Monte Carlo program.

Until now, the program has relied on a division of the Brillouin zone into cubes that was formed around the mesh points, where the band structure was known. The mesh points were at the center of the cubes, simply because the method requires the knowledge of the energy and energy gradient only at the center of the cubes.

During the present work, the program that calculates scattering rates has been modified, and no longer relies on the cubes to form around the mesh points. The energy and energy gradient can be given at any point in \vec{k} -space, thanks to the interpolation schemes in section 3.2. The layout and the size of the cubes can now be changed, without changing the underlying cubic mesh of discrete points, where the band structure is known. One of the weaknesses to the modified program is that the wavefunctions are only given at the mesh points, and the overlap factors are therefore calculated using the wavefunctions from the nearest mesh points. This should not be a big problem if the underlying mesh of discrete points is not too coarse.

In the present work, the underlying $33 \times 33 \times 33$ mesh of discrete points, was used as a basis for the division of the \vec{k} -space. The \vec{k} -space was divided up into $32 \times 32 \times 32$ cubes, where the mesh points coincide with the corners of the cubes. As illustrated in figure 3.6.

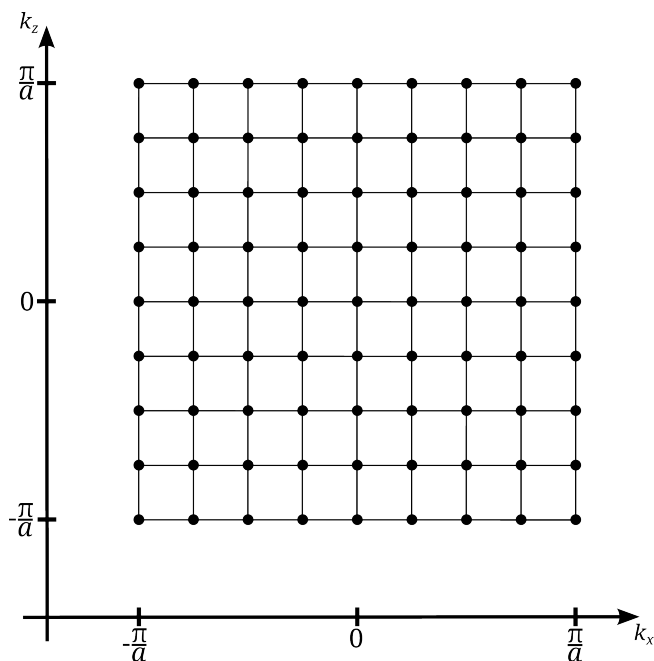


Figure 3.6: Illustrating how the \vec{k} -space is divided up into cubes, for scattering rate calculations. The mesh points are shown with black dots.

The program flow for the scattering rate calculations is rather simple. Given an initial band n , initial state \vec{k} , and the initial energy $E_n(\vec{k})$, the scattering rate to band n' caused

by mechanism m is calculated as follows:

- Select a cube i , and use the center of the cube, \vec{k}_i , to estimate the energy transition, and thereby the final energy E_f^i .
- Check if the final energy E_f^i is between the maximum and minimum energy found in the cube i in band n' .
- If the check in the previous point fails, the weight for the cube i is zero, $\mathbb{W}_i = 0$.
- Otherwise, the cube i contains the final energy. Then:
 - Interpolate the energy and gradient at the center of the cube, and use the values at the center to find the vector to the constant energy plane, \vec{k}_{\parallel} .
 - Calculate the cross-section area $S(k_{\parallel})$.
 - Calculate the squared matrix element using $q = |\vec{k}_i + \vec{k}_{\parallel} - \vec{k}|$, and the overlap factor using the nearest mesh point wavefunctions.
 - Finally, calculate the weight \mathbb{W}_i using equation 3.14.
- Continue to the next cube until the weights for all cubes are calculated. At the end, sum up the weights from all cubes to get the scattering rate.

3.4 Scattering rate interpolation

The numerical calculation of scattering rates is quite CPU intensive and time consuming. Therefore, calculating the scattering rates during a simulation would make the Full Band Monte Carlo program inconveniently slow. The scattering rates are therefore pre-calculated and stored at the same cubic mesh as the band structure, and interpolated during simulations. The interpolation routine is similar to the energy and gradient interpolation routines, but avoids the \vec{k} -space derivatives of the scattering rates. After finding the eight mesh points that surround the arbitrary \vec{k} , the scattering rate from each of the mesh points is multiplied by appropriate weights (3.2), and finally summed up.

$$S_{nn'}^m(\vec{k}) \approx \sum_{\lambda=1}^8 S_{nn'}^m(\vec{k}_{\lambda}) \cdot W_{\lambda}(\vec{k}). \quad (3.29)$$

The interpolation routine also includes some checks, before returning the interpolated value. When dealing with optical phonon emission (both polar and nonpolar), the routine explicitly checks if the carrier energy is actually high enough to emit an optical phonon. These checks must be seen in the context of explicitly calculated compared to interpolated scattering rates.

Suppose a carrier with energy just below the optical phonon energy. When the scattering rate for optical intraband emission is calculated explicitly, the final energy will not be found inside any of the cubes, and the scattering rate becomes zero. However, if the carrier's \vec{k} is changed slightly, so the carrier's energy becomes just above the optical phonon

energy, the same scattering rate becomes $\neq 0$. However, if the scattering rate is interpolated, the two scenarios will result in almost the same rate that is $\neq 0$. This may cause trouble when searching after final states. If an "illegal" scattering is chosen, no final states will be found. And the checks are meant to avoid such situations, by making sure that if a returned rate is $\neq 0$, then the final energy is within the energy range of the final band.

3.5 Selection of final states

When a carrier reaches the end of a flight, it gets instantly scattered from its initial state \vec{k} to a final state \vec{k}' . This section will focus on how this final state is selected in the Full Band Monte Carlo program.

The selection of final states is done in two parts. First a selection of a cube where the final state is to be found. Then a selection of the final state \vec{k}' , that represents the desired final energy, within the selected cube.

3.5.1 Selecting final cube

The cube to be selected is one of the cubes used in scattering rate calculations. When the scattering rates are calculated, the cubes are assigned different weights. These weights represent how much the final states inside each cube contribute to the scattering rate. The probability to pick out a cube should therefore be proportional to the cube's contribution to the scattering rate, ie the cube's weight.

The selection of a final cube could be done using the same method that is applied to selection of scattering mechanism. But the method would require all of the cube weights to be calculated. Which could of course be done, but calculating, typically, several thousand cube weights does not seem to be very efficient during simulations.

Fischetti and Laux used a rejection technique to choose the final cube, which does not require all of the cube weights. This rejection method is also currently implemented in the Full Band Monte Carlo program. The method goes as follows (for a given initial state \vec{k} , initial band n , mechanism m and final band n'):

- A search is performed over all cubes, where all the cubes that contain the desired final energy are stored in a list. The list contains all the possible final cubes. During the search, only the final energy is calculated for each cube, and compared to the energy spanned by the cube.
- Then, two random numbers are generated, r_1 and r_2 , which are uniformly distributed between 0 and 1. r_1 is used to suggest one of the possible final cubes, say cube i . The weight, \mathbb{W}_i , for the suggested cube is then calculated.
- Weight \mathbb{W}_i is compared to $r_2 \cdot \mathbb{W}_{MAX}$, where \mathbb{W}_{MAX} is the maximum of the possible cube weights. If $\mathbb{W}_i \geq r_2 \cdot \mathbb{W}_{MAX}$, the suggested cube i is chosen as the final cube.
- Else, if $\mathbb{W}_i < r_2 \cdot \mathbb{W}_{MAX}$, the cube is rejected. And the whole procedure, starting with generation of two random numbers, is repeated until a randomly suggested cube is chosen as the final cube.

This rejection method selects the final cube with the proper probability, as long as the the value \mathbb{W}_{MAX} is higher than any of cube weights. However, choosing \mathbb{W}_{MAX} too high, may result in an extremely high rejection rate, thereby reducing the efficiency of the method. It is important to notice, that \mathbb{W}_{MAX} has to be chosen without actually calculating the cube weights. Choosing a suitable value for \mathbb{W}_{MAX} is outside the scope of this work, but some thoughts have been made on the topic:

- The cube weights are given by the equation 3.14. So one could in principle use the maximum *observed* value for each of the factors in equation 3.14, to estimate the maximum possible cube weight. But, as a simple test showed, the product of the maximum of each factor lead to a very high value, even higher than the scattering rate. In which case even the scattering rate will be a better value for \mathbb{W}_{MAX} than the product of the maximum factors, because none of the cube weights will exceed the scattering rate for obvious reasons.
- A different approach, to find a value for \mathbb{W}_{MAX} , could involve the power of observations. The idea is to observe the calculated cube weights, and save the maximum values. These observations should be done separately, for example during scattering rate calculations, where all cube weights are being calculated anyway.

Another weakness to the rejection method, is the fact that the cube weights can vary a lot for some scattering mechanisms. This is typically the case for the ionized impurity scattering and sometimes also for the polar optical phonon scattering, where the matrix element varies rapidly between the final cubes. A few of the cube weights could be orders of magnitude higher than the rest, which will result in very high rejection rate. Figure 3.7 shows a typical plot of the cube weights in case of ionized impurity scattering, illustrating the problem.

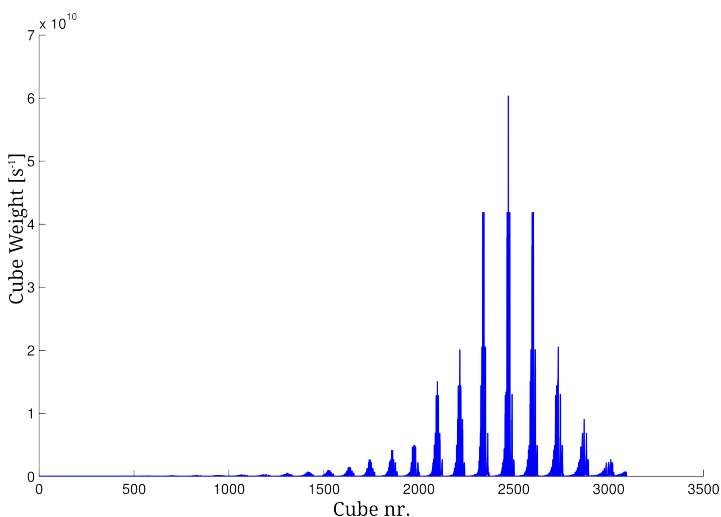


Figure 3.7: Plot of the final cube weights for electron, with energy 0.43 eV along (111)-direction, scattered by ionized impurity.

Figure 3.7 shows clearly that a few of the final cube weights are much higher than the others. Which results in a very high chance of suggesting the cubes with low weights, but rejecting them because of the low weight. A similar distribution of the cube weights can also occur for polar optical phonon scattering, as figure 3.8 shows.

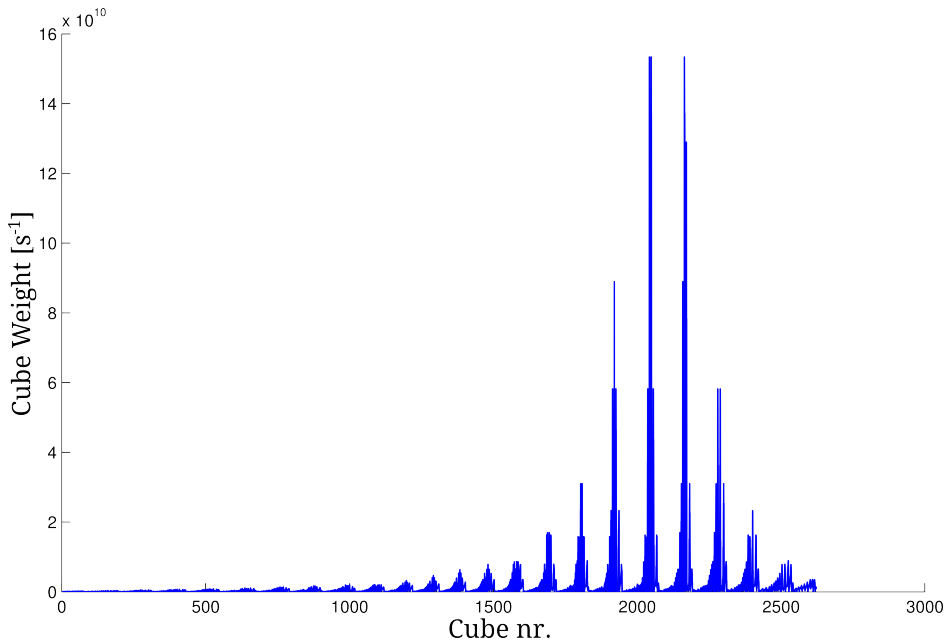


Figure 3.8: Plot of the final cube weights for electron, with energy 0.43 eV along (111)-direction, scattered by polar optical phonon emission.

Also in this case, the cubes with low weights will have a high chance of being suggested, but also most likely be rejected because of the low weight.

In contrast to the ionized impurity scattering and the polar optical phonon scattering, the cube weights are much more evenly distributed for the other scattering mechanisms. As illustrated by figure 3.9, that shows a typical distribution of the cube weights for the acoustic deformation potential phonon emission.

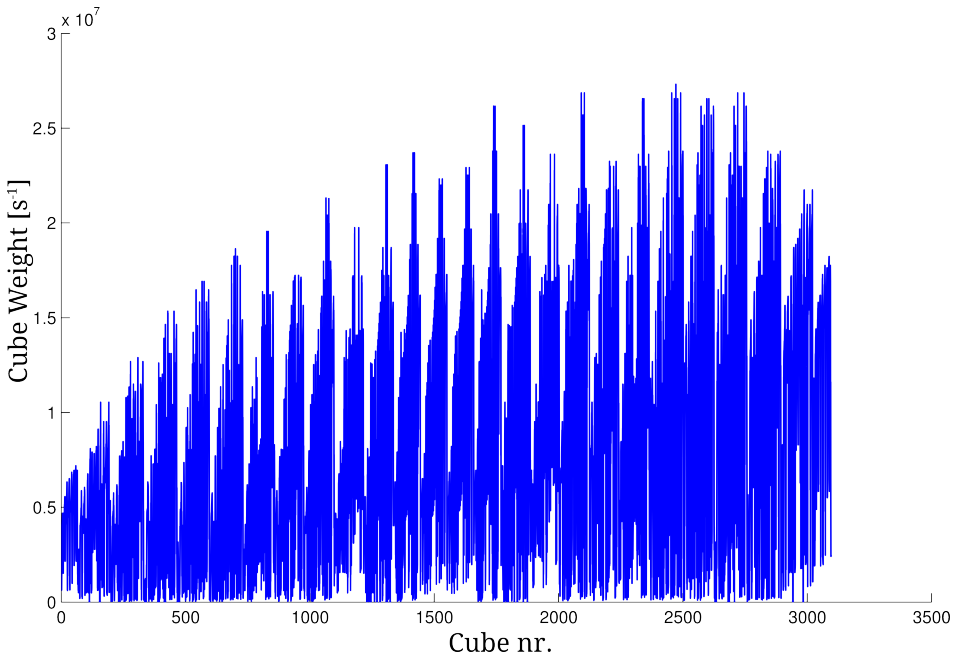


Figure 3.9: Plot of the final cube weights for electron, with energy 0.43 eV along (111)-direction, scattered by acoustic deformation potential phonon emission.

The cube weights in figure 3.9 are very similar, atleast compared to figure 3.8 and 3.7. And in this case the suggested cube will have a relatively large chance of being accepted, and little time will therefore be wasted to suggesting new cubes.

3.5.2 High precision selection of final states

After a final cube has been chosen, a final state within the cube has to be selected. The selection has to be done efficiently, but at the same time it is crucial that the selected final state, \vec{k}' , represents the desired final energy E_f .

Simply choosing the center of the final cube as the final state, \vec{k}' , would be very efficient. However, the error in final energy would be unacceptably large, as the energy represented by the cube center may deviate from the desired final energy by many meV (10^{-3} eV).

Tore Bergslid [11], corrected the final state along the energy gradient, from the center of the cube to the constant energy plane. This correction was reported to give an average error of 2.9 meV in the final energy. However, the energy represented by the chosen final state was always higher than the desired final energy, which lead to artificial heating of the carriers.

A different method was introduced in the specialization project [1] prior to this master's thesis, that offered to select final states with high precision. The derivation of the method is given below:

The energy of the selected final state $E_{n'}(\vec{k}')$ is given by the energy interpolation, described in section 3.2. So in order to select a final state \vec{k}' with a predetermined final energy E_f , one has to somehow invert the expression used to interpolate the energy, the equation 3.3.

First of all, the expression for interpolated energy, given by equation 3.3, is only valid for \vec{k} 's inside the "interpolation" cube, defined by the 8 mesh points surrounding the \vec{k} . And as figure 3.10 shows, any \vec{k} inside the interpolation cube can be expressed by

$$\vec{k} = \vec{k}_1 + \vec{\Delta k} = [k_{x,1} + \Delta k_x, k_{y,1} + \Delta k_y, k_{z,1} + \Delta k_z], \quad (3.30)$$

where $\vec{k}_1 = [k_{x,1}, k_{y,1}, k_{z,1}]$ is the vector to mesh point/corner nr 1, and $\vec{\Delta k} = [\Delta k_x, \Delta k_y, \Delta k_z]$ is the vector between \vec{k}_1 and \vec{k} .

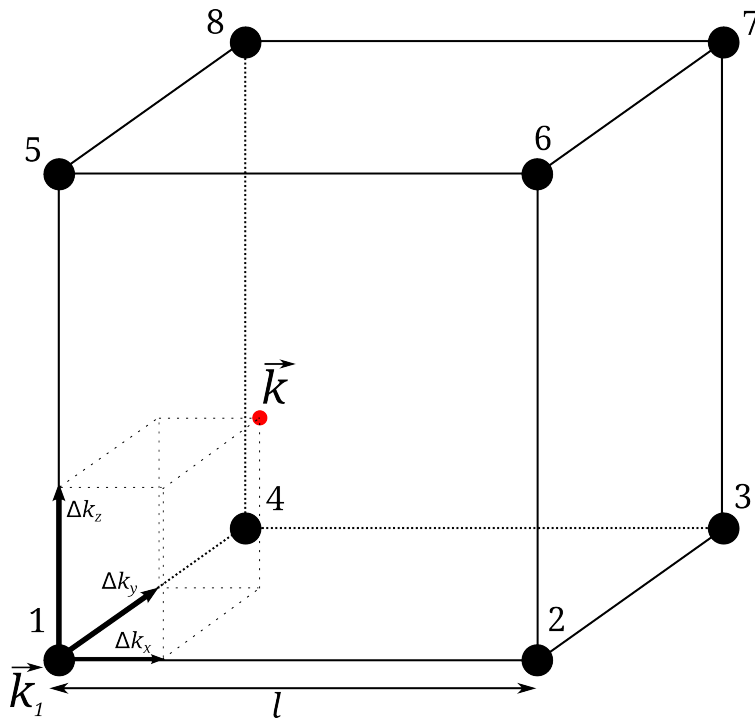


Figure 3.10: Showing an arbitrary \vec{k} (red dot) inside the interpolation cube, with 8 mesh points (black dots) in the corners.

Note, the corner nr 1 is always defined as the mesh point with the lowest coordinates, which makes $0 \leq \Delta k_i \leq l$ by definition.

Similarly to 3.30, can all of the 8 mesh points/corners be expressed by \vec{k}_1 and l :

$$\vec{k}_1 = \vec{k}_1 + [0, 0, 0] = [k_{x,1} + 0, k_{y,1} + 0, k_{z,1} + 0] \quad (3.31a)$$

$$\vec{k}_2 = \vec{k}_1 + [l, 0, 0] = [k_{x,1} + l, k_{y,1} + 0, k_{z,1} + 0] \quad (3.31b)$$

$$\vec{k}_3 = \vec{k}_1 + [l, l, 0] = [k_{x,1} + l, k_{y,1} + l, k_{z,1} + 0] \quad (3.31c)$$

$$\vec{k}_4 = \vec{k}_1 + [0, l, 0] = [k_{x,1} + 0, k_{y,1} + l, k_{z,1} + 0] \quad (3.31d)$$

$$\vec{k}_5 = \vec{k}_1 + [0, 0, l] = [k_{x,1} + 0, k_{y,1} + 0, k_{z,1} + l] \quad (3.31e)$$

$$\vec{k}_6 = \vec{k}_1 + [l, 0, l] = [k_{x,1} + l, k_{y,1} + 0, k_{z,1} + l] \quad (3.31f)$$

$$\vec{k}_7 = \vec{k}_1 + [l, l, l] = [k_{x,1} + l, k_{y,1} + l, k_{z,1} + l] \quad (3.31g)$$

$$\vec{k}_8 = \vec{k}_1 + [0, l, l] = [k_{x,1} + 0, k_{y,1} + l, k_{z,1} + l] \quad (3.31h)$$

where l is the distance between mesh points, as shown in figure 3.10.

Substituting the expressions 3.31 and 3.30 into 3.3, and expanding the sum, gives the (very long) expression for the interpolated energy:

$$\begin{aligned} E_n(\vec{k}) = & \left\{ E_n(\vec{k}_1) + \frac{\partial E_n}{\partial k_x} \Big|_{\vec{k}_1} \Delta k_x + \frac{\partial E_n}{\partial k_y} \Big|_{\vec{k}_1} \Delta k_y + \frac{\partial E_n}{\partial k_z} \Big|_{\vec{k}_1} \Delta k_z \right. \\ & + \frac{\partial^2 E_n}{\partial k_x \partial k_y} \Big|_{\vec{k}_1} \Delta k_x \Delta k_y + \frac{\partial^2 E_n}{\partial k_y \partial k_z} \Big|_{\vec{k}_1} \Delta k_y \Delta k_z \\ & + \frac{\partial^2 E_n}{\partial k_z \partial k_x} \Big|_{\vec{k}_1} \Delta k_z \Delta k_x + \frac{1}{2} \frac{\partial^2 E_n}{\partial k_x^2} \Big|_{\vec{k}_1} (\Delta k_x)^2 + \frac{1}{2} \frac{\partial^2 E_n}{\partial k_y^2} \Big|_{\vec{k}_1} (\Delta k_y)^2 \\ & \left. + \frac{1}{2} \frac{\partial^2 E_n}{\partial k_z^2} \Big|_{\vec{k}_1} (\Delta k_z)^2 \right\} \cdot \left[1 - \frac{|\Delta k_x|}{l} \right] \left[1 - \frac{|\Delta k_y|}{l} \right] \left[1 - \frac{|\Delta k_z|}{l} \right] \\ & + \left\{ E_n(\vec{k}_2) + \frac{\partial E_n}{\partial k_x} \Big|_{\vec{k}_2} (\Delta k_x - l) + \frac{\partial E_n}{\partial k_y} \Big|_{\vec{k}_2} \Delta k_y + \frac{\partial E_n}{\partial k_z} \Big|_{\vec{k}_2} \Delta k_z \right. \\ & + \frac{\partial^2 E_n}{\partial k_x \partial k_y} \Big|_{\vec{k}_2} (\Delta k_x - l) \Delta k_y + \frac{\partial^2 E_n}{\partial k_y \partial k_z} \Big|_{\vec{k}_2} \Delta k_y \Delta k_z \\ & + \frac{\partial^2 E_n}{\partial k_z \partial k_x} \Big|_{\vec{k}_2} \Delta k_z (\Delta k_x - l) + \frac{1}{2} \frac{\partial^2 E_n}{\partial k_x^2} \Big|_{\vec{k}_2} (\Delta k_x - l)^2 + \frac{1}{2} \frac{\partial^2 E_n}{\partial k_y^2} \Big|_{\vec{k}_2} (\Delta k_y)^2 \\ & \left. + \frac{1}{2} \frac{\partial^2 E_n}{\partial k_z^2} \Big|_{\vec{k}_2} (\Delta k_z)^2 \right\} \cdot \left[1 - \frac{|\Delta k_x - l|}{l} \right] \left[1 - \frac{|\Delta k_y|}{l} \right] \left[1 - \frac{|\Delta k_z|}{l} \right] \end{aligned}$$

$$\begin{aligned}
& + \left\{ E_n(\vec{k}_3) + \frac{\partial E_n}{\partial k_x} \Big|_{\vec{k}_3} (\Delta k_x - l) + \frac{\partial E_n}{\partial k_y} \Big|_{\vec{k}_3} (\Delta k_y - l) + \frac{\partial E_n}{\partial k_z} \Big|_{\vec{k}_3} \Delta k_z \right. \\
& + \frac{\partial^2 E_n}{\partial k_x \partial k_y} \Big|_{\vec{k}_3} (\Delta k_x - l)(\Delta k_y - l) + \frac{\partial^2 E_n}{\partial k_y \partial k_z} \Big|_{\vec{k}_3} (\Delta k_y - l)\Delta k_z \\
& + \frac{\partial^2 E_n}{\partial k_z \partial k_x} \Big|_{\vec{k}_3} \Delta k_z(\Delta k_x - l) + \frac{1}{2} \frac{\partial^2 E_n}{\partial k_x^2} \Big|_{\vec{k}_3} (\Delta k_x - l)^2 + \frac{1}{2} \frac{\partial^2 E_n}{\partial k_y^2} \Big|_{\vec{k}_3} (\Delta k_y - l)^2 \\
& \left. + \frac{1}{2} \frac{\partial^2 E_n}{\partial k_z^2} \Big|_{\vec{k}_3} (\Delta k_z)^2 \right\} \cdot \left[1 - \frac{|\Delta k_x - l|}{l} \right] \left[1 - \frac{|\Delta k_y - l|}{l} \right] \left[1 - \frac{|\Delta k_z|}{l} \right] \\
& + \left\{ E_n(\vec{k}_4) + \frac{\partial E_n}{\partial k_x} \Big|_{\vec{k}_4} \Delta k_x + \frac{\partial E_n}{\partial k_y} \Big|_{\vec{k}_4} (\Delta k_y - l) + \frac{\partial E_n}{\partial k_z} \Big|_{\vec{k}_4} \Delta k_z \right. \\
& + \frac{\partial^2 E_n}{\partial k_x \partial k_y} \Big|_{\vec{k}_4} \Delta k_x(\Delta k_y - l) + \frac{\partial^2 E_n}{\partial k_y \partial k_z} \Big|_{\vec{k}_4} (\Delta k_y - l)\Delta k_z \\
& + \frac{\partial^2 E_n}{\partial k_z \partial k_x} \Big|_{\vec{k}_4} \Delta k_z \Delta k_x + \frac{1}{2} \frac{\partial^2 E_n}{\partial k_x^2} \Big|_{\vec{k}_4} (\Delta k_x)^2 + \frac{1}{2} \frac{\partial^2 E_n}{\partial k_y^2} \Big|_{\vec{k}_4} (\Delta k_y - l)^2 \\
& \left. + \frac{1}{2} \frac{\partial^2 E_n}{\partial k_z^2} \Big|_{\vec{k}_4} (\Delta k_z)^2 \right\} \cdot \left[1 - \frac{|\Delta k_x|}{l} \right] \left[1 - \frac{|\Delta k_y - l|}{l} \right] \left[1 - \frac{|\Delta k_z|}{l} \right] \\
& + \left\{ E_n(\vec{k}_5) + \frac{\partial E_n}{\partial k_x} \Big|_{\vec{k}_5} \Delta k_x + \frac{\partial E_n}{\partial k_y} \Big|_{\vec{k}_5} \Delta k_y + \frac{\partial E_n}{\partial k_z} \Big|_{\vec{k}_5} (\Delta k_z - l) \right. \\
& + \frac{\partial^2 E_n}{\partial k_x \partial k_y} \Big|_{\vec{k}_5} \Delta k_x \Delta k_y + \frac{\partial^2 E_n}{\partial k_y \partial k_z} \Big|_{\vec{k}_5} \Delta k_y(\Delta k_z - l) \\
& + \frac{\partial^2 E_n}{\partial k_z \partial k_x} \Big|_{\vec{k}_5} (\Delta k_z - l)\Delta k_x + \frac{1}{2} \frac{\partial^2 E_n}{\partial k_x^2} \Big|_{\vec{k}_5} (\Delta k_x)^2 + \frac{1}{2} \frac{\partial^2 E_n}{\partial k_y^2} \Big|_{\vec{k}_5} (\Delta k_y)^2 \\
& \left. + \frac{1}{2} \frac{\partial^2 E_n}{\partial k_z^2} \Big|_{\vec{k}_5} (\Delta k_z - l)^2 \right\} \cdot \left[1 - \frac{|\Delta k_x|}{l} \right] \left[1 - \frac{|\Delta k_y|}{l} \right] \left[1 - \frac{|\Delta k_z - l|}{l} \right] \\
& + \left\{ E_n(\vec{k}_6) + \frac{\partial E_n}{\partial k_x} \Big|_{\vec{k}_6} (\Delta k_x - l) + \frac{\partial E_n}{\partial k_y} \Big|_{\vec{k}_6} \Delta k_y + \frac{\partial E_n}{\partial k_z} \Big|_{\vec{k}_6} (\Delta k_z - l) \right. \\
& + \frac{\partial^2 E_n}{\partial k_x \partial k_y} \Big|_{\vec{k}_6} (\Delta k_x - l)\Delta k_y + \frac{\partial^2 E_n}{\partial k_y \partial k_z} \Big|_{\vec{k}_6} \Delta k_y(\Delta k_z - l) \\
& + \frac{\partial^2 E_n}{\partial k_z \partial k_x} \Big|_{\vec{k}_6} (\Delta k_z - l)(\Delta k_x - l) + \frac{1}{2} \frac{\partial^2 E_n}{\partial k_x^2} \Big|_{\vec{k}_6} (\Delta k_x - l)^2 + \frac{1}{2} \frac{\partial^2 E_n}{\partial k_y^2} \Big|_{\vec{k}_6} (\Delta k_y)^2 \\
& \left. + \frac{1}{2} \frac{\partial^2 E_n}{\partial k_z^2} \Big|_{\vec{k}_6} (\Delta k_z - l)^2 \right\} \cdot \left[1 - \frac{|\Delta k_x - l|}{l} \right] \left[1 - \frac{|\Delta k_y|}{l} \right] \left[1 - \frac{|\Delta k_z - l|}{l} \right]
\end{aligned} \tag{3.32}$$

$$\begin{aligned}
& + \left\{ E_n(\vec{k}_7) + \frac{\partial E_n}{\partial k_x} \Big|_{\vec{k}_7} (\Delta k_x - l) + \frac{\partial E_n}{\partial k_y} \Big|_{\vec{k}_7} (\Delta k_y - l) + \frac{\partial E_n}{\partial k_z} \Big|_{\vec{k}_7} (\Delta k_z - l) \right. \\
& + \frac{\partial^2 E_n}{\partial k_x \partial k_y} \Big|_{\vec{k}_7} (\Delta k_x - l)(\Delta k_y - l) + \frac{\partial^2 E_n}{\partial k_y \partial k_z} \Big|_{\vec{k}_7} (\Delta k_y - l)(\Delta k_z - l) \\
& + \frac{\partial^2 E_n}{\partial k_z \partial k_x} \Big|_{\vec{k}_7} (\Delta k_z - l)(\Delta k_x - l) + \frac{1}{2} \frac{\partial^2 E_n}{\partial k_x^2} \Big|_{\vec{k}_7} (\Delta k_x - l)^2 + \frac{1}{2} \frac{\partial^2 E_n}{\partial k_y^2} \Big|_{\vec{k}_7} (\Delta k_y - l)^2 \\
& \left. + \frac{1}{2} \frac{\partial^2 E_n}{\partial k_z^2} \Big|_{\vec{k}_7} (\Delta k_z - l)^2 \right\} \cdot \left[1 - \frac{|\Delta k_x - l|}{l} \right] \left[1 - \frac{|\Delta k_y - l|}{l} \right] \left[1 - \frac{|\Delta k_z - l|}{l} \right] \\
& + \left\{ E_n(\vec{k}_8) + \frac{\partial E_n}{\partial k_x} \Big|_{\vec{k}_8} \Delta k_x + \frac{\partial E_n}{\partial k_y} \Big|_{\vec{k}_8} (\Delta k_y - l) + \frac{\partial E_n}{\partial k_z} \Big|_{\vec{k}_8} (\Delta k_z - l) \right. \\
& + \frac{\partial^2 E_n}{\partial k_x \partial k_y} \Big|_{\vec{k}_8} \Delta k_x (\Delta k_y - l) + \frac{\partial^2 E_n}{\partial k_y \partial k_z} \Big|_{\vec{k}_8} (\Delta k_y - l)(\Delta k_z - l) \\
& + \frac{\partial^2 E_n}{\partial k_z \partial k_x} \Big|_{\vec{k}_8} (\Delta k_z - l) \Delta k_x + \frac{1}{2} \frac{\partial^2 E_n}{\partial k_x^2} \Big|_{\vec{k}_8} (\Delta k_x)^2 + \frac{1}{2} \frac{\partial^2 E_n}{\partial k_y^2} \Big|_{\vec{k}_8} (\Delta k_y - l)^2 \\
& \left. + \frac{1}{2} \frac{\partial^2 E_n}{\partial k_z^2} \Big|_{\vec{k}_8} (\Delta k_z - l)^2 \right\} \cdot \left[1 - \frac{|\Delta k_x|}{l} \right] \left[1 - \frac{|\Delta k_y - l|}{l} \right] \left[1 - \frac{|\Delta k_z - l|}{l} \right].
\end{aligned}$$

where $\vec{k} = \vec{k}_1 + \vec{\Delta k}$. Equation 3.32 gives the energy as a function of $(\Delta k_x, \Delta k_y, \Delta k_z)$. The energy contributions from each corner are deliberately kept in curly $\{ \}$ parenthesis, while the corner weights are kept in square $[]$ parenthesis. This is done for slightly better overview.

The absolute values in the square $[]$ parenthesis in equation 3.32 can be eliminated using the identities:

$$\left[1 - \frac{|\Delta k_i|}{l} \right] = \left[\frac{l - \Delta k_i}{l} \right] \quad (3.33a)$$

$$\left[1 - \frac{|\Delta k_i - l|}{l} \right] = \left[\frac{\Delta k_i}{l} \right]. \quad (3.33b)$$

where $i \in x, y, z$, the fact that $0 \leq \Delta k_i \leq l$ has been used.

Replacing the corner weights in equation 3.32, with the identities 3.33, results in the following expression for the interpolated energy, that no longer contains absolute values.

$$\begin{aligned}
E_n(\vec{k}) = & \left\{ E_n(\vec{k}_1) + \frac{\partial E_n}{\partial k_x} \Big|_{\vec{k}_1} \Delta k_x + \frac{\partial E_n}{\partial k_y} \Big|_{\vec{k}_1} \Delta k_y + \frac{\partial E_n}{\partial k_z} \Big|_{\vec{k}_1} \Delta k_z \right. \\
& + \frac{\partial^2 E_n}{\partial k_x \partial k_y} \Big|_{\vec{k}_1} \Delta k_x \Delta k_y + \frac{\partial^2 E_n}{\partial k_y \partial k_z} \Big|_{\vec{k}_1} \Delta k_y \Delta k_z \\
& + \frac{\partial^2 E_n}{\partial k_z \partial k_x} \Big|_{\vec{k}_1} \Delta k_z \Delta k_x + \frac{1}{2} \frac{\partial^2 E_n}{\partial k_x^2} \Big|_{\vec{k}_1} (\Delta k_x)^2 + \frac{1}{2} \frac{\partial^2 E_n}{\partial k_y^2} \Big|_{\vec{k}_1} (\Delta k_y)^2 \\
& \left. + \frac{1}{2} \frac{\partial^2 E_n}{\partial k_z^2} \Big|_{\vec{k}_1} (\Delta k_z)^2 \right\} \cdot \left(\frac{l - \Delta k_x}{l} \right) \left(\frac{l - \Delta k_y}{l} \right) \left(\frac{l - \Delta k_z}{l} \right)
\end{aligned}$$

$$\begin{aligned}
& + \left\{ E_n(\vec{k}_2) + \frac{\partial E_n}{\partial k_x} \Big|_{\vec{k}_2} (\Delta k_x - l) + \frac{\partial E_n}{\partial k_y} \Big|_{\vec{k}_2} \Delta k_y + \frac{\partial E_n}{\partial k_z} \Big|_{\vec{k}_2} \Delta k_z \right. \\
& + \frac{\partial^2 E_n}{\partial k_x \partial k_y} \Big|_{\vec{k}_2} (\Delta k_x - l) \Delta k_y + \frac{\partial^2 E_n}{\partial k_y \partial k_z} \Big|_{\vec{k}_2} \Delta k_y \Delta k_z \\
& + \frac{\partial^2 E_n}{\partial k_z \partial k_x} \Big|_{\vec{k}_2} \Delta k_z (\Delta k_x - l) + \frac{1}{2} \frac{\partial^2 E_n}{\partial k_x^2} \Big|_{\vec{k}_2} (\Delta k_x - l)^2 + \frac{1}{2} \frac{\partial^2 E_n}{\partial k_y^2} \Big|_{\vec{k}_2} (\Delta k_y)^2 \\
& \left. + \frac{1}{2} \frac{\partial^2 E_n}{\partial k_z^2} \Big|_{\vec{k}_2} (\Delta k_z)^2 \right\} \cdot \left(\frac{\Delta k_x}{l} \right) \left(\frac{l - \Delta k_y}{l} \right) \left(\frac{l - \Delta k_z}{l} \right) \\
& + \left\{ E_n(\vec{k}_3) + \frac{\partial E_n}{\partial k_x} \Big|_{\vec{k}_3} (\Delta k_x - l) + \frac{\partial E_n}{\partial k_y} \Big|_{\vec{k}_3} (\Delta k_y - l) + \frac{\partial E_n}{\partial k_z} \Big|_{\vec{k}_3} \Delta k_z \right. \\
& + \frac{\partial^2 E_n}{\partial k_x \partial k_y} \Big|_{\vec{k}_3} (\Delta k_x - l) (\Delta k_y - l) + \frac{\partial^2 E_n}{\partial k_y \partial k_z} \Big|_{\vec{k}_3} (\Delta k_y - l) \Delta k_z \\
& + \frac{\partial^2 E_n}{\partial k_z \partial k_x} \Big|_{\vec{k}_3} \Delta k_z (\Delta k_x - l) + \frac{1}{2} \frac{\partial^2 E_n}{\partial k_x^2} \Big|_{\vec{k}_3} (\Delta k_x - l)^2 + \frac{1}{2} \frac{\partial^2 E_n}{\partial k_y^2} \Big|_{\vec{k}_3} (\Delta k_y - l)^2 \\
& \left. + \frac{1}{2} \frac{\partial^2 E_n}{\partial k_z^2} \Big|_{\vec{k}_3} (\Delta k_z)^2 \right\} \cdot \left(\frac{\Delta k_x}{l} \right) \left(\frac{\Delta k_y}{l} \right) \left(\frac{l - \Delta k_z}{l} \right) \\
& + \left\{ E_n(\vec{k}_4) + \frac{\partial E_n}{\partial k_x} \Big|_{\vec{k}_4} \Delta k_x + \frac{\partial E_n}{\partial k_y} \Big|_{\vec{k}_4} (\Delta k_y - l) + \frac{\partial E_n}{\partial k_z} \Big|_{\vec{k}_4} \Delta k_z \right. \\
& + \frac{\partial^2 E_n}{\partial k_x \partial k_y} \Big|_{\vec{k}_4} \Delta k_x (\Delta k_y - l) + \frac{\partial^2 E_n}{\partial k_y \partial k_z} \Big|_{\vec{k}_4} (\Delta k_y - l) \Delta k_z \\
& + \frac{\partial^2 E_n}{\partial k_z \partial k_x} \Big|_{\vec{k}_4} \Delta k_z \Delta k_x + \frac{1}{2} \frac{\partial^2 E_n}{\partial k_x^2} \Big|_{\vec{k}_4} (\Delta k_x)^2 + \frac{1}{2} \frac{\partial^2 E_n}{\partial k_y^2} \Big|_{\vec{k}_4} (\Delta k_y - l)^2 \\
& \left. + \frac{1}{2} \frac{\partial^2 E_n}{\partial k_z^2} \Big|_{\vec{k}_4} (\Delta k_z)^2 \right\} \cdot \left(\frac{l - \Delta k_x}{l} \right) \left(\frac{\Delta k_y}{l} \right) \left(\frac{l - \Delta k_z}{l} \right) \\
& + \left\{ E_n(\vec{k}_5) + \frac{\partial E_n}{\partial k_x} \Big|_{\vec{k}_5} \Delta k_x + \frac{\partial E_n}{\partial k_y} \Big|_{\vec{k}_5} \Delta k_y + \frac{\partial E_n}{\partial k_z} \Big|_{\vec{k}_5} (\Delta k_z - l) \right. \\
& + \frac{\partial^2 E_n}{\partial k_x \partial k_y} \Big|_{\vec{k}_5} \Delta k_x \Delta k_y + \frac{\partial^2 E_n}{\partial k_y \partial k_z} \Big|_{\vec{k}_5} \Delta k_y (\Delta k_z - l) \\
& + \frac{\partial^2 E_n}{\partial k_z \partial k_x} \Big|_{\vec{k}_5} (\Delta k_z - l) \Delta k_x + \frac{1}{2} \frac{\partial^2 E_n}{\partial k_x^2} \Big|_{\vec{k}_5} (\Delta k_x)^2 + \frac{1}{2} \frac{\partial^2 E_n}{\partial k_y^2} \Big|_{\vec{k}_5} (\Delta k_y)^2 \\
& \left. + \frac{1}{2} \frac{\partial^2 E_n}{\partial k_z^2} \Big|_{\vec{k}_5} (\Delta k_z - l)^2 \right\} \cdot \left(\frac{l - \Delta k_x}{l} \right) \left(\frac{l - \Delta k_y}{l} \right) \left(\frac{\Delta k_z}{l} \right)
\end{aligned} \tag{3.34}$$

$$\begin{aligned}
& + \left\{ E_n(\vec{k}_6) + \frac{\partial E_n}{\partial k_x} \Big|_{\vec{k}_6} (\Delta k_x - l) + \frac{\partial E_n}{\partial k_y} \Big|_{\vec{k}_6} \Delta k_y + \frac{\partial E_n}{\partial k_z} \Big|_{\vec{k}_6} (\Delta k_z - l) \right. \\
& + \frac{\partial^2 E_n}{\partial k_x \partial k_y} \Big|_{\vec{k}_6} (\Delta k_x - l) \Delta k_y + \frac{\partial^2 E_n}{\partial k_y \partial k_z} \Big|_{\vec{k}_6} \Delta k_y (\Delta k_z - l) \\
& + \frac{\partial^2 E_n}{\partial k_z \partial k_x} \Big|_{\vec{k}_6} (\Delta k_z - l) (\Delta k_x - l) + \frac{1}{2} \frac{\partial^2 E_n}{\partial k_x^2} \Big|_{\vec{k}_6} (\Delta k_x - l)^2 + \frac{1}{2} \frac{\partial^2 E_n}{\partial k_y^2} \Big|_{\vec{k}_6} (\Delta k_y)^2 \\
& \left. + \frac{1}{2} \frac{\partial^2 E_n}{\partial k_z^2} \Big|_{\vec{k}_6} (\Delta k_z - l)^2 \right\} \cdot \left(\frac{\Delta k_x}{l} \right) \left(\frac{l - \Delta k_y}{l} \right) \left(\frac{\Delta k_z}{l} \right) \\
& + \left\{ E_n(\vec{k}_7) + \frac{\partial E_n}{\partial k_x} \Big|_{\vec{k}_7} (\Delta k_x - l) + \frac{\partial E_n}{\partial k_y} \Big|_{\vec{k}_7} (\Delta k_y - l) + \frac{\partial E_n}{\partial k_z} \Big|_{\vec{k}_7} (\Delta k_z - l) \right. \\
& + \frac{\partial^2 E_n}{\partial k_x \partial k_y} \Big|_{\vec{k}_7} (\Delta k_x - l) (\Delta k_y - l) + \frac{\partial^2 E_n}{\partial k_y \partial k_z} \Big|_{\vec{k}_7} (\Delta k_y - l) (\Delta k_z - l) \\
& + \frac{\partial^2 E_n}{\partial k_z \partial k_x} \Big|_{\vec{k}_7} (\Delta k_z - l) (\Delta k_x - l) + \frac{1}{2} \frac{\partial^2 E_n}{\partial k_x^2} \Big|_{\vec{k}_7} (\Delta k_x - l)^2 \\
& \left. + \frac{1}{2} \frac{\partial^2 E_n}{\partial k_y^2} \Big|_{\vec{k}_7} (\Delta k_y - l)^2 + \frac{1}{2} \frac{\partial^2 E_n}{\partial k_z^2} \Big|_{\vec{k}_7} (\Delta k_z - l)^2 \right\} \cdot \left(\frac{\Delta k_x}{l} \right) \left(\frac{\Delta k_y}{l} \right) \left(\frac{\Delta k_z}{l} \right) \\
& + \left\{ E_n(\vec{k}_8) + \frac{\partial E_n}{\partial k_x} \Big|_{\vec{k}_8} \Delta k_x + \frac{\partial E_n}{\partial k_y} \Big|_{\vec{k}_8} (\Delta k_y - l) + \frac{\partial E_n}{\partial k_z} \Big|_{\vec{k}_8} (\Delta k_z - l) \right. \\
& + \frac{\partial^2 E_n}{\partial k_x \partial k_y} \Big|_{\vec{k}_8} \Delta k_x (\Delta k_y - l) + \frac{\partial^2 E_n}{\partial k_y \partial k_z} \Big|_{\vec{k}_8} (\Delta k_y - l) (\Delta k_z - l) \\
& + \frac{\partial^2 E_n}{\partial k_z \partial k_x} \Big|_{\vec{k}_8} (\Delta k_z - l) \Delta k_x + \frac{1}{2} \frac{\partial^2 E_n}{\partial k_x^2} \Big|_{\vec{k}_8} (\Delta k_x)^2 + \frac{1}{2} \frac{\partial^2 E_n}{\partial k_y^2} \Big|_{\vec{k}_8} (\Delta k_y - l)^2 \\
& \left. + \frac{1}{2} \frac{\partial^2 E_n}{\partial k_z^2} \Big|_{\vec{k}_8} (\Delta k_z - l)^2 \right\} \cdot \left(\frac{l - \Delta k_x}{l} \right) \left(\frac{\Delta k_y}{l} \right) \left(\frac{\Delta k_z}{l} \right)
\end{aligned}$$

where $\vec{k} = \vec{k}_1 + [\Delta k_x, \Delta k_y, \Delta k_z]$.

The equation 3.34, describing the interpolated energy inside an "interpolation" cube, may look very complicated, but is actually a 5th order polynomial of the 3 variables Δk_x , Δk_y and Δk_z .

Inversion of the energy is equivalent to finding a solution $(\Delta k_x, \Delta k_y, \Delta k_z)$ for a given energy. Finding a general solution $(\Delta k_x, \Delta k_y, \Delta k_z)$ for the 5th order polynomial is extremely difficult or maybe even impossible. However, if the $(\Delta k_x, \Delta k_y, \Delta k_z)$ represent a straight line, the 5th order polynomial of 3 variables becomes a 5th order polynomial of only 1 variable. Which is simply because any straight line can be parametrized by only 1 free variable. This means that the energy along any straight line inside the "interpolation" cube can be written in the form

$$E(x) = C_0 + C_1 x + C_2 x^2 + C_3 x^3 + C_4 x^4 + C_5 x^5 \quad (3.35)$$

where x is the free parameter, and the coefficients $C_{0,1,2,3,4,5}$ depend on the actual parametrization of the straight line (and of course corner point energy and derivatives). This is easily seen when substituting $(\Delta k_x, \Delta k_y, \Delta k_z)$ in equation 3.34 by a general parametrization of a straight line, given by $(a_1 + b_1x, a_2 + b_2x, a_3 + b_3x)$, where x is the free variable and $a_{1,2,3}, b_{1,2,3}$ are constants.

A solution x' of the 5th order polynomial (3.35), can be found numerically, for a given energy E' . And the $\vec{\Delta k}' = [\Delta k'_x, \Delta k'_y, \Delta k'_z]$ associated with the energy E' is given by the specific parametrization. The resulting $\vec{k}' = \vec{k}_1 + \vec{\Delta k}'$ will therefore have the given energy E' . Or in other words, the interpolated energy at \vec{k}' will be equal to E' .

One important thing must be noted: the method described above can be used to find \vec{k}' with the desired energy E' , only within an "interpolation" cube. However, the cube that is selected as the final cube, is deliberately chosen to be identical to the "interpolation" cube. This allows the method described above to be used directly to select a final state \vec{k}' representing the final energy E_f within the chosen final cube.

There is also no guarantee that a given straight line in the final cube will contain the desired energy E_f , in which case no solution x' will be found. So the search after a final state is performed along several carefully chosen straight lines inside the final cube, in order to maximize the probability of finding a final state. The parametrization of the 7 lines, that are currently implemented, is given in the table below.

Line nr.	$(\Delta x, \Delta y, \Delta z)$
1.	$(x, l/2, l/2)$
2.	$(l/2, x, l/2)$
3.	$(l/2, l/2, x)$
4.	(x, x, x)
5.	$(l - x, x, x)$
6.	$(l - x, l - x, x)$
7.	$(x, l - x, x)$

Table 3.1: The 7 lines given by the parametrization of $\vec{\Delta k}$, x is the free variable, and l is the side length of the final cube.

The 7 carefully chosen lines, inside the final cube, are shown in figure 3.11. That also shows that all of the 7 lines are *inside* the final cube, which makes them exclusive for the chosen final cube. Fischetti and Laux [7] used a somewhat similar approach, where they placed the final states on predetermined lines. But most of the lines they used were on the border of the cube, and were therefore shared between the neighbouring cubes, making the lines non exclusive. Which could lead to accumulation of the final states on the shared lines. This accumulation is avoided in this work because, as mentioned, all of the lines are exclusive for the final cubes.

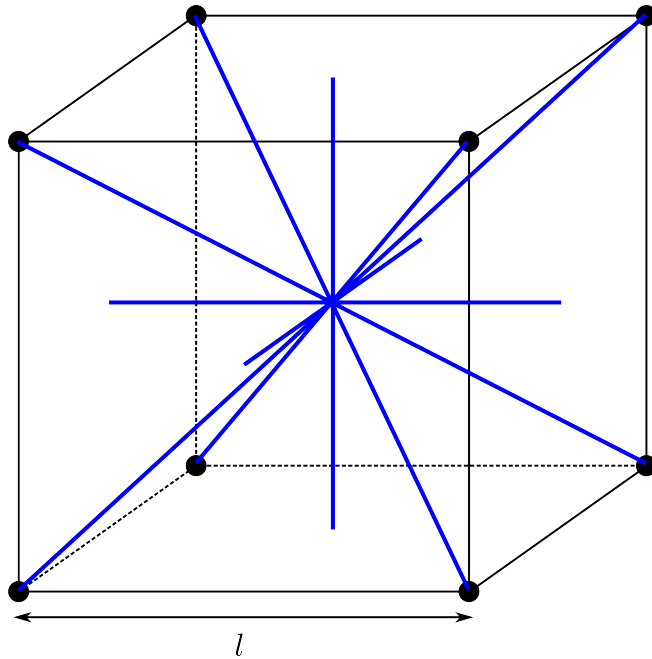


Figure 3.11: Showing the 7 lines in the final cube, along which the final state is found.

The program flow for the selection of the final state within the final cube is fairly simple. Given a final cube and the desired final energy E_f : The coefficients, for the energy along the 7 lines inside the final cube, are calculated using the expressions given in appendix B. Then for each of the lines, the solution x' of the 5th order polynomial is found numerically, before converted to a \vec{k}' using the parametrization of the line in question and \vec{k}_1 . In most cases, several of the lines contain the desired energy, each resulting in a \vec{k}' , one of them is picked out at random to be the final state \vec{k}' . The chosen final state \vec{k}' should now represent the desired final energy E_f .

This method of selecting final states within the final cube, proved to be very precise, during testing in the specialization project [1]. In fact, an error less than 10^{-6} eV in the final state energy was easily achieved. While this high precision method of finding final states is clearly more CPU intensive than the mentioned inaccurate alternatives, the high increase in precision should outweigh the small increase in simulation runtime.

Results

In this chapter the most important results of the present work will be shown. The first section covers on the calculated scattering rates for both electrons and holes, that are important to perform the actual Monte Carlo simulations. The following section will show some actual simulation results, to demonstrate a properly working Full Band model. Before the electron mobility in $\text{Hg}_{0.72}\text{Cd}_{0.28}\text{Te}$ is calculated in the final section of this chapter.

All of the calculations and simulations were performed for $\text{Hg}_{0.72}\text{Cd}_{0.28}\text{Te}$ at 77K, and in order to include the ionized impurity scattering, the impurity density was set to $1.0 \cdot 10^{17} \text{ cm}^{-3}$ (equivalent to heavily doped MCT). The rest of the simulation parameters are given in the appendix A.

The band structure for $\text{Hg}_{0.72}\text{Cd}_{0.28}\text{Te}$ was already shown in section 3.1, but only the light- and heavy-hole bands are considered when simulating holes, and only the first conduction band is used for electrons. The split-off band is omitted, since it requires the holes to have very high energies and is therefore rarely occupied. The same applies to the higher conduction bands, that requires even higher electron energies to be occupied.

4.1 Scattering rates

The calculated scattering rates in the (111)-direction are presented below. These calculations are closely related to the *ab initio* scattering rates calculated by Bjørnar Karlsen [5], as the used band structure is essentially the same. The main difference between the scattering rate calculations performed in this work and Bjørnar Karlsen's, are the different mesh sizes, and the method used to estimate the maximum and minimum energy spanned by a final cube. Karlsen estimated the energy span by a simple linear extrapolation from the cube center, but in this work, the energy spanned by each final cube is found by a brute force technique. Where the energy was interpolated at many points inside each cube and the maximum/minimum value was saved.

Acoustic deformation potential phonon scattering

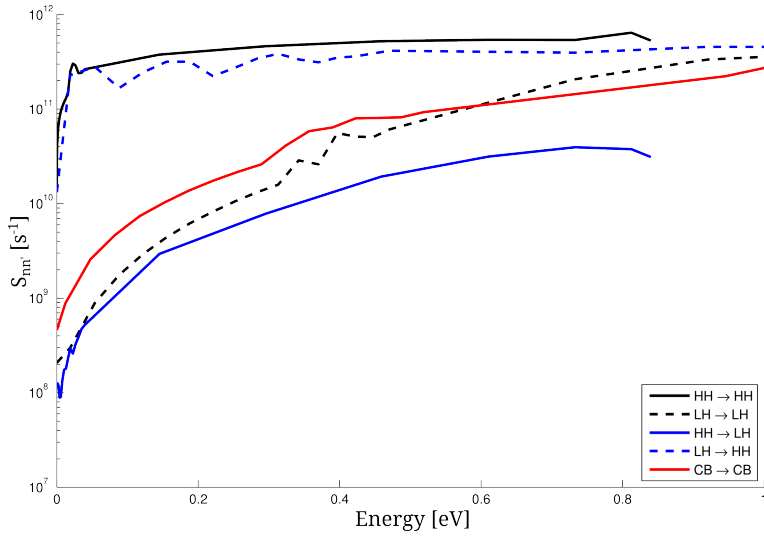


Figure 4.1: Acoustic deformation potential phonon absorption scattering rates, in the (111)-direction.

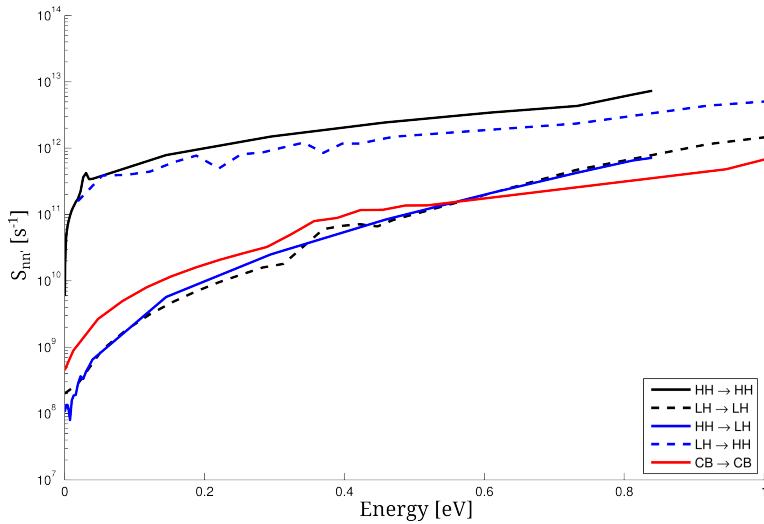


Figure 4.2: Acoustic deformation potential phonon emission scattering rates, in the (111)-direction.

Polar optical phonon scattering

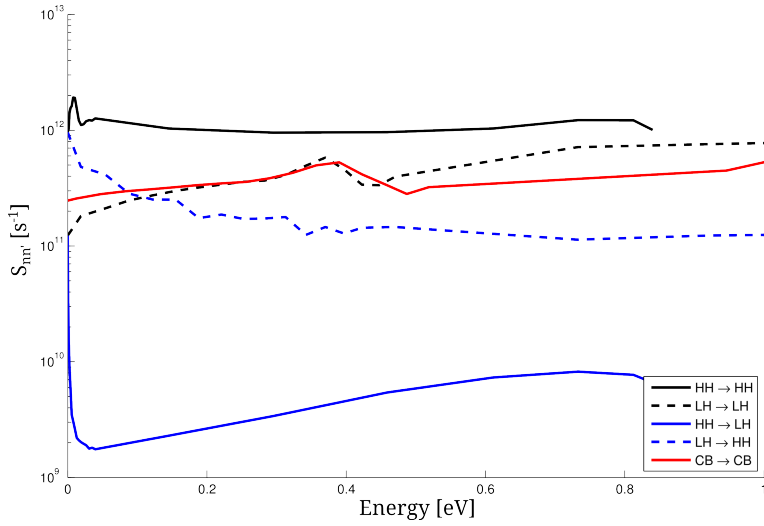


Figure 4.3: Polar optical phonon absorption scattering rates, in the (111)-direction.

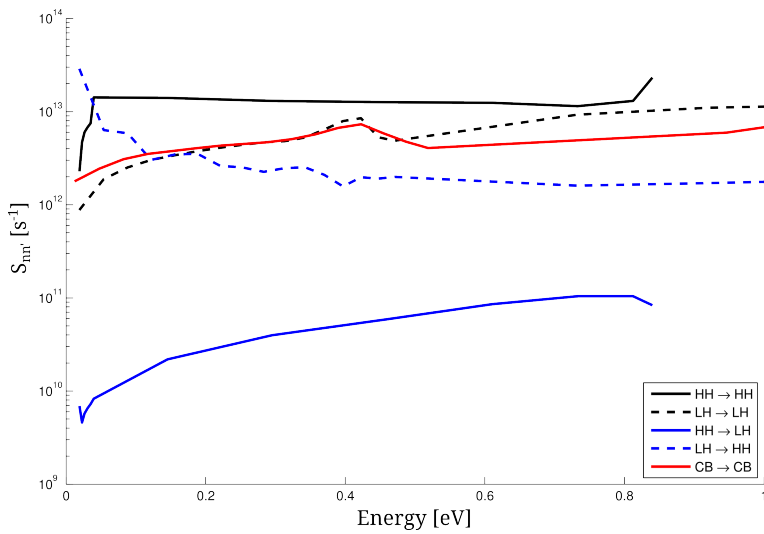


Figure 4.4: Polar optical phonon emission scattering rates, in the (111)-direction.

Nonpolar optical phonon scattering

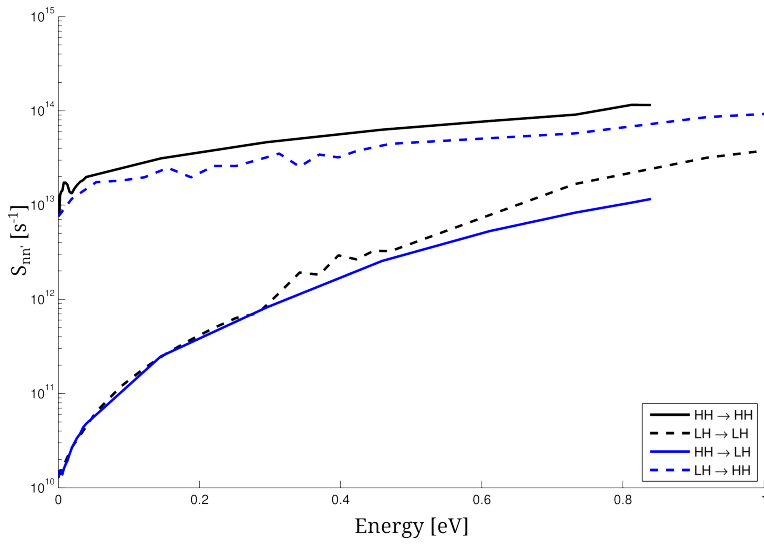


Figure 4.5: Nonpolar optical phonon absorption scattering rates, in the (111)-direction.

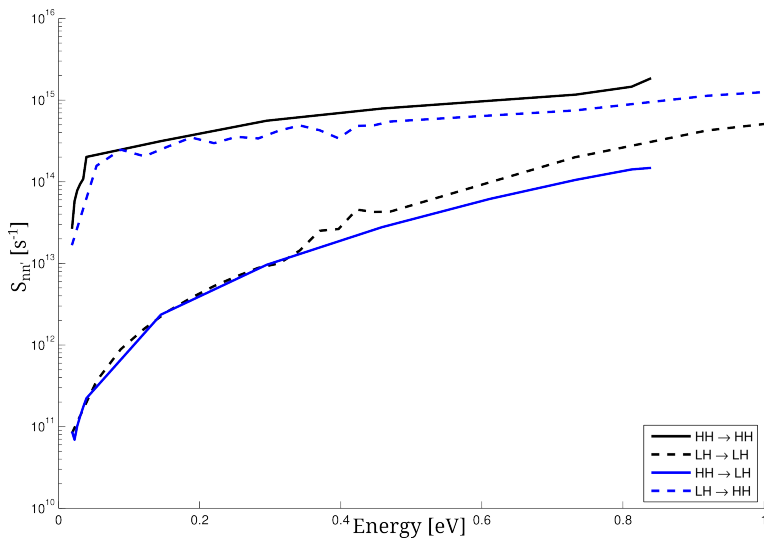


Figure 4.6: Nonpolar optical phonon emission scattering rates, in the (111)-direction.

Ionized impurity scattering

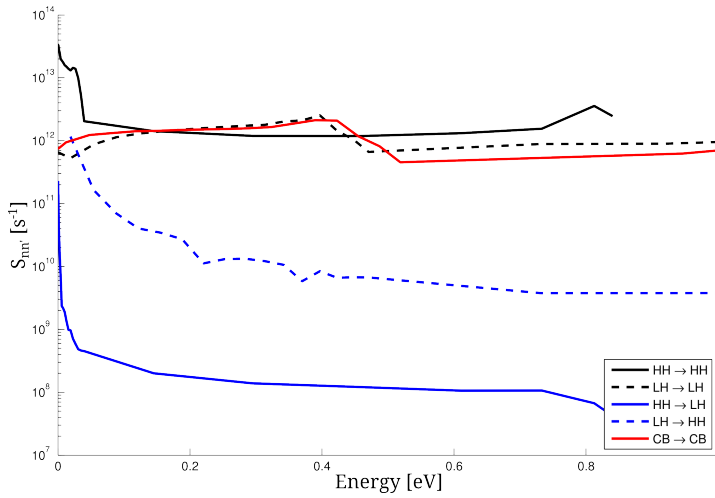


Figure 4.7: Ionized impurity scattering rates, in the (111)-direction.

Alloy scattering

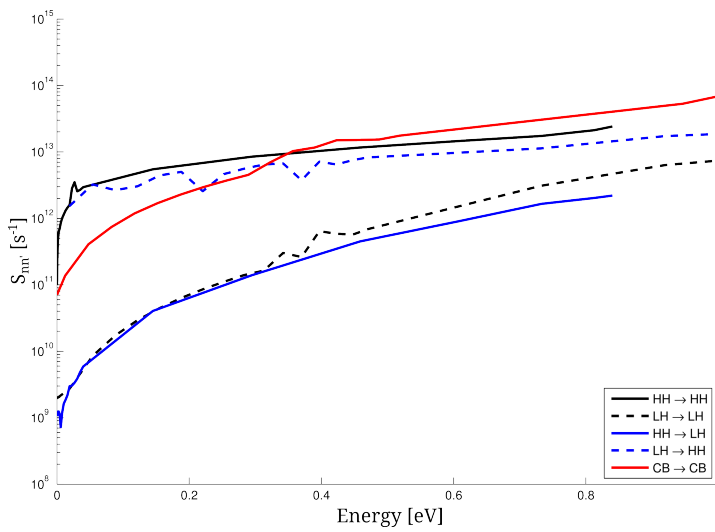


Figure 4.8: Alloy scattering rates, in the (111)-direction.

All of the scattering rates are roughly the same as the the ones calculated by Bjørnar Karlsen [3], and the differences are caused by the slight differences between the calculations. Also the difficulties Karlsen encountered while calculating the electron scattering rates appear to be solved.

The scattering by optical phonons, alloy and ionized impurities are the most prevalent scattering mechanisms for $\text{Hg}_{0.72}\text{Cd}_{0.28}\text{Te}$ at 77K, and should therefore always be included in Monte Carlo simulations. The scattering rates for acoustic phonons are significantly lower than the other mechanisms, and could in principle be neglected in Monte Carlo simulations. However, all of the mechanisms mentioned above are always included in the Monte Carlo simulations of this work.

4.2 Monte Carlo simulations

This section contains the results of some Monte Carlo simulations of both electrons and holes in $\text{Hg}_{0.72}\text{Cd}_{0.28}\text{Te}$ at 77K, where the purpose is to show that the implemented Full Band model works properly.

The first simulations were performed without any external field, where the carriers were randomly distributed around the center of the Brillouin zone. Figures 4.9 and 4.10 shows the results from a 5 ps long simulation.

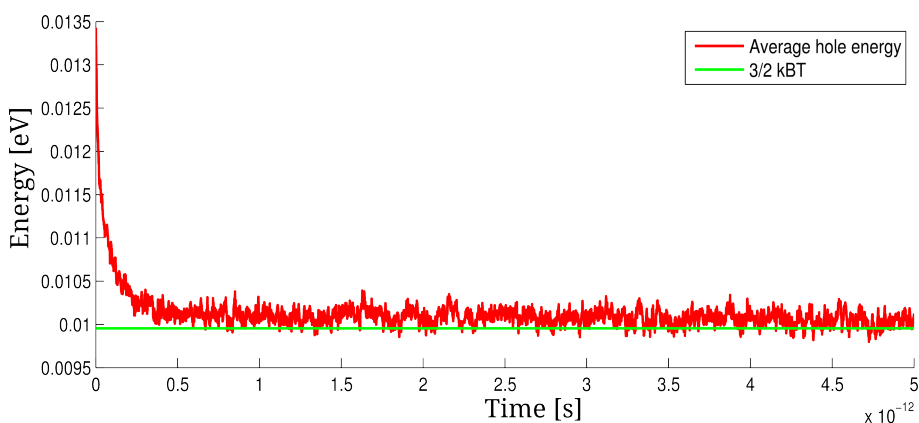


Figure 4.9: Evolution of the average hole energy during a bulk simulation without external fields.

The holes in figure 4.9 seems cool down quickly to an average energy around $\frac{3}{2}k_B T$, that is the theoretical average energy for parabolic bands. But the bands used in this work are not exactly parabolic, so some deviation from $\frac{3}{2}k_B T$ is expected. The average hole energy is also steady after cooling down, showing no sign of artificial heating.

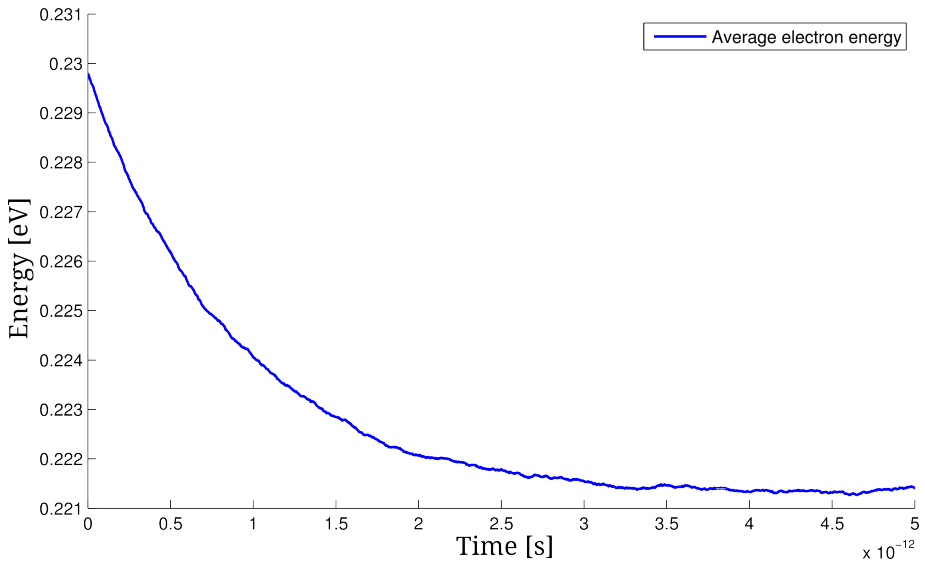
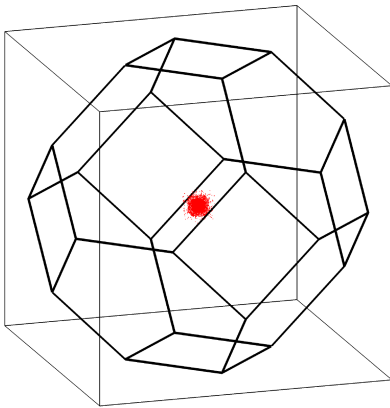
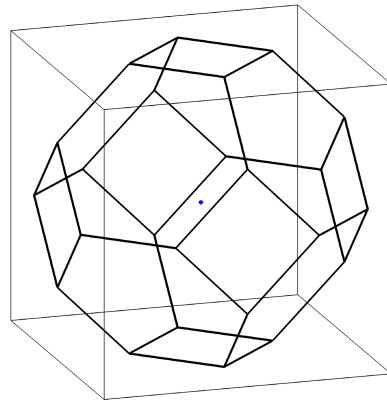


Figure 4.10: Evolution of the average electron energy during a bulk simulation without external fields.

The average electron energy shown in figure 4.10, also cools down fairly quickly to an energy slightly above the band gap energy $E_g = 0.2184$ eV. The cooling down of electrons is considerably slower than for holes, which is expected, since the electron scattering rates are considerably lower than scattering rates for holes.



(a) Distribution of holes (red dots) in 1st BZ at equilibrium (no external fields).



(b) Distribution of electrons (blue dots) in 1st BZ at equilibrium (no external fields).

Similar (but longer) simulations were performed in order to find the equilibrium distribution of electrons and holes. The equilibrium distribution was saved, and used as a starting

point for the other simulations.

Figures 4.11a and 4.11b shows how the electrons and holes are distributed in the 1st Brillouin zone, after the equilibrium is reached. Both types of carriers gather nicely at the zone center, and the magnified versions of the plots shows that the carriers are evenly distributed in all directions. The holes are clearly much more spread out than the electrons, which is exactly what could be expected from the band structure. Most of the holes are located in the heavy-hole band at 77K, that is very "flat" around $\vec{k} = 0$, allowing even the holes with low energies to spread pretty far out from $\vec{k} = 0$. While the conduction band where all the electrons are located, is very "steep" around the zone center, so only electrons with high energy can be found far from $\vec{k} = 0$, which is a rare case at 77K without any external fields.

When an external electric field is applied, the carriers get accelerated by the field and gain more and more energy. The carriers will at the same time get relaxed by phonon emission scattering, but will still have a better chance of gaining high energies. Which means that the carriers get spread further out from the zone center. The actual distributions of carriers in the Brillouin zone for low electric fields in $\text{Hg}_{0.72}\text{Cd}_{0.28}\text{Te}$, is very similar to figures 4.11a and 4.11b. More and more carriers are naturally found further away from $\vec{k} = 0$, but it is difficult to see it from a 3D plot, for low fields. However, the conduction band in $\text{Hg}_{0.72}\text{Cd}_{0.28}\text{Te}$ is anisotropic for high electron energies, which means that the electrons with very high energies will prefer some part of the Brillouin zone over others. This was observed by turning the electric field up as high as 50 kV/cm. Figure 4.11 shows the resulting distributions of electrons.

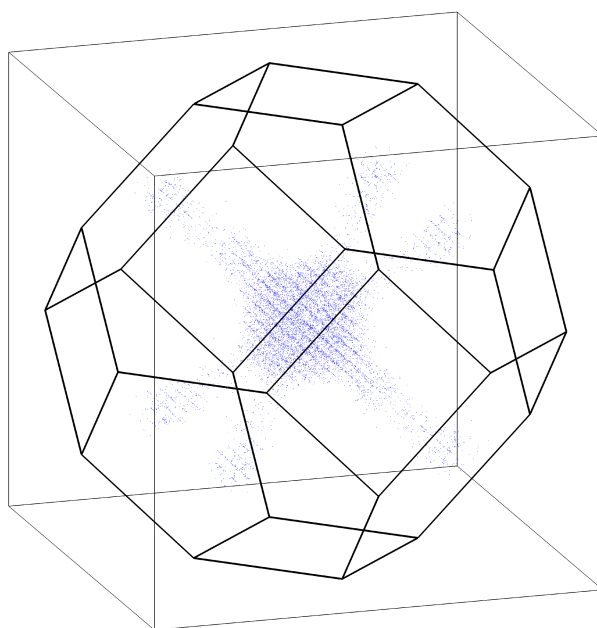


Figure 4.11: Distribution of electrons (blue dots) in 1st BZ at steady state, with electric field at 50 kV/cm in \hat{k}_x direction.

Most of the electrons are still gathered around the center of the 1st BZ, but they spread out a lot more than for low electric fields. Also, quite a few of the electrons are found far away from the zone center, in which case they tend to accumulate towards the L -points. The band plot in figure 3.2 shows that the L -valleys are extremely narrow in the conduction band in MCT, specially compared to the L -valleys in for instance GaAs. However, some of the electrons with high energy are still found in the L -valleys in MCT.

The fact that the electrons seem to be distributed evenly between the 6 L -points, is a clear indication that the carriers wavevector is being properly randomized in scattering events. Figure 4.11 also illustrates one of the strengths of the Full Band model. The fact that the band structure is given over the whole Brillouin zone, allows the carriers to continuously move over the full zone. While analytical band models are often constrained to small parts of the Brillouin zone, and the only way particles can move from one part of the zone to another, is by additional, high q , "intervalley" scattering mechanisms that take care of these "special" events. Particles can thus be transported to different valleys by continuous migration or scattered directly into the valleys by the large-wavevector "intervalley"-phonons. The simulation examples show that migration can on its own be a strong mechanism for L valley occupation.

4.3 Electron Mobility in bulk $\text{Hg}_{0.72}\text{Cd}_{0.28}\text{Te}$

As the previous section showed, the Full Band model appears to be working properly during bulk simulations of $\text{Hg}_{0.72}\text{Cd}_{0.28}\text{Te}$, for both electrons and holes, with and without external electric fields. The program also seems to be stable when it comes to consistency in the reproduced results, as well as the runtime of the simulations. And with that in mind, it was decided to use the Full Band Monte Carlo program to calculate the electron mobility in $\text{Hg}_{0.72}\text{Cd}_{0.28}\text{Te}$.

The simulations were initialized with equilibrium distribution of the electrons, and an external electric field (in \hat{k}_x -direction) was turned on at $t = 0$. The average drift velocity (parallel to the field) of the electrons was measured after the steady state was achieved. Figure 4.12 shows how the average electron velocity is evolving during a simulation, for several different electric fields.

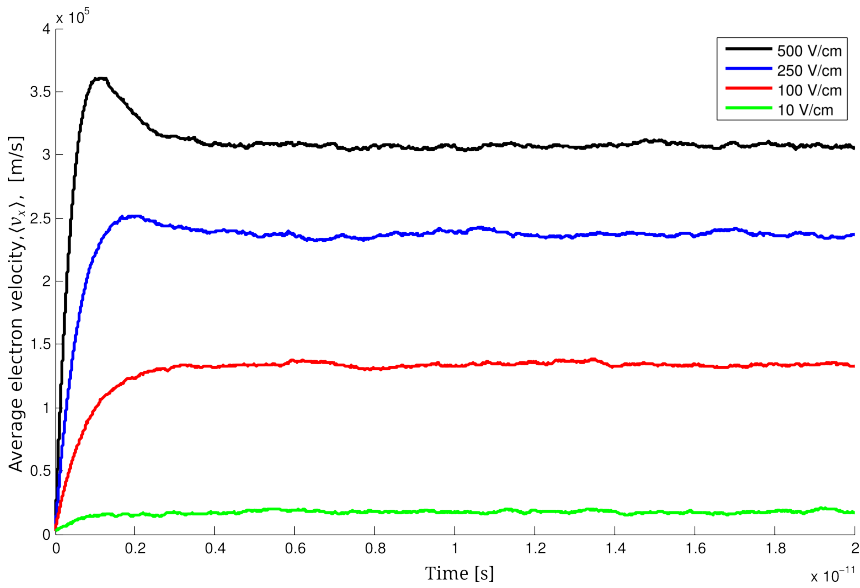


Figure 4.12: Evolution of average electron velocity (parallel to electric field) in time.

The average electron velocity, shown in figure 4.12, increases very quickly before converging the steady state level after approximately 4 ps. Velocity overshoot is observed around 1 – 2 ps into the simulations for electric fields above approximately 250 V/cm. The steady state average electron velocity was measured first after 10 ps into the simulations, in order to be confident that the steady state was actually reached. And a summary of the results are given in table 4.1.

Electric field [V/m]	Drift velocity [m/s]	Calculated mobility [cm^2/Vs]	Number of electrons	Simulation runtime
1000	17628	176280	50000	2h16m54s
2500	40237	160950	50000	2h16m35s
5000	75615	151231	50000	2h20m59s
10000	134402	134402	50000	2h21m52s
15000	177998	118665	50000	2h17m02s
20000	210916	105458	50000	2h18m02s
25000	237462	94985	50000	2h19m41s
30000	257268	85756	50000	2h20m00s
35000	274687	78482	50000	2h21m39s
40000	288084	72021	50000	2h23m14s
45000	299858	66635	50000	2h28m31s
50000	307475	61495	50000	2h30m32s

Table 4.1: Summary of the Monte Carlo simulations that were used to calculate electron mobility in $\text{Hg}_{0.72}\text{Cd}_{0.28}\text{Te}$.

The electron drift velocity is plotted against the electric field in figure 4.13.

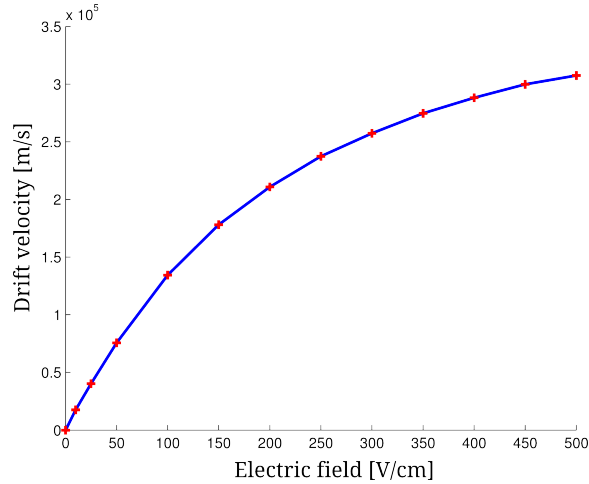


Figure 4.13: Measured electron drift velocity (parallel to electric field), plotted against the electric field.

The resulting velocity-field curve in figure 4.13 is qualitatively very similar to the much cited simulation results reported by Bjørnar Lund [12]. However, the simulations by Lund [12] was performed for the alloy fraction $x = 0.205$ and lower doping. But despite the differences, the resulting velocity-field curve in figure 4.13 seems to be very plausible. The velocity-field curve in figure 4.13 shows that the drift velocity becomes nonlinear at very low electric fields, and the calculated electron mobility (table 4.1) seems to be in a very good agreement with the reported values of $\sim 10^5 \text{ cm}^2/\text{Vs}$. This is another good indication that the Full Band Monte Carlo program is working properly.

The electron mobility calculations in this work were, as mentioned, performed as a part of the testing of the Full Band model. But if the purpose is to actually explore the electron mobility in $\text{Hg}_{0.72}\text{Cd}_{0.28}\text{Te}$, one should consider including degeneracy effects, such as varying screening length and Pauli exclusion principle. A switch for incorporating the Pauli exclusion principle is available in the Monte Carlo program, but it was not possible to test it extensively and properly due to lack of time. A self-consistent screening length calculation was developed for the Monte Carlo program by Øyvind Skåring [13] [14]. As reported by Lund [12], these degeneracy effects seem to significantly affect the electron mobility in HgCdTe .

Conclusions

During this work the following important improvements have been made to the Full Band Monte Carlo program:

- The program is now able to simulate charge transport in $\text{Hg}_{0.72}\text{Cd}_{0.28}\text{Te}$, thanks to introductions of a new *ab initio* numerical band structure.
- All necessary changes has been made to enable simulation of electrons, including:
 - The routine handling the calculation of the scattering rates has been generalized to include calculation of electron scattering rates, in addition to holes.
 - A new routine `escatter` has been written, that takes care of electron scattering.
 - The routine that selects final states has been modified to find final states for electrons in the conduction band.
- Major improvements have been made to the routine that selects final states:
 - The high-precision method, that was proposed in the specialization project [1] to select final states with proper energy, has been implemented.
 - The q -dependence of the final energy has been included in selection of final cubes.
 - The routine has been generalized, and now automatically recognizes the final band and type of carrier, based on the initial state and the chosen scattering mechanism.
- The layout of the underlying cubic mesh of discrete points has been changed to a more intuitive and convenient layout. And all of the interpolation routines have been adapted accordingly.
- The routine handling the calculation of scattering rates has been modified to use interpolated quantities. Which allows the layout of the cubes, that are used in these calculations, to be independent of the mesh points.

-
- Mobility calculations have been enabled for both electrons and holes.

However, the most important achievement that was accomplished during this work, is a stable and properly working Full Band Monte Carlo program, capable of simulating both electrons and holes in bulk $\text{Hg}_{0.72}\text{Cd}_{0.28}\text{Te}$. The program is also capable of calculating bulk mobility, producing plausible and acceptable results.

5.1 Future work

Even though the Monte Carlo software has been significantly improved during this work, there is still a lot of room for further development and improvement. Some suggestions for the future work are presented below:

- Include the *ab initio* wavefunctions, produced by ABINIT [2] (or other software), in the calculation of the overlap factors.
- The selection of final cubes could be done more effectively by a better estimation of the maximum value for the cube weights. This could significantly reduce the simulation runtime, and should therefore be considered.
- Allow the scattering events to take place at arbitrary times between the time steps, by properly implementing the Yorston Method.
- Include effects such as hot-phonons and Pauli exclusion principle. Both effects were available in the analytical version of the program, and implementing these into the Full Band version should be a fairly manageable task.
- Some of the main parts of the program, such as calculations of scattering rates and selection of final cubes, are very CPU intensive. However, these parts consists of many smaller independent calculations, and could in principle be performed in parallel to reduce the runtime. Parallel parts of the program should be considered if the simulations become very long.
- A recently published article [15] (dated May 19, 2014!), addresses how supercell electronic structures can be "unfolded" back to a standard zincblende Brillouin zone (used in the MC program). This long awaited approach opens up the opportunity to get the band structure for alloy compounds from the widely used supercell calculations, and such "backfolder" was already requested by Bjørnar Karlsen [3]. It should be very interesting to test this new approach, not only for the purpose of this MC program, but also in a MC context on a worldwide basis.

Bibliography

- [1] Juri Selvåg. High precision method for energy conserving post-scattering states in a Full Band Monte Carlo charge transport model. Specialization project, Norwegian University of Science and Technology, 2013.
- [2] Program ABINIT, <http://www.abinit.org/>.
- [3] Bjørnar Karlsen. Calculation of phonon and alloy scattering rates in zincblende structure semiconductors using 14×14 kp and "ab initio" pseudopotential methods. Master's thesis, Norwegian University of Science and Technology, 2013.
- [4] Ronald M Yorston. Free-flight time generation in the monte carlo simulation of carrier transport in semiconductors. *Journal of computational physics*, 64(1):177–194, 1986.
- [5] Einar Halvorsen. Numerical calculation of valence band and hole scattering rates in gaas. Master's thesis, Norges Tekniske Høgskole, 1991.
- [6] Program WIEN2k, <http://www.wien2k.at/>.
- [7] Massimo V Fischetti and Steven E Laux. Monte carlo analysis of electron transport in small semiconductor devices including band-structure and space-charge effects. *Physical Review B*, 38(14):9721, 1988.
- [8] G Gilat and LJ Raubenheimer. Accurate numerical method for calculating frequency-distribution functions in solids. *Physical Review*, 144(2):390, 1966.
- [9] T Brudevoll, TA Fjeldly, J Baek, and MS Shur. Scattering rates for holes near the valence-band edge in semiconductors. *Journal of applied physics*, 67(12):7373–7382, 1990.
- [10] Brian K Ridley. *Quantum processes in semiconductors*. Oxford University Press, 2013.
- [11] Tore Sivertsen Bergslid. Implementing a full-band monte carlo model for zincblende structure semiconductors. Master's thesis, Norwegian University of Science and Technology, 2013.

-
- [12] Bjørnar Lund. *Monte Carlo simulation of charge transport in semiconductors and semiconductor devices*. PhD thesis, The Norwegian Institute of Technology, 1992.
- [13] Øyvind Skåring. Hot phonon, carrier-carrier, and dynamic screening algorithms for semiconductor simulation. Specialization project, Norwegian University of Science and Technology, 2009.
- [14] Øyvind Skåring. Ultrashort relaxation dynamics in laser excited semiconductors. Master's thesis, Norwegian University of Science and Technology, 2010.
- [15] O Rubel, A Bokhanchuk, SJ Ahmed, and E Assmann. Unfolding the band structure of disordered solids: from localization to high-mobility kane fermions. *arXiv preprint arXiv:1405.4218*, 2014.

Appendix A: List of parameters

The table below contains a list of parameters that are used in scattering rate calculations and in the Monte Carlo simulations of the present work.

Symbol	Value	Variable	Explanation
T	77 K	T	Temperature
x	0.28	XFRAC	Alloy fraction of CdTe
ρ	7.406 g/cm ³	RHO	Mass density
ε_∞	12.25	EPSINF	High frequency relative dielectric constant
ε_s	16.58	EPSS	Low frequency relative dielectric constant
$\hbar\omega_0$	0.0178 eV	HW0	Optical phonon energy
N_i	$1.0 \cdot 10^{17}$ cm ⁻³	NIMP	Concentration of ionized impurities
E_1	7.00eV/5.60eV	D(2)	Acoustic deformation potential (for GaAs) (electrons/holes)
v_s	4570 m/s	S	Average sound velocity
$(DK)^2$	$3.16 \cdot 10^3$ eV ² /Å ²	DKSQR	Squared optical phonon coupling constant
DV	1.5 eV/0.3 eV	DV(2)	Alloy scattering potential (electrons/holes)
Δt	$1.0 \cdot 10^{-15}$ s	TIME	Simulation time step
–	$1.0 \cdot 10^{-6}$ eV	FETOL	Energy tolerance used in high precision selection of final states

Appendix B: Expressions for the coefficients

As stated in section 3.5.2, the energy along any of the 7 lines can be written in the form $E(x) = C_0 + C_1x + C_2x^2 + C_3x^3 + C_4x^4 + C_5x^5$.

The coefficients are of course different for different lines, and the expressions for all of them are presented below. The lines are identified by the parametrization is of $(\Delta k_x, \Delta k_y, \Delta k_z)$, expressed by the free variable x and the side length of the final cubes l .

The coefficients are generally found by inserting the parametrization of any straight line, $(\Delta k_x, \Delta k_y, \Delta k_z)$, into equation 3.34 and collecting terms.

Line number 1: $\vec{\Delta k} = (\Delta k_x, \Delta k_y, \Delta k_z)$ is given by $(x, \frac{l}{2}, \frac{l}{2})$

$$\begin{aligned}
 C_0 = & \frac{1}{4}E_n(\vec{k}_4) - \frac{l}{8} \frac{\partial E_n}{\partial k_y} \Big|_{\vec{k}_8} - \frac{l}{8} \frac{\partial E_n}{\partial k_z} \Big|_{\vec{k}_8} + \frac{l^2}{32} \frac{\partial^2 E_n}{\partial k_y^2} \Big|_{\vec{k}_8} + \frac{l^2}{32} \frac{\partial^2 E_n}{\partial k_z^2} \Big|_{\vec{k}_8} + \frac{l^2}{16} \frac{\partial^2 E_n}{\partial k_y \partial k_z} \Big|_{\vec{k}_8} \\
 & + \frac{l}{8} \frac{\partial E_n}{\partial k_y} \Big|_{\vec{k}_1} + \frac{l}{8} \frac{\partial E_n}{\partial k_z} \Big|_{\vec{k}_1} + \frac{l^2}{32} \frac{\partial^2 E_n}{\partial k_y^2} \Big|_{\vec{k}_1} + \frac{l^2}{32} \frac{\partial^2 E_n}{\partial k_z^2} \Big|_{\vec{k}_1} + \frac{l^2}{16} \frac{\partial^2 E_n}{\partial k_y \partial k_z} \Big|_{\vec{k}_1} - \frac{l}{8} \frac{\partial E_n}{\partial k_y} \Big|_{\vec{k}_4} \\
 & + \frac{l}{8} \frac{\partial E_n}{\partial k_z} \Big|_{\vec{k}_4} + \frac{l^2}{32} \frac{\partial^2 E_n}{\partial k_y^2} \Big|_{\vec{k}_4} + \frac{l^2}{32} \frac{\partial^2 E_n}{\partial k_z^2} \Big|_{\vec{k}_4} - \frac{l^2}{16} \frac{\partial^2 E_n}{\partial k_y \partial k_z} \Big|_{\vec{k}_4} + \frac{l}{8} \frac{\partial E_n}{\partial k_y} \Big|_{\vec{k}_5} - \frac{l}{8} \frac{\partial E_n}{\partial k_z} \Big|_{\vec{k}_5} \\
 & + \frac{l^2}{32} \frac{\partial^2 E_n}{\partial k_y^2} \Big|_{\vec{k}_5} + \frac{l^2}{32} \frac{\partial^2 E_n}{\partial k_z^2} \Big|_{\vec{k}_5} - \frac{l^2}{16} \frac{\partial^2 E_n}{\partial k_y \partial k_z} \Big|_{\vec{k}_5} + \frac{1}{4}E_n(\vec{k}_8) + \frac{1}{4}E_n(\vec{k}_1) + \frac{1}{4}E_n(\vec{k}_5)
 \end{aligned}$$

$$\begin{aligned}
C_2 = & \frac{1}{8} \frac{\partial^2 E_n}{\partial k_x^2} \Big|_{\vec{k}_5} - \frac{1}{8} \frac{\partial^2 E_n}{\partial k_x \partial k_y} \Big|_{\vec{k}_5} + \frac{1}{8} \frac{\partial^2 E_n}{\partial k_z \partial k_x} \Big|_{\vec{k}_5} - \frac{1}{4l} \frac{\partial E_n}{\partial k_x} \Big|_{\vec{k}_1} + \frac{1}{4l} \frac{\partial E_n}{\partial k_x} \Big|_{\vec{k}_2} + \frac{1}{4l} \frac{\partial E_n}{\partial k_x} \Big|_{\vec{k}_3} \\
& - \frac{1}{4l} \frac{\partial E_n}{\partial k_x} \Big|_{\vec{k}_4} - \frac{1}{4l} \frac{\partial E_n}{\partial k_x} \Big|_{\vec{k}_5} + \frac{1}{4l} \frac{\partial E_n}{\partial k_x} \Big|_{\vec{k}_6} + \frac{1}{4l} \frac{\partial E_n}{\partial k_x} \Big|_{\vec{k}_7} - \frac{1}{4l} \frac{\partial E_n}{\partial k_x} \Big|_{\vec{k}_8} + \frac{1}{8} \frac{\partial^2 E_n}{\partial k_x^2} \Big|_{\vec{k}_4} \\
& + \frac{1}{8} \frac{\partial^2 E_n}{\partial k_x \partial k_y} \Big|_{\vec{k}_4} - \frac{1}{8} \frac{\partial^2 E_n}{\partial k_z \partial k_x} \Big|_{\vec{k}_4} - \frac{1}{4} \frac{\partial^2 E_n}{\partial k_x^2} \Big|_{\vec{k}_7} - \frac{1}{8} \frac{\partial^2 E_n}{\partial k_x \partial k_y} \Big|_{\vec{k}_7} - \frac{1}{8} \frac{\partial^2 E_n}{\partial k_z \partial k_x} \Big|_{\vec{k}_7} \\
& - \frac{1}{4} \frac{\partial^2 E_n}{\partial k_x^2} \Big|_{\vec{k}_3} - \frac{1}{8} \frac{\partial^2 E_n}{\partial k_x \partial k_y} \Big|_{\vec{k}_3} + \frac{1}{8} \frac{\partial^2 E_n}{\partial k_z \partial k_x} \Big|_{\vec{k}_3} + \frac{1}{8} \frac{\partial^2 E_n}{\partial k_x^2} \Big|_{\vec{k}_8} + \frac{1}{8} \frac{\partial^2 E_n}{\partial k_x \partial k_y} \Big|_{\vec{k}_8} \\
& + \frac{1}{8} \frac{\partial^2 E_n}{\partial k_z \partial k_x} \Big|_{\vec{k}_8} - \frac{1}{4} \frac{\partial^2 E_n}{\partial k_x^2} \Big|_{\vec{k}_2} + \frac{1}{8} \frac{\partial^2 E_n}{\partial k_x \partial k_y} \Big|_{\vec{k}_2} + \frac{1}{8} \frac{\partial^2 E_n}{\partial k_z \partial k_x} \Big|_{\vec{k}_2} + \frac{1}{8} \frac{\partial^2 E_n}{\partial k_x^2} \Big|_{\vec{k}_1} \\
& - \frac{1}{8} \frac{\partial^2 E_n}{\partial k_x \partial k_y} \Big|_{\vec{k}_1} - \frac{1}{8} \frac{\partial^2 E_n}{\partial k_z \partial k_x} \Big|_{\vec{k}_1} - \frac{1}{4} \frac{\partial^2 E_n}{\partial k_x^2} \Big|_{\vec{k}_6} + \frac{1}{8} \frac{\partial^2 E_n}{\partial k_x \partial k_y} \Big|_{\vec{k}_6} - \frac{1}{8} \frac{\partial^2 E_n}{\partial k_z \partial k_x} \Big|_{\vec{k}_6}
\end{aligned}$$

$$\begin{aligned}
C_3 = & \frac{1}{8l} \frac{\partial^2 E_n}{\partial k_x^2} \Big|_{\vec{k}_7} + \frac{1}{8l} \frac{\partial^2 E_n}{\partial k_x^2} \Big|_{\vec{k}_2} - \frac{1}{8l} \frac{\partial^2 E_n}{\partial k_x^2} \Big|_{\vec{k}_4} + \frac{1}{8l} \frac{\partial^2 E_n}{\partial k_x^2} \Big|_{\vec{k}_6} \\
& - \frac{1}{8l} \frac{\partial^2 E_n}{\partial k_x^2} \Big|_{\vec{k}_1} - \frac{1}{8l} \frac{\partial^2 E_n}{\partial k_x^2} \Big|_{\vec{k}_8} - \frac{1}{8l} \frac{\partial^2 E_n}{\partial k_x^2} \Big|_{\vec{k}_5} + \frac{1}{8l} \frac{\partial^2 E_n}{\partial k_x^2} \Big|_{\vec{k}_3}
\end{aligned}$$

$$C_4 = 0$$

$$C_5 = 0$$

Line number 2: $\vec{\Delta}k = (\Delta k_x, \Delta k_y, \Delta k_z)$ is given by $(\frac{l}{2}, x, \frac{l}{2})$

$$\begin{aligned}
C_0 = & \frac{1}{4} E_n(\vec{k}_5) + \frac{1}{4} E_n(\vec{k}_6) + \frac{1}{4} E_n(\vec{k}_2) + \frac{1}{4} E_n(\vec{k}_1) + \frac{l^2}{16} \frac{\partial^2 E_n}{\partial k_z \partial k_x} \Big|_{\vec{k}_6} \\
& + \frac{l^2}{16} \frac{\partial^2 E_n}{\partial k_z \partial k_x} \Big|_{\vec{k}_1} + \frac{l}{8} \frac{\partial E_n}{\partial k_x} \Big|_{\vec{k}_1} + \frac{l^2}{32} \frac{\partial^2 E_n}{\partial k_x^2} \Big|_{\vec{k}_1} + \frac{l}{8} \frac{\partial E_n}{\partial k_z} \Big|_{\vec{k}_1} + \frac{l^2}{32} \frac{\partial^2 E_n}{\partial k_x^2} \Big|_{\vec{k}_2} \\
& - \frac{l}{8} \frac{\partial E_n}{\partial k_z} \Big|_{\vec{k}_5} - \frac{l}{8} \frac{\partial E_n}{\partial k_x} \Big|_{\vec{k}_2} + \frac{l}{8} \frac{\partial E_n}{\partial k_z} \Big|_{\vec{k}_2} + \frac{l^2}{32} \frac{\partial^2 E_n}{\partial k_z^2} \Big|_{\vec{k}_6} - \frac{l}{8} \frac{\partial E_n}{\partial k_z} \Big|_{\vec{k}_6} \\
& + \frac{l^2}{32} \frac{\partial^2 E_n}{\partial k_z^2} \Big|_{\vec{k}_2} - \frac{l^2}{16} \frac{\partial^2 E_n}{\partial k_z \partial k_x} \Big|_{\vec{k}_2} + \frac{l}{8} \frac{\partial E_n}{\partial k_x} \Big|_{\vec{k}_5} + \frac{l^2}{32} \frac{\partial^2 E_n}{\partial k_z^2} \Big|_{\vec{k}_1} \\
& + \frac{l^2}{32} \frac{\partial^2 E_n}{\partial k_x^2} \Big|_{\vec{k}_5} + \frac{l^2}{32} \frac{\partial^2 E_n}{\partial k_z^2} \Big|_{\vec{k}_5} - \frac{l^2}{16} \frac{\partial^2 E_n}{\partial k_z \partial k_x} \Big|_{\vec{k}_5} - \frac{l}{8} \frac{\partial E_n}{\partial k_x} \Big|_{\vec{k}_6} + \frac{l^2}{32} \frac{\partial^2 E_n}{\partial k_x^2} \Big|_{\vec{k}_6}
\end{aligned}$$

$$\begin{aligned}
C_2 = & \frac{1}{4l} \frac{\partial E_n}{\partial k_y} \Big|_{\vec{k}_8} - \frac{1}{4l} \frac{\partial E_n}{\partial k_y} \Big|_{\vec{k}_5} - \frac{1}{4l} \frac{\partial E_n}{\partial k_y} \Big|_{\vec{k}_6} + \frac{1}{4l} \frac{\partial E_n}{\partial k_y} \Big|_{\vec{k}_7} - \frac{1}{4l} \frac{\partial E_n}{\partial k_y} \Big|_{\vec{k}_2} \\
& + \frac{1}{4l} \frac{\partial E_n}{\partial k_y} \Big|_{\vec{k}_3} + \frac{1}{4l} \frac{\partial E_n}{\partial k_y} \Big|_{\vec{k}_4} - \frac{1}{4l} \frac{\partial E_n}{\partial k_y} \Big|_{\vec{k}_1} + \frac{1}{8} \frac{\partial^2 E_n}{\partial k_y^2} \Big|_{\vec{k}_5} - \frac{1}{8} \frac{\partial^2 E_n}{\partial k_x \partial k_y} \Big|_{\vec{k}_5} \\
& + \frac{1}{8} \frac{\partial^2 E_n}{\partial k_y \partial k_z} \Big|_{\vec{k}_5} - \frac{1}{4} \frac{\partial^2 E_n}{\partial k_y^2} \Big|_{\vec{k}_4} + \frac{1}{8} \frac{\partial^2 E_n}{\partial k_x \partial k_y} \Big|_{\vec{k}_4} + \frac{1}{8} \frac{\partial^2 E_n}{\partial k_y \partial k_z} \Big|_{\vec{k}_4} - \frac{1}{4} \frac{\partial^2 E_n}{\partial k_y^2} \Big|_{\vec{k}_7} \\
& - \frac{1}{8} \frac{\partial^2 E_n}{\partial k_x \partial k_y} \Big|_{\vec{k}_7} - \frac{1}{8} \frac{\partial^2 E_n}{\partial k_y \partial k_z} \Big|_{\vec{k}_7} - \frac{1}{4} \frac{\partial^2 E_n}{\partial k_y^2} \Big|_{\vec{k}_3} - \frac{1}{8} \frac{\partial^2 E_n}{\partial k_x \partial k_y} \Big|_{\vec{k}_3} \\
& + \frac{1}{8} \frac{\partial^2 E_n}{\partial k_y \partial k_z} \Big|_{\vec{k}_3} - \frac{1}{4} \frac{\partial^2 E_n}{\partial k_y^2} \Big|_{\vec{k}_8} + \frac{1}{8} \frac{\partial^2 E_n}{\partial k_x \partial k_y} \Big|_{\vec{k}_8} - \frac{1}{8} \frac{\partial^2 E_n}{\partial k_y \partial k_z} \Big|_{\vec{k}_8} + \frac{1}{8} \frac{\partial^2 E_n}{\partial k_y^2} \Big|_{\vec{k}_2} \\
& + \frac{1}{8} \frac{\partial^2 E_n}{\partial k_x \partial k_y} \Big|_{\vec{k}_2} - \frac{1}{8} \frac{\partial^2 E_n}{\partial k_y \partial k_z} \Big|_{\vec{k}_2} + \frac{1}{8} \frac{\partial^2 E_n}{\partial k_y^2} \Big|_{\vec{k}_1} - \frac{1}{8} \frac{\partial^2 E_n}{\partial k_x \partial k_y} \Big|_{\vec{k}_1} \\
& - \frac{1}{8} \frac{\partial^2 E_n}{\partial k_y \partial k_z} \Big|_{\vec{k}_1} + \frac{1}{8} \frac{\partial^2 E_n}{\partial k_y^2} \Big|_{\vec{k}_6} + \frac{1}{8} \frac{\partial^2 E_n}{\partial k_x \partial k_y} \Big|_{\vec{k}_6} + \frac{1}{8} \frac{\partial^2 E_n}{\partial k_y \partial k_z} \Big|_{\vec{k}_6}
\end{aligned}$$

$$\begin{aligned}
C_3 = & -\frac{1}{8l} \frac{\partial^2 E_n}{\partial k_y^2} \Big|_{\vec{k}_6} + \frac{1}{8l} \frac{\partial^2 E_n}{\partial k_y^2} \Big|_{\vec{k}_8} + \frac{1}{8l} \frac{\partial^2 E_n}{\partial k_y^2} \Big|_{\vec{k}_4} - \frac{1}{8l} \frac{\partial^2 E_n}{\partial k_y^2} \Big|_{\vec{k}_2} \\
& - \frac{1}{8l} \frac{\partial^2 E_n}{\partial k_y^2} \Big|_{\vec{k}_5} + \frac{1}{8l} \frac{\partial^2 E_n}{\partial k_y^2} \Big|_{\vec{k}_7} + \frac{1}{8l} \frac{\partial^2 E_n}{\partial k_y^2} \Big|_{\vec{k}_3} - \frac{1}{8l} \frac{\partial^2 E_n}{\partial k_y^2} \Big|_{\vec{k}_1}
\end{aligned}$$

$$C_4 = 0$$

$$C_5 = 0$$

Line number 3: $\vec{\Delta}k = (\Delta k_x, \Delta k_y, \Delta k_z)$ is given by $(\frac{l}{2}, \frac{l}{2}, x)$

$$\begin{aligned}
C_0 = & \frac{l}{8} \frac{\partial E_n}{\partial k_x} \Big|_{\vec{k}_1} + \frac{l^2}{32} \frac{\partial^2 E_n}{\partial k_x^2} \Big|_{\vec{k}_1} - \frac{l}{8} \frac{\partial E_n}{\partial k_x} \Big|_{\vec{k}_2} + \frac{l^2}{32} \frac{\partial^2 E_n}{\partial k_x^2} \Big|_{\vec{k}_2} + \frac{l^2}{16} \frac{\partial^2 E_n}{\partial k_x \partial k_y} \Big|_{\vec{k}_1} \\
& + \frac{l}{8} \frac{\partial E_n}{\partial k_y} \Big|_{\vec{k}_2} + \frac{l^2}{32} \frac{\partial^2 E_n}{\partial k_y^2} \Big|_{\vec{k}_2} - \frac{l^2}{16} \frac{\partial^2 E_n}{\partial k_x \partial k_y} \Big|_{\vec{k}_2} - \frac{l}{8} \frac{\partial E_n}{\partial k_x} \Big|_{\vec{k}_3} - \frac{l}{8} \frac{\partial E_n}{\partial k_y} \Big|_{\vec{k}_3} \\
& + \frac{l^2}{32} \frac{\partial^2 E_n}{\partial k_x^2} \Big|_{\vec{k}_3} + \frac{l^2}{32} \frac{\partial^2 E_n}{\partial k_y^2} \Big|_{\vec{k}_3} + \frac{l^2}{16} \frac{\partial^2 E_n}{\partial k_x \partial k_y} \Big|_{\vec{k}_3} + \frac{l}{8} \frac{\partial E_n}{\partial k_x} \Big|_{\vec{k}_4} \\
& + \frac{l^2}{32} \frac{\partial^2 E_n}{\partial k_x^2} \Big|_{\vec{k}_4} - \frac{l^2}{16} \frac{\partial^2 E_n}{\partial k_x \partial k_y} \Big|_{\vec{k}_4} + \frac{1}{4} E_n(\vec{k}_4) + \frac{l}{8} \frac{\partial E_n}{\partial k_y} \Big|_{\vec{k}_1} + \frac{l^2}{32} \frac{\partial^2 E_n}{\partial k_y^2} \Big|_{\vec{k}_1} \\
& - \frac{l}{8} \frac{\partial E_n}{\partial k_y} \Big|_{\vec{k}_4} + \frac{l^2}{32} \frac{\partial^2 E_n}{\partial k_y^2} \Big|_{\vec{k}_4} + \frac{1}{4} E_n(\vec{k}_3) + \frac{1}{4} E_n(\vec{k}_2) + \frac{1}{4} E_n(\vec{k}_1)
\end{aligned}$$

$$\begin{aligned}
C_2 = & \frac{1}{4l} \frac{\partial E_n}{\partial k_z} \Big|_{\vec{k}_7} + \frac{1}{4l} \frac{\partial E_n}{\partial k_z} \Big|_{\vec{k}_8} - \frac{1}{4l} \frac{\partial E_n}{\partial k_z} \Big|_{\vec{k}_3} - \frac{1}{4l} \frac{\partial E_n}{\partial k_z} \Big|_{\vec{k}_4} + \frac{1}{4l} \frac{\partial E_n}{\partial k_z} \Big|_{\vec{k}_5} \\
& - \frac{1}{4l} \frac{\partial E_n}{\partial k_z} \Big|_{\vec{k}_1} - \frac{1}{4l} \frac{\partial E_n}{\partial k_z} \Big|_{\vec{k}_2} + \frac{1}{4l} \frac{\partial E_n}{\partial k_z} \Big|_{\vec{k}_6} - \frac{1}{4} \frac{\partial^2 E_n}{\partial k_z^2} \Big|_{\vec{k}_5} + \frac{1}{8} \frac{\partial^2 E_n}{\partial k_y \partial k_z} \Big|_{\vec{k}_5} \\
& + \frac{1}{8} \frac{\partial^2 E_n}{\partial k_z \partial k_x} \Big|_{\vec{k}_5} + \frac{1}{8} \frac{\partial^2 E_n}{\partial k_z^2} \Big|_{\vec{k}_4} + \frac{1}{8} \frac{\partial^2 E_n}{\partial k_y \partial k_z} \Big|_{\vec{k}_4} - \frac{1}{8} \frac{\partial^2 E_n}{\partial k_z \partial k_x} \Big|_{\vec{k}_4} \\
& - \frac{1}{4} \frac{\partial^2 E_n}{\partial k_z^2} \Big|_{\vec{k}_7} - \frac{1}{8} \frac{\partial^2 E_n}{\partial k_y \partial k_z} \Big|_{\vec{k}_7} - \frac{1}{8} \frac{\partial^2 E_n}{\partial k_z \partial k_x} \Big|_{\vec{k}_7} + \frac{1}{8} \frac{\partial^2 E_n}{\partial k_z^2} \Big|_{\vec{k}_3} + \frac{1}{8} \frac{\partial^2 E_n}{\partial k_y \partial k_z} \Big|_{\vec{k}_3} \\
& + \frac{1}{8} \frac{\partial^2 E_n}{\partial k_z \partial k_x} \Big|_{\vec{k}_3} - \frac{1}{4} \frac{\partial^2 E_n}{\partial k_z^2} \Big|_{\vec{k}_8} - \frac{1}{8} \frac{\partial^2 E_n}{\partial k_y \partial k_z} \Big|_{\vec{k}_8} + \frac{1}{8} \frac{\partial^2 E_n}{\partial k_z \partial k_x} \Big|_{\vec{k}_8} \\
& + \frac{1}{8} \frac{\partial^2 E_n}{\partial k_z^2} \Big|_{\vec{k}_2} - \frac{1}{8} \frac{\partial^2 E_n}{\partial k_y \partial k_z} \Big|_{\vec{k}_2} + \frac{1}{8} \frac{\partial^2 E_n}{\partial k_z \partial k_x} \Big|_{\vec{k}_2} + \frac{1}{8} \frac{\partial^2 E_n}{\partial k_z^2} \Big|_{\vec{k}_1} - \frac{1}{8} \frac{\partial^2 E_n}{\partial k_y \partial k_z} \Big|_{\vec{k}_1} \\
& - \frac{1}{8} \frac{\partial^2 E_n}{\partial k_z \partial k_x} \Big|_{\vec{k}_1} - \frac{1}{4} \frac{\partial^2 E_n}{\partial k_z^2} \Big|_{\vec{k}_6} + \frac{1}{8} \frac{\partial^2 E_n}{\partial k_y \partial k_z} \Big|_{\vec{k}_6} - \frac{1}{8} \frac{\partial^2 E_n}{\partial k_z \partial k_x} \Big|_{\vec{k}_6}
\end{aligned}$$

$$\begin{aligned}
C_3 = & \frac{1}{8l} \frac{\partial^2 E_n}{\partial k_z^2} \Big|_{\vec{k}_8} - \frac{1}{8l} \frac{\partial^2 E_n}{\partial k_z^2} \Big|_{\vec{k}_3} + \frac{1}{8l} \frac{\partial^2 E_n}{\partial k_z^2} \Big|_{\vec{k}_7} + \frac{1}{8l} \frac{\partial^2 E_n}{\partial k_z^2} \Big|_{\vec{k}_5} \\
& - \frac{1}{8l} \frac{\partial^2 E_n}{\partial k_z^2} \Big|_{\vec{k}_2} + \frac{1}{8l} \frac{\partial^2 E_n}{\partial k_z^2} \Big|_{\vec{k}_6} - \frac{1}{8l} \frac{\partial^2 E_n}{\partial k_z^2} \Big|_{\vec{k}_4} - \frac{1}{8l} \frac{\partial^2 E_n}{\partial k_z^2} \Big|_{\vec{k}_1}
\end{aligned}$$

$$C_4 = 0$$

$$C_5 = 0$$

Line number 4: $\vec{\Delta k} = (\Delta k_x, \Delta k_y, \Delta k_z)$ is given by (x, x, x)

$$C_0 = E_n(\vec{k}_1)$$

$$\begin{aligned}
C_1 = & -\frac{3}{l} E_n(\vec{k}_1) + \frac{1}{l} E_n(\vec{k}_5) + \frac{1}{l} E_n(\vec{k}_2) - \frac{\partial E_n}{\partial k_z} \Big|_{\vec{k}_5} + \frac{\partial E_n}{\partial k_z} \Big|_{\vec{k}_1} + \frac{l}{2} \frac{\partial^2 E_n}{\partial k_x^2} \Big|_{\vec{k}_2} \\
& + \frac{l}{2} \frac{\partial^2 E_n}{\partial k_z^2} \Big|_{\vec{k}_5} + \frac{\partial E_n}{\partial k_y} \Big|_{\vec{k}_1} - \frac{\partial E_n}{\partial k_y} \Big|_{\vec{k}_4} - \frac{\partial E_n}{\partial k_x} \Big|_{\vec{k}_2} + \frac{1}{l} E_n(\vec{k}_4) + \frac{\partial E_n}{\partial k_x} \Big|_{\vec{k}_1} + \frac{l}{2} \frac{\partial^2 E_n}{\partial k_y^2} \Big|_{\vec{k}_4}
\end{aligned}$$

$$\begin{aligned}
C_2 = & -\frac{2}{l^2} E_n(\vec{k}_5) + \frac{1}{l^2} E_n(\vec{k}_3) + \frac{1}{l^2} E_n(\vec{k}_8) + \frac{1}{l^2} E_n(\vec{k}_6) - \frac{2}{l^2} E_n(\vec{k}_4) + \frac{3}{l^2} E_n(\vec{k}_1) \\
& - \frac{2}{l^2} E_n(\vec{k}_2) - \frac{1}{l} \frac{\partial E_n}{\partial k_y} \Big|_{\vec{k}_8} + \frac{1}{l} \frac{\partial E_n}{\partial k_y} \Big|_{\vec{k}_5} + \frac{1}{l} \frac{\partial E_n}{\partial k_y} \Big|_{\vec{k}_2} - \frac{1}{l} \frac{\partial E_n}{\partial k_y} \Big|_{\vec{k}_3} + \frac{3}{l} \frac{\partial E_n}{\partial k_y} \Big|_{\vec{k}_4} \\
& - \frac{3}{l} \frac{\partial E_n}{\partial k_y} \Big|_{\vec{k}_1} - \frac{1}{l} \frac{\partial E_n}{\partial k_z} \Big|_{\vec{k}_8} + \frac{1}{l} \frac{\partial E_n}{\partial k_z} \Big|_{\vec{k}_4} + \frac{3}{l} \frac{\partial E_n}{\partial k_z} \Big|_{\vec{k}_5} - \frac{3}{l} \frac{\partial E_n}{\partial k_z} \Big|_{\vec{k}_1} + \frac{1}{l} \frac{\partial E_n}{\partial k_z} \Big|_{\vec{k}_2} \\
& - \frac{1}{l} \frac{\partial E_n}{\partial k_z} \Big|_{\vec{k}_6} - 2 \frac{\partial^2 E_n}{\partial k_z^2} \Big|_{\vec{k}_5} - \frac{\partial^2 E_n}{\partial k_y \partial k_z} \Big|_{\vec{k}_5} - \frac{\partial^2 E_n}{\partial k_z \partial k_x} \Big|_{\vec{k}_5} - \frac{3}{l} \frac{\partial E_n}{\partial k_x} \Big|_{\vec{k}_1} \\
& + \frac{3}{l} \frac{\partial E_n}{\partial k_x} \Big|_{\vec{k}_2} - \frac{1}{l} \frac{\partial E_n}{\partial k_x} \Big|_{\vec{k}_3} + \frac{1}{l} \frac{\partial E_n}{\partial k_x} \Big|_{\vec{k}_4} + \frac{1}{l} \frac{\partial E_n}{\partial k_x} \Big|_{\vec{k}_5} - \frac{1}{l} \frac{\partial E_n}{\partial k_x} \Big|_{\vec{k}_6} - 2 \frac{\partial^2 E_n}{\partial k_y^2} \Big|_{\vec{k}_4} \\
& - \frac{\partial^2 E_n}{\partial k_x \partial k_y} \Big|_{\vec{k}_4} - \frac{\partial^2 E_n}{\partial k_y \partial k_z} \Big|_{\vec{k}_4} + \frac{1}{2} \frac{\partial^2 E_n}{\partial k_x^2} \Big|_{\vec{k}_3} + \frac{1}{2} \frac{\partial^2 E_n}{\partial k_y^2} \Big|_{\vec{k}_3} + \frac{\partial^2 E_n}{\partial k_x \partial k_y} \Big|_{\vec{k}_3} \\
& + \frac{1}{2} \frac{\partial^2 E_n}{\partial k_y^2} \Big|_{\vec{k}_8} + \frac{1}{2} \frac{\partial^2 E_n}{\partial k_z^2} \Big|_{\vec{k}_8} + \frac{\partial^2 E_n}{\partial k_y \partial k_z} \Big|_{\vec{k}_8} - 2 \frac{\partial^2 E_n}{\partial k_x^2} \Big|_{\vec{k}_2} - \frac{\partial^2 E_n}{\partial k_x \partial k_y} \Big|_{\vec{k}_2} \\
& - \frac{\partial^2 E_n}{\partial k_z \partial k_x} \Big|_{\vec{k}_2} + \frac{1}{2} \frac{\partial^2 E_n}{\partial k_x^2} \Big|_{\vec{k}_1} + \frac{1}{2} \frac{\partial^2 E_n}{\partial k_y^2} \Big|_{\vec{k}_1} + \frac{1}{2} \frac{\partial^2 E_n}{\partial k_z^2} \Big|_{\vec{k}_1} + \frac{\partial^2 E_n}{\partial k_x \partial k_y} \Big|_{\vec{k}_1} \\
& + \frac{\partial^2 E_n}{\partial k_y \partial k_z} \Big|_{\vec{k}_1} + \frac{\partial^2 E_n}{\partial k_z \partial k_x} \Big|_{\vec{k}_1} + \frac{1}{2} \frac{\partial^2 E_n}{\partial k_x^2} \Big|_{\vec{k}_6} + \frac{1}{2} \frac{\partial^2 E_n}{\partial k_z^2} \Big|_{\vec{k}_6} + \frac{\partial^2 E_n}{\partial k_z \partial k_x} \Big|_{\vec{k}_6}
\end{aligned}$$

$$\begin{aligned}
C_5 = & -\frac{1}{l^3} \frac{\partial^2 E_n}{\partial k_x \partial k_y} \Big|_{\vec{k}_3} + \frac{1}{l^3} \frac{\partial^2 E_n}{\partial k_z \partial k_x} \Big|_{\vec{k}_7} + \frac{1}{l^3} \frac{\partial^2 E_n}{\partial k_x \partial k_y} \Big|_{\vec{k}_7} + \frac{1}{l^3} \frac{\partial^2 E_n}{\partial k_y \partial k_z} \Big|_{\vec{k}_7} + \frac{1}{l^3} \frac{\partial^2 E_n}{\partial k_x \partial k_y} \Big|_{\vec{k}_5} \\
& + \frac{1}{l^3} \frac{\partial^2 E_n}{\partial k_y \partial k_z} \Big|_{\vec{k}_5} + \frac{1}{l^3} \frac{\partial^2 E_n}{\partial k_z \partial k_x} \Big|_{\vec{k}_5} + \frac{1}{2l^3} \frac{\partial^2 E_n}{\partial k_z^2} \Big|_{\vec{k}_7} + \frac{1}{2l^3} \frac{\partial^2 E_n}{\partial k_x^2} \Big|_{\vec{k}_5} + \frac{1}{2l^3} \frac{\partial^2 E_n}{\partial k_y^2} \Big|_{\vec{k}_5} \\
& + \frac{1}{2l^3} \frac{\partial^2 E_n}{\partial k_z^2} \Big|_{\vec{k}_5} + \frac{1}{2l^3} \frac{\partial^2 E_n}{\partial k_x^2} \Big|_{\vec{k}_4} + \frac{1}{2l^3} \frac{\partial^2 E_n}{\partial k_y^2} \Big|_{\vec{k}_4} + \frac{1}{2l^3} \frac{\partial^2 E_n}{\partial k_z^2} \Big|_{\vec{k}_4} + \frac{1}{l^3} \frac{\partial^2 E_n}{\partial k_x \partial k_y} \Big|_{\vec{k}_4} \\
& + \frac{1}{l^3} \frac{\partial^2 E_n}{\partial k_y \partial k_z} \Big|_{\vec{k}_4} + \frac{1}{l^3} \frac{\partial^2 E_n}{\partial k_z \partial k_x} \Big|_{\vec{k}_4} + \frac{1}{l^3} \frac{\partial^2 E_n}{\partial k_x \partial k_y} \Big|_{\vec{k}_2} + \frac{1}{l^3} \frac{\partial^2 E_n}{\partial k_y \partial k_z} \Big|_{\vec{k}_2} \\
& + \frac{1}{l^3} \frac{\partial^2 E_n}{\partial k_z \partial k_x} \Big|_{\vec{k}_2} - \frac{1}{2l^2} \frac{\partial^2 E_n}{\partial k_x^2} \Big|_{\vec{k}_8} - \frac{1}{2l^3} \frac{\partial^2 E_n}{\partial k_y^2} \Big|_{\vec{k}_8} - \frac{1}{2l^3} \frac{\partial^2 E_n}{\partial k_z^2} \Big|_{\vec{k}_8} - \frac{1}{l^3} \frac{\partial^2 E_n}{\partial k_x \partial k_y} \Big|_{\vec{k}_8} \\
& - \frac{1}{l^3} \frac{\partial^2 E_n}{\partial k_y \partial k_z} \Big|_{\vec{k}_8} - \frac{1}{l^3} \frac{\partial^2 E_n}{\partial k_z \partial k_x} \Big|_{\vec{k}_8} - \frac{1}{l^3} \frac{\partial^2 E_n}{\partial k_y \partial k_z} \Big|_{\vec{k}_3} - \frac{1}{l^3} \frac{\partial^2 E_n}{\partial k_z \partial k_x} \Big|_{\vec{k}_3} \\
& - \frac{1}{2l^3} \frac{\partial^2 E_n}{\partial k_x^2} \Big|_{\vec{k}_3} - \frac{1}{2l^3} \frac{\partial^2 E_n}{\partial k_y^2} \Big|_{\vec{k}_3} - \frac{1}{2l^3} \frac{\partial^2 E_n}{\partial k_z^2} \Big|_{\vec{k}_3} - \frac{1}{2l^3} \frac{\partial^2 E_n}{\partial k_x^2} \Big|_{\vec{k}_1} - \frac{1}{2l^3} \frac{\partial^2 E_n}{\partial k_y^2} \Big|_{\vec{k}_1} \\
& - \frac{1}{2l^3} \frac{\partial^2 E_n}{\partial k_z^2} \Big|_{\vec{k}_1} - \frac{1}{l^3} \frac{\partial^2 E_n}{\partial k_x \partial k_y} \Big|_{\vec{k}_1} - \frac{1}{l^3} \frac{\partial^2 E_n}{\partial k_y \partial k_z} \Big|_{\vec{k}_1} - \frac{1}{l^3} \frac{\partial^2 E_n}{\partial k_z \partial k_x} \Big|_{\vec{k}_1} + \frac{1}{2l^3} \frac{\partial^2 E_n}{\partial k_x^2} \Big|_{\vec{k}_2} \\
& + \frac{1}{2l^3} \frac{\partial^2 E_n}{\partial k_y^2} \Big|_{\vec{k}_2} + \frac{1}{2l^3} \frac{\partial^2 E_n}{\partial k_z^2} \Big|_{\vec{k}_2} - \frac{1}{2l^3} \frac{\partial^2 E_n}{\partial k_x^2} \Big|_{\vec{k}_6} - \frac{1}{2l^3} \frac{\partial^2 E_n}{\partial k_y^2} \Big|_{\vec{k}_6} - \frac{1}{2l^3} \frac{\partial^2 E_n}{\partial k_z^2} \Big|_{\vec{k}_6} \\
& - \frac{1}{l^3} \frac{\partial^2 E_n}{\partial k_x \partial k_y} \Big|_{\vec{k}_6} - \frac{1}{l^3} \frac{\partial^2 E_n}{\partial k_y \partial k_z} \Big|_{\vec{k}_6} - \frac{1}{l^3} \frac{\partial^2 E_n}{\partial k_z \partial k_x} \Big|_{\vec{k}_6} + \frac{1}{2l^3} \frac{\partial^2 E_n}{\partial k_x^2} \Big|_{\vec{k}_7} + \frac{1}{2l^3} \frac{\partial^2 E_n}{\partial k_y^2} \Big|_{\vec{k}_7}
\end{aligned}$$

Line number 5: $\vec{\Delta k} = (\Delta k_x, \Delta k_y, \Delta k_z)$ is given by $(l - x, x, x)$

$$C_0 = E_n(\vec{k}_2)$$

$$\begin{aligned}
C_1 = & -\frac{\partial E_n}{\partial k_z} \Big|_{\vec{k}_6} + \frac{1}{l} E_n(\vec{k}_1) + \frac{\partial E_n}{\partial k_x} \Big|_{\vec{k}_1} + \frac{l}{2} \frac{\partial^2 E_n}{\partial k_y^2} \Big|_{\vec{k}_3} - \frac{3}{l} E_n(\vec{k}_2) + \frac{\partial E_n}{\partial k_y} \Big|_{\vec{k}_2} + \frac{\partial E_n}{\partial k_z} \Big|_{\vec{k}_2} \\
& - \frac{\partial E_n}{\partial k_y} \Big|_{\vec{k}_3} + \frac{1}{l} E_n(\vec{k}_3) + \frac{l}{2} \frac{\partial^2 E_n}{\partial k_x^2} \Big|_{\vec{k}_1} - \frac{\partial E_n}{\partial k_x} \Big|_{\vec{k}_2} + \frac{l}{2} \frac{\partial^2 E_n}{\partial k_z^2} \Big|_{\vec{k}_6} + \frac{1}{l} E_n(\vec{k}_6)
\end{aligned}$$

$$\begin{aligned}
C_2 = & \frac{1}{l^2} E_n(\vec{k}_5) - \frac{2}{l^2} E_n(\vec{k}_3) - \frac{2}{l^2} E_n(\vec{k}_6) + \frac{1}{l^2} E_n(\vec{k}_4) - \frac{2}{l^2} E_n(\vec{k}_1) + \frac{3}{l^2} E_n(\vec{k}_2) \\
& + \frac{1}{l} \frac{\partial E_n}{\partial k_y} \Big|_{\vec{k}_6} - \frac{1}{l} \frac{\partial E_n}{\partial k_y} \Big|_{\vec{k}_7} - \frac{3}{l} \frac{\partial E_n}{\partial k_y} \Big|_{\vec{k}_2} + \frac{3}{l} \frac{\partial E_n}{\partial k_y} \Big|_{\vec{k}_3} - \frac{1}{l} \frac{\partial E_n}{\partial k_y} \Big|_{\vec{k}_4} + \frac{1}{l} \frac{\partial E_n}{\partial k_y} \Big|_{\vec{k}_1} \\
& - \frac{1}{l} \frac{\partial E_n}{\partial k_z} \Big|_{\vec{k}_7} + \frac{1}{l} \frac{\partial E_n}{\partial k_z} \Big|_{\vec{k}_3} - \frac{1}{l} \frac{\partial E_n}{\partial k_z} \Big|_{\vec{k}_5} + \frac{1}{l} \frac{\partial E_n}{\partial k_z} \Big|_{\vec{k}_1} - \frac{3}{l} \frac{\partial E_n}{\partial k_z} \Big|_{\vec{k}_2} + \frac{3}{l} \frac{\partial E_n}{\partial k_z} \Big|_{\vec{k}_6} \\
& + \frac{1}{2} \frac{\partial^2 E_n}{\partial k_x^2} \Big|_{\vec{k}_5} + \frac{1}{2} \frac{\partial^2 E_n}{\partial k_z^2} \Big|_{\vec{k}_5} - \frac{\partial^2 E_n}{\partial k_z \partial k_x} \Big|_{\vec{k}_5} - \frac{3}{l} \frac{\partial E_n}{\partial k_x} \Big|_{\vec{k}_1} + \frac{3}{l} \frac{\partial E_n}{\partial k_x} \Big|_{\vec{k}_2} \\
& - \frac{1}{l} \frac{\partial E_n}{\partial k_x} \Big|_{\vec{k}_3} + \frac{1}{l} \frac{\partial E_n}{\partial k_x} \Big|_{\vec{k}_4} + \frac{1}{l} \frac{\partial E_n}{\partial k_x} \Big|_{\vec{k}_5} - \frac{1}{l} \frac{\partial E_n}{\partial k_x} \Big|_{\vec{k}_6} + \frac{1}{l^2} E_n(\vec{k}_7) + \frac{1}{2} \frac{\partial^2 E_n}{\partial k_x^2} \Big|_{\vec{k}_4} \\
& + \frac{1}{2} \frac{\partial^2 E_n}{\partial k_y^2} \Big|_{\vec{k}_4} - \frac{\partial^2 E_n}{\partial k_x \partial k_y} \Big|_{\vec{k}_4} + \frac{1}{2} \frac{\partial^2 E_n}{\partial k_y^2} \Big|_{\vec{k}_7} + \frac{1}{2} \frac{\partial^2 E_n}{\partial k_z^2} \Big|_{\vec{k}_7} + \frac{\partial^2 E_n}{\partial k_y \partial k_z} \Big|_{\vec{k}_7} \\
& - 2 \frac{\partial^2 E_n}{\partial k_y^2} \Big|_{\vec{k}_3} + \frac{\partial^2 E_n}{\partial k_x \partial k_y} \Big|_{\vec{k}_3} - \frac{\partial^2 E_n}{\partial k_y \partial k_z} \Big|_{\vec{k}_3} + \frac{1}{2} \frac{\partial^2 E_n}{\partial k_x^2} \Big|_{\vec{k}_2} + \frac{1}{2} \frac{\partial^2 E_n}{\partial k_y^2} \Big|_{\vec{k}_2} \\
& + \frac{1}{2} \frac{\partial^2 E_n}{\partial k_z^2} \Big|_{\vec{k}_2} - \frac{\partial^2 E_n}{\partial k_x \partial k_y} \Big|_{\vec{k}_2} + \frac{\partial^2 E_n}{\partial k_y \partial k_z} \Big|_{\vec{k}_2} - \frac{\partial^2 E_n}{\partial k_z \partial k_x} \Big|_{\vec{k}_2} - 2 \frac{\partial^2 E_n}{\partial k_x^2} \Big|_{\vec{k}_1} \\
& + \frac{\partial^2 E_n}{\partial k_x \partial k_y} \Big|_{\vec{k}_1} + \frac{\partial^2 E_n}{\partial k_z \partial k_x} \Big|_{\vec{k}_1} - 2 \frac{\partial^2 E_n}{\partial k_z^2} \Big|_{\vec{k}_6} - \frac{\partial^2 E_n}{\partial k_y \partial k_z} \Big|_{\vec{k}_6} + \frac{\partial^2 E_n}{\partial k_z \partial k_x} \Big|_{\vec{k}_6}
\end{aligned}$$

$$\begin{aligned}
C_5 = & -\frac{1}{l^3} \frac{\partial^2 E_n}{\partial k_x \partial k_y} \Big|_{\vec{k}_3} + \frac{1}{l^3} \frac{\partial^2 E_n}{\partial k_z \partial k_x} \Big|_{\vec{k}_7} + \frac{1}{l^3} \frac{\partial^2 E_n}{\partial k_x \partial k_y} \Big|_{\vec{k}_7} - \frac{1}{l^3} \frac{\partial^2 E_n}{\partial k_y \partial k_z} \Big|_{\vec{k}_7} + \frac{1}{l^3} \frac{\partial^2 E_n}{\partial k_x \partial k_y} \Big|_{\vec{k}_5} \\
& - \frac{1}{l^3} \frac{\partial^2 E_n}{\partial k_y \partial k_z} \Big|_{\vec{k}_5} + \frac{1}{l^3} \frac{\partial^2 E_n}{\partial k_z \partial k_x} \Big|_{\vec{k}_5} - \frac{1}{2l^3} \frac{\partial^2 E_n}{\partial k_z^2} \Big|_{\vec{k}_7} - \frac{1}{2l^3} \frac{\partial^2 E_n}{\partial k_x^2} \Big|_{\vec{k}_5} - \frac{1}{2l^3} \frac{\partial^2 E_n}{\partial k_y^2} \Big|_{\vec{k}_5} \\
& - \frac{1}{2l^3} \frac{\partial^2 E_n}{\partial k_z^2} \Big|_{\vec{k}_5} - \frac{1}{2l^3} \frac{\partial^2 E_n}{\partial k_x^2} \Big|_{\vec{k}_4} - \frac{1}{2l^3} \frac{\partial^2 E_n}{\partial k_y^2} \Big|_{\vec{k}_4} - \frac{1}{2l^3} \frac{\partial^2 E_n}{\partial k_z^2} \Big|_{\vec{k}_4} + \frac{1}{l^3} \frac{\partial^2 E_n}{\partial k_x \partial k_y} \Big|_{\vec{k}_4} \\
& - \frac{1}{l^3} \frac{\partial^2 E_n}{\partial k_y \partial k_z} \Big|_{\vec{k}_4} + \frac{1}{l^3} \frac{\partial^2 E_n}{\partial k_z \partial k_x} \Big|_{\vec{k}_4} + \frac{1}{l^3} \frac{\partial^2 E_n}{\partial k_x \partial k_y} \Big|_{\vec{k}_2} - \frac{1}{l^3} \frac{\partial^2 E_n}{\partial k_y \partial k_z} \Big|_{\vec{k}_2} \\
& + \frac{1}{l^3} \frac{\partial^2 E_n}{\partial k_z \partial k_x} \Big|_{\vec{k}_2} + \frac{1}{2l^3} \frac{\partial^2 E_n}{\partial k_x^2} \Big|_{\vec{k}_8} + \frac{1}{2l^3} \frac{\partial^2 E_n}{\partial k_y^2} \Big|_{\vec{k}_8} + \frac{1}{2l^3} \frac{\partial^2 E_n}{\partial k_z^2} \Big|_{\vec{k}_8} - \frac{1}{l^3} \frac{\partial^2 E_n}{\partial k_x \partial k_y} \Big|_{\vec{k}_8} \\
& + \frac{1}{l^3} \frac{\partial^2 E_n}{\partial k_y \partial k_z} \Big|_{\vec{k}_8} - \frac{1}{l^3} \frac{\partial^2 E_n}{\partial k_z \partial k_x} \Big|_{\vec{k}_8} + \frac{1}{l^3} \frac{\partial^2 E_n}{\partial k_y \partial k_z} \Big|_{\vec{k}_3} - \frac{1}{l^3} \frac{\partial^2 E_n}{\partial k_z \partial k_x} \Big|_{\vec{k}_3} \\
& + \frac{1}{2l^3} \frac{\partial^2 E_n}{\partial k_x^2} \Big|_{\vec{k}_3} + \frac{1}{2l^3} \frac{\partial^2 E_n}{\partial k_y^2} \Big|_{\vec{k}_3} + \frac{1}{2l^3} \frac{\partial^2 E_n}{\partial k_z^2} \Big|_{\vec{k}_3} + \frac{1}{2l^3} \frac{\partial^2 E_n}{\partial k_x^2} \Big|_{\vec{k}_1} + \frac{1}{2l^3} \frac{\partial^2 E_n}{\partial k_y^2} \Big|_{\vec{k}_1} \\
& + \frac{1}{2l^3} \frac{\partial^2 E_n}{\partial k_z^2} \Big|_{\vec{k}_1} - \frac{1}{l^3} \frac{\partial^2 E_n}{\partial k_x \partial k_y} \Big|_{\vec{k}_1} + \frac{1}{l^3} \frac{\partial^2 E_n}{\partial k_y \partial k_z} \Big|_{\vec{k}_1} - \frac{1}{l^3} \frac{\partial^2 E_n}{\partial k_z \partial k_x} \Big|_{\vec{k}_1} - \frac{1}{2l^3} \frac{\partial^2 E_n}{\partial k_x^2} \Big|_{\vec{k}_2} \\
& - \frac{1}{2l^3} \frac{\partial^2 E_n}{\partial k_y^2} \Big|_{\vec{k}_2} - \frac{1}{2l^3} \frac{\partial^2 E_n}{\partial k_z^2} \Big|_{\vec{k}_2} + \frac{1}{2l^3} \frac{\partial^2 E_n}{\partial k_x^2} \Big|_{\vec{k}_6} + \frac{1}{2l^3} \frac{\partial^2 E_n}{\partial k_y^2} \Big|_{\vec{k}_6} + \frac{1}{2l^3} \frac{\partial^2 E_n}{\partial k_z^2} \Big|_{\vec{k}_6} \\
& - \frac{1}{l^3} \frac{\partial^2 E_n}{\partial k_x \partial k_y} \Big|_{\vec{k}_6} + \frac{1}{l^3} \frac{\partial^2 E_n}{\partial k_y \partial k_z} \Big|_{\vec{k}_6} - \frac{1}{l^3} \frac{\partial^2 E_n}{\partial k_z \partial k_x} \Big|_{\vec{k}_6} - \frac{1}{2l^3} \frac{\partial^2 E_n}{\partial k_x^2} \Big|_{\vec{k}_7} - \frac{1}{2l^3} \frac{\partial^2 E_n}{\partial k_y^2} \Big|_{\vec{k}_7}
\end{aligned}$$

Line number 6: $\vec{\Delta k} = (\Delta k_x, \Delta k_y, \Delta k_z)$ is given by $(l - x, l - x, x)$

$$C_0 = E_n(\vec{k}_3)$$

$$\begin{aligned}
C_1 = & -\frac{\partial E_n}{\partial k_y} \Big|_{\vec{k}_3} + \frac{l}{2} \frac{\partial^2 E_n}{\partial k_x^2} \Big|_{\vec{k}_4} + \frac{l}{2} \frac{\partial^2 E_n}{\partial k_z^2} \Big|_{\vec{k}_7} - \frac{3}{l} E_n(\vec{k}_3) + \frac{l}{2} \frac{\partial^2 E_n}{\partial k_y^2} \Big|_{\vec{k}_2} + \frac{1}{l} E_n(\vec{k}_4) \\
& - \frac{\partial E_n}{\partial k_z} \Big|_{\vec{k}_7} + \frac{\partial E_n}{\partial k_z} \Big|_{\vec{k}_3} + \frac{\partial E_n}{\partial k_y} \Big|_{\vec{k}_2} - \frac{\partial E_n}{\partial k_x} \Big|_{\vec{k}_3} + \frac{1}{l} E_n(\vec{k}_2) + \frac{1}{l} E_n(\vec{k}_7) + \frac{\partial E_n}{\partial k_x} \Big|_{\vec{k}_4}
\end{aligned}$$

$$\begin{aligned}
C_2 = & \frac{3}{l^2} E_n(\vec{k}_3) + \frac{1}{l^2} E_n(\vec{k}_8) + \frac{1}{l^2} E_n(\vec{k}_6) - \frac{2}{l^2} E_n(\vec{k}_4) + \frac{1}{l^2} E_n(\vec{k}_1) - \frac{2}{l^2} E_n(\vec{k}_2) \\
& + \frac{1}{l} \frac{\partial E_n}{\partial k_y} \Big|_{\vec{k}_6} - \frac{1}{l} \frac{\partial E_n}{\partial k_y} \Big|_{\vec{k}_7} - \frac{3}{l} \frac{\partial E_n}{\partial k_y} \Big|_{\vec{k}_2} + \frac{3}{l} \frac{\partial E_n}{\partial k_y} \Big|_{\vec{k}_3} - \frac{1}{l} \frac{\partial E_n}{\partial k_y} \Big|_{\vec{k}_4} + \frac{1}{l} \frac{\partial E_n}{\partial k_y} \Big|_{\vec{k}_1} \\
& + \frac{3}{l} \frac{\partial E_n}{\partial k_z} \Big|_{\vec{k}_7} - \frac{1}{l} \frac{\partial E_n}{\partial k_z} \Big|_{\vec{k}_8} - \frac{3}{l} \frac{\partial E_n}{\partial k_z} \Big|_{\vec{k}_3} + \frac{1}{l} \frac{\partial E_n}{\partial k_z} \Big|_{\vec{k}_4} + \frac{1}{l} \frac{\partial E_n}{\partial k_z} \Big|_{\vec{k}_2} - \frac{1}{l} \frac{\partial E_n}{\partial k_z} \Big|_{\vec{k}_6} \\
& + \frac{1}{l} \frac{\partial E_n}{\partial k_x} \Big|_{\vec{k}_1} - \frac{1}{l} \frac{\partial E_n}{\partial k_x} \Big|_{\vec{k}_2} + \frac{3}{l} \frac{\partial E_n}{\partial k_x} \Big|_{\vec{k}_3} - \frac{3}{l} \frac{\partial E_n}{\partial k_x} \Big|_{\vec{k}_4} - \frac{1}{l} \frac{\partial E_n}{\partial k_x} \Big|_{\vec{k}_7} + \frac{1}{l} \frac{\partial E_n}{\partial k_x} \Big|_{\vec{k}_8} \\
& - \frac{2}{l^2} E_n(\vec{k}_7) - 2 \frac{\partial^2 E_n}{\partial k_x^2} \Big|_{\vec{k}_4} - \frac{\partial^2 E_n}{\partial k_x \partial k_y} \Big|_{\vec{k}_4} + \frac{\partial^2 E_n}{\partial k_z \partial k_x} \Big|_{\vec{k}_4} - 2 \frac{\partial^2 E_n}{\partial k_z^2} \Big|_{\vec{k}_7} \\
& + \frac{\partial^2 E_n}{\partial k_y \partial k_z} \Big|_{\vec{k}_7} + \frac{\partial^2 E_n}{\partial k_z \partial k_x} \Big|_{\vec{k}_7} + \frac{1}{2} \frac{\partial^2 E_n}{\partial k_x^2} \Big|_{\vec{k}_3} + \frac{1}{2} \frac{\partial^2 E_n}{\partial k_y^2} \Big|_{\vec{k}_3} + \frac{1}{2} \frac{\partial^2 E_n}{\partial k_z^2} \Big|_{\vec{k}_3} \\
& + \frac{\partial^2 E_n}{\partial k_x \partial k_y} \Big|_{\vec{k}_3} - \frac{\partial^2 E_n}{\partial k_y \partial k_z} \Big|_{\vec{k}_3} - \frac{\partial^2 E_n}{\partial k_z \partial k_x} \Big|_{\vec{k}_3} + \frac{1}{2} \frac{\partial^2 E_n}{\partial k_x^2} \Big|_{\vec{k}_8} + \frac{1}{2} \frac{\partial^2 E_n}{\partial k_z^2} \Big|_{\vec{k}_8} \\
& - \frac{\partial^2 E_n}{\partial k_z \partial k_x} \Big|_{\vec{k}_8} - 2 \frac{\partial^2 E_n}{\partial k_y^2} \Big|_{\vec{k}_2} - \frac{\partial^2 E_n}{\partial k_x \partial k_y} \Big|_{\vec{k}_2} + \frac{\partial^2 E_n}{\partial k_y \partial k_z} \Big|_{\vec{k}_2} + \frac{1}{2} \frac{\partial^2 E_n}{\partial k_x^2} \Big|_{\vec{k}_1} \\
& + \frac{1}{2} \frac{\partial^2 E_n}{\partial k_y^2} \Big|_{\vec{k}_1} + \frac{\partial^2 E_n}{\partial k_x \partial k_y} \Big|_{\vec{k}_1} + \frac{1}{2} \frac{\partial^2 E_n}{\partial k_y^2} \Big|_{\vec{k}_6} + \frac{1}{2} \frac{\partial^2 E_n}{\partial k_z^2} \Big|_{\vec{k}_6} - \frac{\partial^2 E_n}{\partial k_y \partial k_z} \Big|_{\vec{k}_6}
\end{aligned}$$

$$\begin{aligned}
C_5 = & -\frac{1}{l^3} \frac{\partial^2 E_n}{\partial k_x \partial k_y} \Big|_{\vec{k}_3} - \frac{1}{l^3} \frac{\partial^2 E_n}{\partial k_z \partial k_x} \Big|_{\vec{k}_7} + \frac{1}{l^3} \frac{\partial^2 E_n}{\partial k_x \partial k_y} \Big|_{\vec{k}_7} - \frac{1}{l^3} \frac{\partial^2 E_n}{\partial k_y \partial k_z} \Big|_{\vec{k}_7} + \frac{1}{l^3} \frac{\partial^2 E_n}{\partial k_x \partial k_y} \Big|_{\vec{k}_5} \\
& - \frac{1}{l^3} \frac{\partial^2 E_n}{\partial k_y \partial k_z} \Big|_{\vec{k}_5} - \frac{1}{l^3} \frac{\partial^2 E_n}{\partial k_z \partial k_x} \Big|_{\vec{k}_5} + \frac{1}{2l^3} \frac{\partial^2 E_n}{\partial k_z^2} \Big|_{\vec{k}_7} + \frac{1}{2l^3} \frac{\partial^2 E_n}{\partial k_x^2} \Big|_{\vec{k}_5} + \frac{1}{2l^3} \frac{\partial^2 E_n}{\partial k_y^2} \Big|_{\vec{k}_5} \\
& + \frac{1}{2l^3} \frac{\partial^2 E_n}{\partial k_z^2} \Big|_{\vec{k}_5} + \frac{1}{2l^3} \frac{\partial^2 E_n}{\partial k_x^2} \Big|_{\vec{k}_4} + \frac{1}{2l^3} \frac{\partial^2 E_n}{\partial k_y^2} \Big|_{\vec{k}_4} + \frac{1}{2l^3} \frac{\partial^2 E_n}{\partial k_z^2} \Big|_{\vec{k}_4} + \frac{1}{l^3} \frac{\partial^2 E_n}{\partial k_x \partial k_y} \Big|_{\vec{k}_4} \\
& - \frac{1}{l^3} \frac{\partial^2 E_n}{\partial k_y \partial k_z} \Big|_{\vec{k}_4} - \frac{1}{l^3} \frac{\partial^2 E_n}{\partial k_z \partial k_x} \Big|_{\vec{k}_4} + \frac{1}{l^3} \frac{\partial^2 E_n}{\partial k_x \partial k_y} \Big|_{\vec{k}_2} - \frac{1}{l^3} \frac{\partial^2 E_n}{\partial k_y \partial k_z} \Big|_{\vec{k}_2} \\
& - \frac{1}{l^3} \frac{\partial^2 E_n}{\partial k_z \partial k_x} \Big|_{\vec{k}_2} - \frac{1}{2l^3} \frac{\partial^2 E_n}{\partial k_x^2} \Big|_{\vec{k}_8} - \frac{1}{2l^3} \frac{\partial^2 E_n}{\partial k_y^2} \Big|_{\vec{k}_8} - \frac{1}{2l^3} \frac{\partial^2 E_n}{\partial k_z^2} \Big|_{\vec{k}_8} - \frac{1}{l^3} \frac{\partial^2 E_n}{\partial k_x \partial k_y} \Big|_{\vec{k}_8} \\
& + \frac{1}{l^3} \frac{\partial^2 E_n}{\partial k_y \partial k_z} \Big|_{\vec{k}_8} + \frac{1}{l^3} \frac{\partial^2 E_n}{\partial k_z \partial k_x} \Big|_{\vec{k}_8} + \frac{1}{l^3} \frac{\partial^2 E_n}{\partial k_y \partial k_z} \Big|_{\vec{k}_3} + \frac{1}{l^3} \frac{\partial^2 E_n}{\partial k_z \partial k_x} \Big|_{\vec{k}_3} \\
& - \frac{1}{2l^3} \frac{\partial^2 E_n}{\partial k_x^2} \Big|_{\vec{k}_3} - \frac{1}{2l^3} \frac{\partial^2 E_n}{\partial k_y^2} \Big|_{\vec{k}_3} - \frac{1}{2l^3} \frac{\partial^2 E_n}{\partial k_z^2} \Big|_{\vec{k}_3} - \frac{1}{2l^3} \frac{\partial^2 E_n}{\partial k_x^2} \Big|_{\vec{k}_1} - \frac{1}{2l^3} \frac{\partial^2 E_n}{\partial k_y^2} \Big|_{\vec{k}_1} \\
& - \frac{1}{2l^3} \frac{\partial^2 E_n}{\partial k_z^2} \Big|_{\vec{k}_1} - \frac{1}{l^3} \frac{\partial^2 E_n}{\partial k_x \partial k_y} \Big|_{\vec{k}_1} + \frac{1}{l^3} \frac{\partial^2 E_n}{\partial k_y \partial k_z} \Big|_{\vec{k}_1} + \frac{1}{l^3} \frac{\partial^2 E_n}{\partial k_z \partial k_x} \Big|_{\vec{k}_1} + \frac{1}{2l^3} \frac{\partial^2 E_n}{\partial k_x^2} \Big|_{\vec{k}_2} \\
& + \frac{1}{2l^3} \frac{\partial^2 E_n}{\partial k_y^2} \Big|_{\vec{k}_2} + \frac{1}{2l^3} \frac{\partial^2 E_n}{\partial k_z^2} \Big|_{\vec{k}_2} - \frac{1}{2l^3} \frac{\partial^2 E_n}{\partial k_x^2} \Big|_{\vec{k}_6} - \frac{1}{2l^3} \frac{\partial^2 E_n}{\partial k_y^2} \Big|_{\vec{k}_6} - \frac{1}{2l^3} \frac{\partial^2 E_n}{\partial k_z^2} \Big|_{\vec{k}_6} \\
& - \frac{1}{l^3} \frac{\partial^2 E_n}{\partial k_x \partial k_y} \Big|_{\vec{k}_6} + \frac{1}{l^3} \frac{\partial^2 E_n}{\partial k_y \partial k_z} \Big|_{\vec{k}_6} + \frac{1}{l^3} \frac{\partial^2 E_n}{\partial k_z \partial k_x} \Big|_{\vec{k}_6} + \frac{1}{2l^3} \frac{\partial^2 E_n}{\partial k_x^2} \Big|_{\vec{k}_7} + \frac{1}{2l^3} \frac{\partial^2 E_n}{\partial k_y^2} \Big|_{\vec{k}_7}
\end{aligned}$$

Line number 7: $\vec{\Delta k} = (\Delta k_x, \Delta k_y, \Delta k_z)$ is given by $(x, l - x, x)$

$$C_0 = E_n(\vec{k}_4)$$

$$\begin{aligned}
C_1 = & \frac{1}{l} E_n(\vec{k}_3) + \frac{\partial E_n}{\partial k_x} \Big|_{\vec{k}_4} + \frac{\partial E_n}{\partial k_z} \Big|_{\vec{k}_4} + \frac{l}{2} \frac{\partial^2 E_n}{\partial k_y^2} \Big|_{\vec{k}_1} - \frac{3}{l} E_n(\vec{k}_4) + \frac{\partial E_n}{\partial k_y} \Big|_{\vec{k}_1} + \frac{l}{2} \frac{\partial^2 E_n}{\partial k_x^2} \Big|_{\vec{k}_3} \\
& - \frac{\partial E_n}{\partial k_x} \Big|_{\vec{k}_3} - \frac{\partial E_n}{\partial k_y} \Big|_{\vec{k}_4} + \frac{l}{2} \frac{\partial^2 E_n}{\partial k_z^2} \Big|_{\vec{k}_8} - \frac{\partial E_n}{\partial k_z} \Big|_{\vec{k}_8} + \frac{1}{l} E_n(\vec{k}_8) + \frac{1}{l} E_n(\vec{k}_1)
\end{aligned}$$

$$\begin{aligned}
C_2 = & \frac{1}{l^2} E_n(\vec{k}_5) - \frac{2}{l^2} E_n(\vec{k}_3) - \frac{2}{l^2} E_n(\vec{k}_8) + \frac{3}{l^2} E_n(\vec{k}_4) - \frac{2}{l^2} E_n(\vec{k}_1) + \frac{1}{l^2} E_n(\vec{k}_2) \\
& - \frac{1}{l} \frac{\partial E_n}{\partial k_y} \Big|_{\vec{k}_8} + \frac{1}{l} \frac{\partial E_n}{\partial k_y} \Big|_{\vec{k}_5} + \frac{1}{l} \frac{\partial E_n}{\partial k_y} \Big|_{\vec{k}_2} - \frac{1}{l} \frac{\partial E_n}{\partial k_y} \Big|_{\vec{k}_3} + \frac{3}{l} \frac{\partial E_n}{\partial k_y} \Big|_{\vec{k}_4} - \frac{3}{l} \frac{\partial E_n}{\partial k_y} \Big|_{\vec{k}_1} \\
& - \frac{1}{l} \frac{\partial E_n}{\partial k_z} \Big|_{\vec{k}_7} + \frac{3}{l} \frac{\partial E_n}{\partial k_z} \Big|_{\vec{k}_8} + \frac{1}{l} \frac{\partial E_n}{\partial k_z} \Big|_{\vec{k}_3} - \frac{3}{l} \frac{\partial E_n}{\partial k_z} \Big|_{\vec{k}_4} - \frac{1}{l} \frac{\partial E_n}{\partial k_z} \Big|_{\vec{k}_5} + \frac{1}{l} \frac{\partial E_n}{\partial k_z} \Big|_{\vec{k}_1} \\
& + \frac{1}{2} \frac{\partial^2 E_n}{\partial k_y^2} \Big|_{\vec{k}_5} + \frac{1}{2} \frac{\partial^2 E_n}{\partial k_z^2} \Big|_{\vec{k}_5} - \frac{\partial^2 E_n}{\partial k_y \partial k_z} \Big|_{\vec{k}_5} + \frac{1}{l} \frac{\partial E_n}{\partial k_x} \Big|_{\vec{k}_1} - \frac{1}{l} \frac{\partial E_n}{\partial k_x} \Big|_{\vec{k}_2} \\
& + \frac{3}{l} \frac{\partial E_n}{\partial k_x} \Big|_{\vec{k}_3} - \frac{3}{l} \frac{\partial E_n}{\partial k_x} \Big|_{\vec{k}_4} - \frac{1}{l} \frac{\partial E_n}{\partial k_x} \Big|_{\vec{k}_7} + \frac{1}{l} \frac{\partial E_n}{\partial k_x} \Big|_{\vec{k}_8} + \frac{1}{l^2} E_n(\vec{k}_7) + \frac{1}{2} \frac{\partial^2 E_n}{\partial k_x^2} \Big|_{\vec{k}_4} \\
& + \frac{1}{2} \frac{\partial^2 E_n}{\partial k_y^2} \Big|_{\vec{k}_4} + \frac{1}{2} \frac{\partial^2 E_n}{\partial k_z^2} \Big|_{\vec{k}_4} - \frac{\partial^2 E_n}{\partial k_x \partial k_y} \Big|_{\vec{k}_4} - \frac{\partial^2 E_n}{\partial k_y \partial k_z} \Big|_{\vec{k}_4} + \frac{\partial^2 E_n}{\partial k_z \partial k_x} \Big|_{\vec{k}_4} \\
& + \frac{1}{2} \frac{\partial^2 E_n}{\partial k_x^2} \Big|_{\vec{k}_7} + \frac{1}{2} \frac{\partial^2 E_n}{\partial k_z^2} \Big|_{\vec{k}_7} + \frac{\partial^2 E_n}{\partial k_z \partial k_x} \Big|_{\vec{k}_7} - 2 \frac{\partial^2 E_n}{\partial k_x^2} \Big|_{\vec{k}_3} + \frac{\partial^2 E_n}{\partial k_x \partial k_y} \Big|_{\vec{k}_3} \\
& - \frac{\partial^2 E_n}{\partial k_z \partial k_x} \Big|_{\vec{k}_3} - 2 \frac{\partial^2 E_n}{\partial k_z^2} \Big|_{\vec{k}_8} + \frac{\partial^2 E_n}{\partial k_y \partial k_z} \Big|_{\vec{k}_8} - \frac{\partial^2 E_n}{\partial k_z \partial k_x} \Big|_{\vec{k}_8} + \frac{1}{2} \frac{\partial^2 E_n}{\partial k_x^2} \Big|_{\vec{k}_2} \\
& + \frac{1}{2} \frac{\partial^2 E_n}{\partial k_y^2} \Big|_{\vec{k}_2} - \frac{\partial^2 E_n}{\partial k_x \partial k_y} \Big|_{\vec{k}_2} - 2 \frac{\partial^2 E_n}{\partial k_y^2} \Big|_{\vec{k}_1} + \frac{\partial^2 E_n}{\partial k_x \partial k_y} \Big|_{\vec{k}_1} + \frac{\partial^2 E_n}{\partial k_y \partial k_z} \Big|_{\vec{k}_1}
\end{aligned}$$
